Thermoeconomical Analysis and Optimization of a Hybrid Solar-Thermal Power Plant Using a Genetic Algorithm

Duarte Pereira de Araújo Coutinho

Thesis to obtain the Master of Science Degree in

Mechanical Engineering

Supervisors: Prof. Aires José Pinto dos Santos
Prof. Viriato Sérgio de Almeida Semião

Examination Committee

Chairperson: Prof. Edgar Caetano Fernandes
Supervisor: Prof. Aires José Pinto dos Santos
Member of the Committee: Prof. Carlos Augusto Santos Silva

January 2021

To my family.

Acknowledgements

I would like to express my deepest appreciation to my supervisors, Professor Aires Santos and Professor Viriato Semião, for their guidance and support throughout this work. It was a challenging journey full of ups and downs, and their combined experience and availability enabled me to overcome the obstacles that I found on the way.

I would also like to thank Jorge Rodrigues, for passing me on the algorithm that he developed during his master thesis, which served as a starting point for my work, as well as for the help he gave me regarding the use of that same algorithm.

To my family and friends, of course, an enormous thank you for all the support you gave me during this period of hard work, and for helping me stay motivated.

Abstract

Climate change is among the issues of the century, and one that is already felt at a global scale on the form of increasing average temperatures, natural catastrophes such as droughts and wildfires, melting of the glaciers, etc. At the same time, the demand for fossil fuels as a primary energy source continues to increase, which will inevitably lead to the exhaustion of existent reserves during the upcoming decades. These issues cannot be overlooked and transitioning towards renewable energy sources is mandatory. Concentrating solar power (CSP) technologies are an attractive option with many advantages such as the possibility to integrate an existent power cycle.

A thermoeconomic model for a small-scale hybrid solar-thermal power plant has been developed to study its performance under different operating conditions. The proposed system consists of a combined Rankine-Brayton cycle with a solar receiver and fossil fuel combustor working in series as heat sources to the topping cycle. An evolutionary algorithm was employed to conduct a multi-objective optimization of such system, and the result was a set of Pareto-optimal designs which were compared to a pre-defined reference design. Resulting optimized designs yield levelized electricity costs as low as 0.179 USD/kWh, as opposed to the 0.237 USD/kWh associated with the base design. Average 1st and 2nd law efficiencies of up to 27.97 % and 33.53 % were achieved, respectively, which represent increases of up to 7.71 % and 7.31 %. Finally, average solar shares of up to 65 % are possible for optimal designs versus the 58.4 % yielded by the reference design.

Keywords

Thermoeconomics, Concentrating Solar Power, Multi-Objective Optimization, Evolutionary Algorithms

Resumo

As alterações climatéricas são um dos principais tópicos do século, e fazem-se sentir atualmente através de fenómenos como o aquecimento global, catástrofes naturais, desaparecimento dos glaciares, etc. Ao mesmo tempo, a utilização de combustíveis fósseis como fonte de energia primária continua a aumentar, o que levará inevitavelmente à exaustão das reservas existentes durante as próximas décadas. Estas questões não podem ser ignoradas, e a transição energética no sentido das fontes renováveis é indispensável. As tecnologias solares térmicas são uma opção atrativa com variadas vantagens tais como a possibilidade de integração num ciclo de potência existente.

Um modelo termoeconómico para uma pequena central de geração elétrica do tipo solar térmico híbrido foi desenvolvido com o objetivo de estudar o respetivo desempenho em diferentes condições operacionais. O modelo proposto consiste num ciclo combinado de Rankine e Brayton, com um sistema de coleção solar e uma câmara de combustão a gás natural a funcionar em série como fontes de calor para o ciclo de Brayton. Um algoritmo evolucionário foi utilizado para conduzir uma otimização multiobjectivo do sistema, o que resultou num conjunto de soluções ótimas (frente de Pareto) que foram posteriormente comparadas com uma solução de referência previamente definida. A otimização possibilitou alcançar custos de geração elétrica na ordem dos 0,179 $US/kWh, o que representa uma redução bastante significativa comparando com o custo associado à solução de referência (0,237 $US/kWh). Além disso, eficiências energéticas e exergéticas máximas de 27,97 % e 33,53 % foram alcançadas, respetivamente, o que representa aumentos de 7,71 % e 7,31 %. Do ponto de vista ambiental, as soluções ótimas exibem frações solares até 65 %, uma melhoria substancial relativamente ao valor máximo de 58,4 % alcançado pela solução de referência.

Palavras-chave

Análise termoeconómica, Tecnologia Solar Térmica, Otimização Multiobjetivo, Algoritmos Evolucionários

Table of Contents

List of Figures

List of Tables

List of Acronyms

CCPP	Combined Cycle Power Plant.
CSP	Concentrating Solar Power.
DNI	Direct Normal Irradiance.
EA	Evolutionary Algorithm.
EOS	Equation of State.
GA	Genetic Algorithm.
HEX	Heat Exchanger.
HRSG	Heat Recovery Steam Generator.
IRR	Internal Rate of Return
ISCC	Integrated Solar Combined Cycle.
LEC	Levelized Electricity Cost.
LFR	Linear Fresnel Reflector.
LHV	Lower Heating Value
MOO	Multi-Objective Optimization.
NPV	Net Present Value
ORC	Organic Rankine Cycle.
PDC	Parabolic Dish Collector.
PTC	Parabolic Trough Collector.
PV	Photovoltaics.
SPT	Solar Power Tower.
TES	Thermal Energy Storage.
TMY	Typical Meteorological Year

List of Symbols

Greek symbols

α	Radiative absorptivity
σ	Entropy generation, Stefan-Boltzmann constant
ε	2nd law efficiency
η	1st law efficiency
ρ	Specific mass
φ	Maintenance factor

Roman symbols

A	Area
C	Concentration ratio, cost
c	Specific cost
E	Total energy
E_x	Total exergy
e	Specific energy
e_x	Specific exergy
E_{x_d}	Exergy destruction
E_{x_f}	Flow exergy
e_{x_f}	Specific flow exergy
E_{x_q}	Exergy in the form of heat
f	Annuity factor
f_{sol}	Solar share
G_0	Nominal solar influx
g	Gravitational acceleration
H	Annual operating time
h	Specific enthalpy
I_b	Direct beam radiation
I_d	Diffuse radiation
i	Interest rate
K_t	Daily clearness index
K_0	Nominal solar influx
M	Molar mass
m	Mass

n	Lifetime expectancy
p	Pressure
p_r	Compression ratio
Q	Energy in the form of heat
R	Revenue
$\bar{R}$	Ideal gas constant
r	Mass flow ratio
s	Specific entropy
T	Temperature
U	Overall heat transfer coefficient
u	Specific internal energy
V	Volume
v	Linear velocity
v	Specific volume
W	Energy in the form of work
y	Molar fraction
Z_k	Cost of capital investment plus operation and maintenance expenses of each component
z	Elevation

Subscripts

AI	Auto ignition
b	Bottoming cycle
$b, pinch$	Pinch point at the bottoming cycle side of the HRGS
col	Collector
$comb$	Combustor
$comp$	Compressor
$cond$	Condenser
cv	Control volume
e	Out direction
ec	Economizer
eqp	Equipment
ev	Evaporator
GT	Gas turbine
f	Fuel
$f.g.$	Flue gases
$global$	Referring to the combined cycle (Brayton + Rankine)
i	In direction

inv	Investment
$O\&M$	Operation and maintenance
p	Product
rec	Receiver
reg	Regenerator
SB	Stream bifurcation
SS	Stream splitter / valve
ST	Steam turbine
s	Shell
sur	Surroundings
t	Tube
$t,pinch$	Pinch point at the topping cycle side of the HRGS
$0/amb$	Ambient conditions

Superscripts

$\dot{}$	Time derivative
ch	Chemical
th	Thermomechanical

Chapter 1

Introduction

This chapter provides an overview of the work. A brief description of the proposed model and main targets is followed by the motivations and current related state-of-the-art. Finally, the main objectives and contributions of the thesis are brought up, and its structure is defined.

A thermoeconomic model for a small-scale hybrid solar thermal power plant has been developed in a MatLab® environment to study and optimize its performance under different operating conditions. The proposed generation unit was idealized from the energy point of view in a previous master thesis [1], and it consists of a combined cycle with a solar collector field and receiver setup operating in series with a natural gas combustor as heat sources of the Brayton cycle. A seasonal analysis of the system's performance was conducted, as well as a multi-objective optimization viewing the improvement of its operation from an economical, thermodynamic and environmental point of view.

1.1 Motivation

Climate change and energy transition are among the main issues of the century. With the annual average global temperature anomaly currently at +0.99 ºC and rising, many specialists believe that critical tipping points - also known as points of no return - will be reached during the upcoming decades unless extreme measures are taken [2,3]. From the total CO_2 emitted in 2018 (36.58 billion tons), approximately 44 % was related to electricity and heat generation [4–6]. Although yearly emissions of greenhouse gases within this sector are stabilizing or decreasing in some developed nations, the global trend follows the opposite path. At the same time, fossil fuel reserves are being continuously depleted which may lead to scarcity of some of these non-renewable resources in the future, especially in specific regions [7]. Transitioning towards green electricity generation solutions is crucial for the sustainability of our planet, and it must be seen as a global venture, with developed countries assuming a steering role in the process.

The electricity generation unit studied in the current work aims at being predominantly powered by the sun, with natural gas acting as a power and efficiency booster, as well as a backup during solar downtime. It is not an entirely green solution, but it might be useful for applications where 100 % solar powered systems are not feasible or convenient due to associated high costs and/or other eventual complications related to energy storage and distribution. Thus, it is presented as a practical solution for specific scenarios, and a greener alternative to traditionally exclusive fossil fuel systems. Ideally, the

system would use a biofuel and/or incorporate some form of CO_2 capture technology in order to achieve carbon-neutrality.

1.2 State of the art

1.2.1 Combined Cycle Power Plants

According to the International Energy Agency (IEA), steam turbine coal-fired power plants (single Rankine cycle) are still the most widely used plants worldwide [8]. This type of generation facilities is not only quite pollutant but also less efficient than more modern solutions. The lower cost of coal compared to other fuels, such as natural gas, is the main reason why this plants still operate. Standard units fired by coal or oil typically achieve efficiencies of 30-35 %, whereas open cycle gas turbine units (single Brayton) often boast efficiencies in the range of 35-40 %, and natural gas fired combined cycle power plants (CCPP) achieve much greater efficiencies of 50-60 %, the highest values available in the market [9]. Furthermore, the combustion of natural gas yields less pollutants per MW of heat released during combustion than any other commercially used fossil fuel due to its simpler molecular composition (mainly methane - CH_4). Last year, in its World Energy Outlook report, IEA stated that "in 2018, on a lifecycle [analysis] basis, natural gas resulted in 33 % fewer carbon dioxide (CO_2) emissions on average than coal per unit of heat used in the industry and buildings sectors, and 50 % fewer emissions than coal per unit of electricity generated. Coal-to-gas switching can therefore provide "quick wins" for global emissions reductions" [5].

Combined cycle power plants are composed of a primary (topping) and a secondary (bottoming) thermodynamic cycle that are connected and interact with each other via a heat recovery steam generator (HRSG). Typically, a Brayton cycle works as primary, and a Rankine cycle as secondary. In standard CCPPs, the heat delivered to the topping cycle comes from the combustion of fuel after the compression stage, while the entirety of the heat consumed in the Rankine cycle comes from the exhaust gases of the gas turbine. This heat exchange occurs inside the HRSG (see Fig. 1.1). The clear advantages of natural-gas-fired CCPPs over other fossil fuel power plants make this a very interesting technology, hence the expected increase in the number of operating plants in the future.

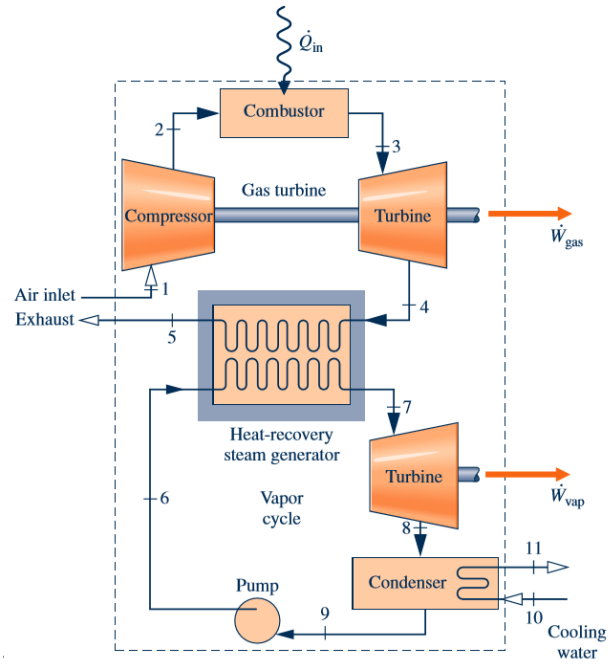

Figure 1. 1 Standard Combined Cycle Power Plant [10]

1.2.2 Concentrating solar power technologies

Planet Earth receives a constant energy flux of roughly 1.4×10^{11} MW from the sun, which means that 71 minutes of solar radiation reaching our planet is equal to the world's primary energy demand for an entire year (14 314 Mtoe in 2018, according to IEA). These values provide an idea of the potential for harnessing the sun's virtually endless energy. At the present time, solar energy represents one of the most relevant renewable energy resources, accounting for 8.9 % of the global electricity produced by renewables in 2018, which represents a share of approximately 2.3 % of the global generation [5].

Solar technologies for power generation can be divided in two categories: solar photovoltaic (PV) and concentrating solar power (CSP). Historically, the investment in PV systems has been far greater than that of CSP, mainly because this type of technology allows for the direct conversion of solar radiation into electricity, while concentrating solar systems convert solar radiation into heat that will be used to generate power. As a result, PV technologies are more mature and therefore the correspondent levelized electricity cost (LEC) is currently lower, with a global average of 0.068 USD/kWh versus 0.182 USD/kWh for CSP in 2019 [11]. According to IEA, the global electricity generation of solar renewables was 604 TWh in 2018, out of which only 12 TWh (roughly 2 %) account for CSP systems. However, CSP technologies offer some advantages such as a greater energy storage potential (in the form of heat), making it a more dispatchable option, and the possibility for direct integration in an operational power cycle such as conventional steam turbine power plants, mitigating construction costs. The relative cost of thermal energy storage (TES) technologies compatible with CSP is much lower comparing to that of electricity storage technologies compatible with PV [12]**.** For these and other reasons, there is a linear growing trend for CSP (8 %), with many large projects currently in operation or under construction (see figure 1.2), however at a lower pace than PV, which is growing at an exponential rete (38 %) [13].

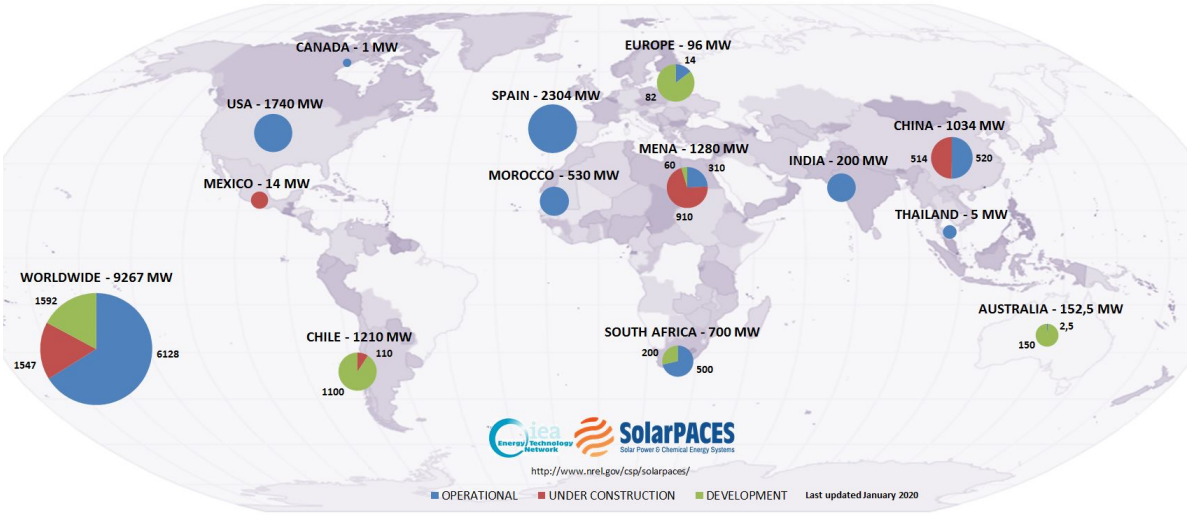

Figure 1. 2 Concentrated Solar Power projects around the World [14]

Concentrating solar power technologies use a set of collectors and/or lenses to reflect incoming solar radiation towards a receiver, where it is converted into heat. This heat can then be transported by a heat transfer fluid - usually a thermal oil - for direct use, production of solar fuels, integration in a power cycle for electricity generation, etc. The solar radiation that reaches a certain surface on the Earth's crust is made of three contributions: direct beam radiation I_b, which comes directly from the sun, diffuse radiation I_d, which is the result of sunlight scattering due to clouds or atmospheric particles, and ground reflected radiation (see figure 1.3).

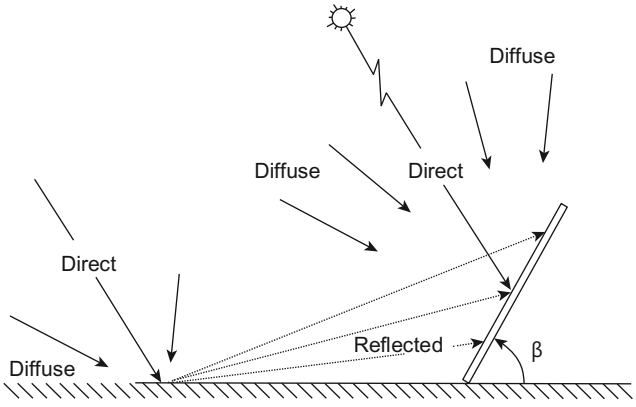

Figure 1. 3 Solar radiation incident on a surface [13]

Unlike PV technology and low temperature non-concentrating solar thermal devices, only direct solar radiation can be successfully exploited with CSP systems, thus sun-tracking mechanisms are usually implemented to achieve higher concentration ratios. A common measure of direct solar radiation for CSP modelling is the direct normal irradiance (DNI), which is the amount of direct beam radiation received per unit of area by a surface that is always perpendicular to this radiation.

1.2.2.1 Solar concentrating technologies

Solar thermal collectors can be sorted out with respect to two distinct categories: stationary collectors and sun-tracking collectors. In their work, Dabiri and Rahimi [16] present three main types of stationary collectors: flat plate collectors (FPC), stationary compound parabolic collectors (CPC), and evacuated tube collectors (ETC). From these three mechanisms, only CPCs can be considered a concentrating solar power technology, since the remaining two do not use concentrators/reflectors to redirect incoming solar radiation towards the receiver. Currently, only sun-tracking mechanisms are suitable for power generation due to their ability to achieve higher concentration ratios, operating temperatures and solar to electricity efficiencies, thus only these type of solar thermal systems will be thoroughly described in this section. Presently, there are four well estabilished sun-tracking CSP technologies with different characteristics, as summarized in table 1.1.

Table 1. 1 Comparison between different sun-tracking CSP technologies [17]

	PTC	SPT	LFR	PDC
Capacity range [MW]	10 - 250	10 - 100	5 - 250	0.01 – 1
Operating temperature range [ºC]	150 - 400	300 - 1200	150 - 400	300 - 1500
Solar concentration ratio	50 - 90	600 - 1000	35 - 170	< 3000
Solar to electricity efficiency	10 - 16	10 - 22	8 - 12	16 – 29
Relative cost	Low	High	Low	Very high
Compatible power cycle (for stand-alone configurations)	Steam Rankine Organic Rankine	Steam Rankine Brayton cycle	Steam Rankine Organic Rankine	Stirling engine Steam Rankine Brayton cycle
Commercial maturity	High	Medium	Medium	Low
Outlook for improvements	Limited	Very significant	Significant	High potential through mass production
Advantages	Long term proved reliability and durability; Modular components; Compatible with combined cycles burning oil or gas;	High efficiency; Compatible with Brayton cycle and combined cycles burning oil or gas; Modular components;	Simple structure and easy construction; Modular units; Compatible with combined cycles burning oil or gas;	High efficiency; Modular units; No need for water cooling;
Disadvantages	Relatively low efficiency; Limited operational temperature; Complex structure; Need water for cooling and cleaning;	High maintenance and equipment costs; Need water for cooling and cleaning;	Relatively low efficiency; Limited operational temperature;	Low commercial matturity; No thermal storage available;

Parabolic Trough Collectors (PTC)

Parabolic trough collectors are composed of a single long linear focus solar collector with a parabolic shape that concentrates incoming solar radiation into a long receiver tube, heating the heat transfer fluid that flows inside. Contrarily to linear Fresnel reflector (LFR) technologies, the collectors and the solar receiver are fixed to one another, thus the sun tracking mechanism drives this assembly as a whole (see fig.1.4).

This is the most mature solar thermal technology, with many worldwide applications from small scale units to major power plants. Most current applications use thermal oils as heat transfer fluids, which quickly degrade at temperatures higher than 398 °C, but the possibility of reaching working temperatures of up to 500 °C using different fluids such as molten salt or compressed gases is described in the literature ([18–20]).

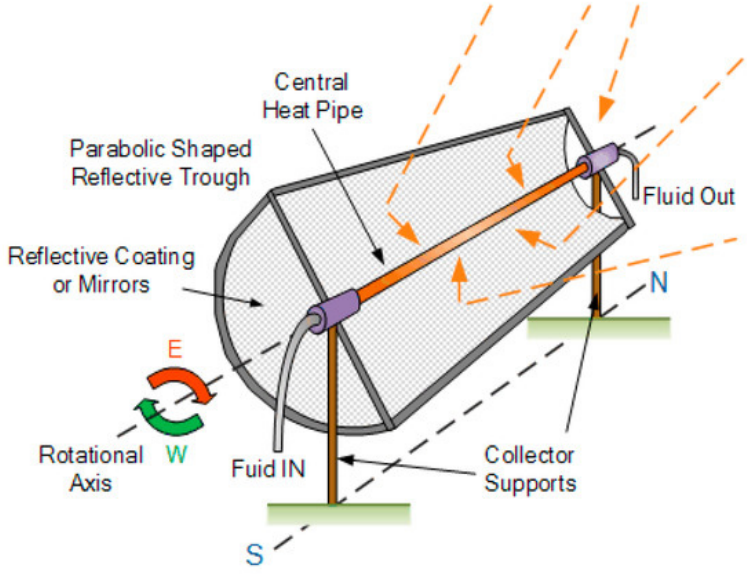

Figure 1. 4 Parabolic Trough Collectors technology [21]

Solar Power Towers (SPT)

Solar power towers consist of a set of independent heliostats that redirect incoming solar radiation towards an elevated central receiver that converts this concentrated radiation into heat (see fig.1.5). The energy is then absorbed by a heat transfer fluid and can be used for many applications such as thermal storage, process heat, and electricity generation. As an alternative, the absorbed radiation can be used to directly drive a chemical reaction, which is an interesting approach with multiple applications (*e.g.* production of solar fuels[1]).

This technology has some major advantages, such as high concentration ratios, output temperatures and generating capacity, with the main disadvantage being its quite high investment cost and limitation to large scale applications (see table 1.1). However, according to Vant-Hull [22], the manufacturing costs of such systems are expected to drop by 15 % for every doubling installed capacity during the upcoming years, which will most likely boost its competitiveness. Many solar tower power plants with installed capacities of several MWe are currently in operation in Spain, USA, India, China, Israel, etc.

[1] Synthetic chemical fuels which are processed using solar energy (*e.g.* production of hydrogen)

Figure 1. 5 Solar Power Tower technology [23]

Linear Fresnel Reflectors (LFR)

Linear Fresnel reflector solar collector systems are composed of many long linear reflectors rotating on their own independent axis that redirect and concentrate incoming solar radiation into a single parabolic receiver tube. The tube is fixed in its place and positioned in such a way that its axis is parallel to the reflector's sun-tracking axis. Each reflector is in a different position relatively to the receiver, so they all assume a different inclination at any given instant in order to successfully focus the direct solar radiation on the target (see fig.1.6). These devices simulate a reflector with a large curvature without the operation and maintenance implications associated with such a system.

LFR technologies are still less mature than parabolic troughs, but the associated costs are droping at a higher rate than that of leading PTCs mainly because the production cost of linear reflectors is tipically lower that that of parabolic reflectors. Furthermore, this type of systems offer some advantages that are exposed in table 1.1. For these reasons, many companies are currently investing in LFR, with the most relevant projects being developed by market giants such as Areva Solar, Solar Power Group, Industrial Solar and Novatec Solar [24].

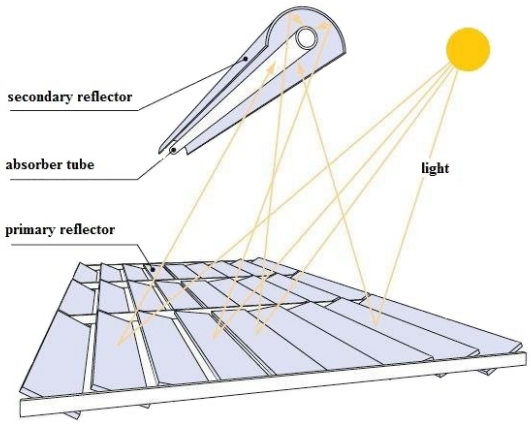

Figure 1. 6 Linear Fresnel Reflector technology [14]

Parabolic Dish Collectors (PDC)

Parabolic dish collectors are composed of a single parabolic shaped mirror that collects incoming solar radiation and reflects it towards a solar receiver, where it is converted into heat and transferred to a heat transfer fluid. The collector and receiver are coupled to each other and the setup is mounted on a bi-axial sun-tracking mechanism (see fig.1.7). Most dish collector systems have a Stirling engine and electrical generator attached to the receiver, allowing for electricity to be directly generated. However, it is also possible to provide a different purpose to the generated energy such as driving ground-based heat engines or using it as process heat [25].

This is the solar thermal technology that boasts the greater concentration ratios, operating temperatures and overall efficiencies, but unfortunately it is also the most costly (see table 1.1). For these reasons, it is most appropriate for small to medium scale independent systems.

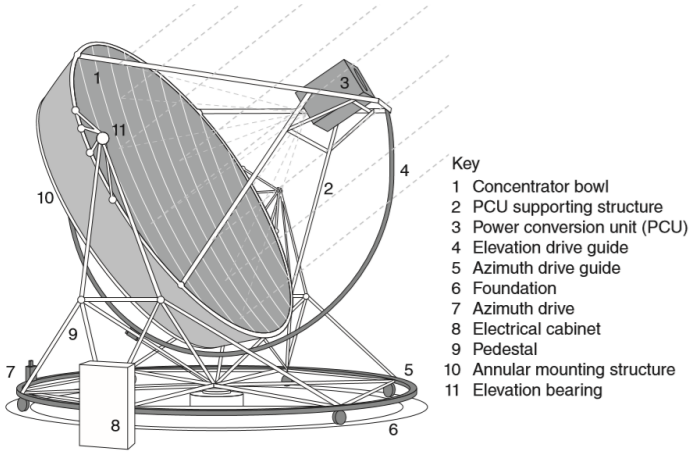

Figure 1. 7 Parabolic Dish Collectors technology [20]

1.2.2.2 Solar thermal power plants

In order to generate electricity, the solar concentration systems are directly or indirectly integrated in a power cycle. Typically, each CSP technology is more suitable to be integrated in a certain type of heat engine, depending on the temperatures achievable by the receiver, which in turn is a function of the collector´s concentration ratio. Systems with lower concentration ratios, such as PTCs or LFRs are usually incorporated in organic Rankine cycles (ORC) or regular steam Rankine cycles, while solutions with higher concentration ratios such as the SPT or PDC are suitable for integration in Stirling engines or Brayton cycles [26]. The current work proposes the integration of a parabolic trough collector (PTC), a device with a relatively low operating temperature range, in the Brayton cycle of a CCPP, which is only

possible due to the existence of a combustor that upgrades the temperature of the working fluid leaving the solar receiver before it enters the gas turbine.

Nowadays, most of the operational solar thermal power plants employ steam turbine cycles, and this trend is expected to continue in the future [12]. The main reasons behind this dominance are the lower costs due to the possibility of employing cheaper and more mature CSP technologies, high reliability, and temperature ranges compatible with existent thermal energy storage technologies. However, as previously mentioned, there are some clear advantages to single Brayton and combined cycle power plants (thermal or fossil fuel powered), such as higher efficiencies and dispatchability, *i.e.*, lower start-up times. According to Spelling [26], "There is only a single commercially available [gas turbine solar thermal power plant], a 100 kWe unit from AORA solar, which has been installed in Israel and Spain". Many R&D projects are currently studying interesting solutions.

1.2.3 Hybrid power plants

The current work focuses on hybrid solar-thermal and fossil fuel power plants, an interesting emerging concept. The clear environmental advantages of renewable solar energy coupled with the dispatchability and reliability of fossil fuels delivers a quite versatile power plant, benefiting from the best of both worlds. Continuous generation of electricity during solar downtimes is assured by the combustor, whose short start-up time allows for the system to work with minimal to non-existent thermal storage, reducing costs. Besides, the integration of these hybrids with CO_2 capture technologies such as pre/post combustion sequestration, oxy-fuel combustion or chemical looping combustion as well as the utilization of so called green fuels such as biodiesel are two quite attractive possibilities that could eventually lead to carbon-neutral systems in the future [12].

Numerous possible configurations for the hybridization of CSP and fossil fuel systems have been reviewed and studied by various authors ([12],[26–30]). In their work, Jin and Hong [31] have identified four main categories of existent hybridization approaches: fossil backup and boosting of solar thermal power plants; solar-aided coal-fired power plants; integrated solar combined cycle (ISCC) plants; and advanced systems. The current study focuses on a model that falls into the last category. According to the authors, advanced hybrid systems are those in which CSP is integrated in a gas turbine cycle, as opposing to other common layouts that couple with steam turbine cycles. It is mentioned in their work that "there are two main categories: systems that use solar heat to preheat the compressor discharge air in a gas turbine cycle; and those that use solar heat to decarbonize fossil fuel for electricity generation". The model proposed in this study fits in the first category.

1.3 Objectives and contribution

Most available thermoeconomic studies on stand-alone and hybrid solar-thermal power plants refer to large-scale steam turbine systems (centralized generation), which is explained by the dominance of

such systems in the solar-thermal market. The use of hybrid solutions for decentralized electric generation is still a poorly explored idea, mainly due to the existence of a cheaper and often more convenient alternative: solar PV. However, as previously described, there are some advantages associated with using CSP technologies for centralized and decentralized electric generation, and so studies such as this one are important to deepen the understanding on the potentials of such applications. With this in mind, the current work focused on the optimization of a hybrid solar thermal microgeneration unit idealized in a previous master thesis [1]. The following steps were taken:

- Develop a thermoeconomic model of the generation unit in a MatLab® environment, enabling the computation of the system's exergy balances and associated costs.
- Assess opportunities for the improvement of the system and simulate the model for different operating conditions.
- Conduct a multi-objective optimization in order to find the system's optimal operating conditions.

1.4 Thesis outline

This thesis is divided in 5 chapters and 2 appendix sections. The introduction (1st chapter) provides an overview of the possible applications of the proposed model as well as a description of the state of the art for CSP technologies. Chapter 2 provides a detailed characterization of the thermodynamic and numerical models used throughout the work. Initially, the theoretical concepts supporting such models are explained. Then, related previous works are addressed followed by descriptions of the model (thermodynamic model) and the algorithm employed in the analysis (numerical model). The third chapter reveals some preliminary conclusions that arose during initial simulations conducted under standard and seasonal conditions. In chapter 4, the multi-objective optimization is characterized, including a description of the considered objective functions, decision variables, performance indicators and obtained results. Finally, the fifth chapter consists on the concluding remarks, where the main conclusions of the thesis as well as some suggestions for future works are presented.

Chapter 2

Modelling

This chapter provides an overview of the model used to conduct the optimization analysis. It starts off with a description of some theoretical concepts that support it, then goes on to summarize previous related works and their respective contributions. Finally, the model itself is described, as well as the computational algorithm that was developed to conduct the numerical simulations.

2.1 Theoretical basis

2.1.1 Integral relations for a control volume

According to the Gibbs phase rule, the number of independent intensive properties (degrees of freedom, *F*) that may be arbitrarily specified in order to fully define the intensive state of a given system is equal to:

$$F = 2 + N - P \tag{2.1}$$

where *N* and *P* stand for the total number of components and phases within the system, respectively. Once this set of independent properties is determined, the values of all other properties will be fixed and may be retrieved from tables, equations of state (EOS), graphics, or computational software. The system proposed in the current work deals with pure substances only, which means that the number of components (*N*) is always equal to one. These substances can assume either single phase ($P = 1$) or phase change condition ($P = 2$), thus the number of independent intensive properties that fully define the system is either two or one, respectively.

The algorithm that was implemented in this study initially defines the thermodynamic state of the fluids in specific stages of the model and then proceeds to compute the thermodynamic states for all the remaining stages using a set of well-established equations coupled with computational software of thermodynamic properties. These equations correspond to the balances of mass, energy, entropy, and exergy within a control volume (CV), and can be expressed by the following integral relations, respectively:

$$\frac{d}{dt}\iiint \rho \, dV + \iint \rho \, \vec{v} \cdot \vec{n} \, dA = 0 \tag{2.2}$$

$$\dot{Q} - \dot{W} = \frac{d}{dt}\iiint \left(u + \frac{v^2}{2} + gz\right)\rho \, dV + \iint \left(h + \frac{v^2}{2} + gz\right)\rho \, \vec{v} \cdot \vec{n} \, dA \tag{2.3}$$

$$\iiint \left(\frac{\dot{Q}}{T}\right)_b dA + \dot{\sigma} = \frac{d}{dt}\iiint s\rho \, dV + \iint s\rho \, \vec{v} \cdot \vec{n} \, dA \tag{2.4}$$

$$\iint \dot{Q}\left(1 - \frac{T_0}{T_b}\right) dA - \dot{W} + p_0 \frac{dV}{dt} - \dot{E}_{x_d} = \frac{d}{dt}\iiint e_x \rho \, dV + \iint e_{x_f} \, \rho \, \vec{v} \cdot \vec{n} \, dA \tag{2.5}$$

where $\dot{\sigma}$, T_0, and T_b stand for the rate of entropy generation, ambient temperature, and heat exchange boundary temperature, respectively. In equation (2.5), the rate of exergy destruction $\dot{E}_{x_d}$, the specific exergy e_x and the specific flow exergy e_{x_f} are equal to:

$$\dot{E}_{x_d} = T_0 \dot{\sigma} \tag{2.6}$$

$$e_x = (u - u_0) + p_0(v - v_0) - T_0(s - s_0) + \frac{v^2}{2} + gz + e_x^{ch} \tag{2.7}$$

$$e_{x_f} = (h - h_0) - T_0(s - s_0) + \frac{v^2}{2} + gz + e_x^{ch} \tag{2.8}$$

In equations (2.7) and (2.8), the last term e_x^{ch} stands for the specific chemical exergy, while the remaining terms represent the thermomechanical exergy. For an ideal gas mixture at T_0, p_0 consisting only of substances present as gases in the environment, the chemical exergy per mol of mixture is equal to:

$$\overline{e_x^{ch}} = \bar{R}T_0 \sum_i y_i ln\left(\frac{y_i}{y_i^e}\right) \tag{2.9}$$

where y_i and y_i^e represent, respectively, the mole fraction of component i in the mixture (at T_0 and p_0) and in the environment. Assuming steady state and neglecting the contribution of potential and kinetic energy terms, the integral relations become:

$$\iint \rho \, \vec{v} \cdot \vec{n} \, dA = 0 \tag{2.10}$$

$$\dot{Q} - \dot{W} = \iint h\rho \, \vec{v} \cdot \vec{n} \, dA \tag{2.11}$$

$$\iint \left(\frac{\dot{Q}}{T}\right)_b dA + \dot{\sigma} = \iint s\rho \, \vec{v} \cdot \vec{n} \, dA \tag{2.12}$$

$$\iint \dot{Q}\left(1 - \frac{T_0}{T_b}\right) dA - \dot{W} - \dot{E}_{x_d} = \iint e_{x_f} \rho \, \vec{v} \cdot \vec{n} \, dA \tag{2.13}$$

2.1.2 Exergy costing

A simple energy and/or exergy analysis of a power system can provide a good overview of its performance under different conditions, but it does not weigh an extremely important factor: economic feasibility. As described by Bejan et al. [32], “thermoeconomics is the branch of engineering that combines exergy analysis and economic analysis to provide the system designer or operator with information not available through conventional energy analysis and economic evaluations but crucial to the design and operation of a cost-effective system”. The terms exergoeconomics, thermoeconomics or exergy costing are also used by many authors referring to this blend between thermodynamic and economic approaches.

Throughout this work, the proposed model was submitted to an exergoeconomic analysis, following the guidelines established by Bejan et al. [32] and the specific exergy costing (SPECO) method. The SPECO method is a “systematic and general methodology for defining and calculating exergetic efficiencies and exergy related costs in thermal systems” [33], that will be described later on.

2.1.3 Multi-Objective Optimization

Optimizing an energy system such as the one being studied is not a straightforward task. Usually there are countless variables that directly affect its performance, and it is virtually impossible to study all of them. Furthermore, there is more than a single way of quantifying the performance of a certain system. One may consider that an optimized design is the one that yields the highest efficiencies, or the lowest specific cost, or the lowest pollutant emissions, and so on. For this reason, a typical approach is to employ evolutionary algorithms (EAs) to conduct multi-objective optimizations (MOOs) [34]. When working with this kind of algorithms, one chooses a set of decision variables, which are considered to be critical parameters for the operation of the system, and a set of objective or fitness functions, which are supposed to quantify the performance of the system and are often conflicting goals. The result of a MOO will be a set of possible solutions that optimize the system with respect to the pre-defined objective functions, also known as Pareto-optimal or non-dominated solutions, that compose the Pareto front. By definition, it is impossible to improve the result of one of the objective functions (a.k.a. fitness value) of a Pareto-optimal solution without hurting the others, which means that it dominates all the solutions that do not belong to the Pareto front. Solution “a” is said to dominate solution “b” if “a” has a better fitness value for at least one of the fitness functions, while maintaining equal fitness values for the remaining fitness functions.

Theoretical definition: *Let us consider, without loss of generality, a multi-objective minimization problem with m decision variables (genes) and n objective functions:*

$$\begin{aligned} &\textit{Minimize} && y = f(x) = \left(f_1(x), \dots, f_n(x)\right) \\ &\textit{where} && x = (x_1, \dots, x_m) \in X \\ & && y = (y_1, \dots, y_n) \in Y \end{aligned}$$

and where x is called decision vector, X parameter space, y objective vector, and Y objective space. A decision vector $a \in X$ is said to dominate a decision vector $b \in X$ (also written as $a \prec b$) if and only if:

$$\begin{aligned} &\forall i \in \{1, \dots, n\}: && f_i(a) \leq f_i(b) \ \cap \\ &\exists j \in \{1, \dots, n\}: && f_j(a) < f_j(b) \end{aligned}$$

Adapted from [35]

The optimization analysis conducted in this work employs an algorithm denominated "*gamultiobj"* which is available in MatLab® optimization toolbox. It is a variant of the state-of-the-art NSGA-II controlled elitist genetic algorithm. Genetic algorithms (GAs) are a specific type of EA that apply the notion of natural selection idealized by Darwin. The first step of any GA is to define the initial population by generating a set of n possible design solutions for the system, which are called individuals or subjects. Different values for each decision variable are assigned to each individual (within a pre-defined range), thus two individuals will have a distinct set of decision variables or genes. Then, the performance of this population will be evaluated through the fitness functions, and a fitness rank will be assigned to each individual accordingly. If individual "a" dominates individual "b" it belongs to a higher rank. Then, the GA will evolve towards the next generation population by removing unwanted low rank individuals and employing two operators that represent natural reproduction processes: crossover and mutation. Crossover involves the selection of pairs of individuals (parents) and the generation of new individuals (offspring or children) that take genes from both parents. Higher rank individuals have a higher chance of becoming parents, so as to encourage the evolution of the algorithm towards the optimal solution(s). Mutation has the purpose of avoiding convergence towards local optima. It takes a randomly selected individual and modifies its genes in a close to arbitrary manner. The algorithm will keep on producing new generations of individuals until it converges, *i.e*., the dominant set of individuals (rank 1) does not change considerably between iterations. The program is terminated once convergence occurs, and the dominant individuals will be considered the Pareto-optimal solutions that compose the Pareto front.

2.2 Previous work

As previously mentioned, the present work proposes a more thorough analysis of one of the models idealized in a previous master thesis (see Rodrigues [1]**)**. The author of that work conducted an energy study of three distinct combined cycle power plants with one concept in common: the integration of a solar receiver in the Brayton cycle. Models number 1 and 3 are hybridized with a fossil fuel combustor

in series, while model number 2 is entirely solar powered. The analysis was conducted for several working fluids, namely: CO_2, Air, N_2, He and H_2 for the Brayton cycle, and R-245fa, R-141b, Cyclohexane, n-Pentane, and Water for the Rankine cycle. Results show that for the defined thermodynamic restrictions, the highest global cycle 1st law efficiency (20.45 %) is achieved for the 3rd model with the fluid pair CO_2 and R-141b. Due to its apparent superiority, the current work focuses on model number 3.

The starting point of Rodrigues's work [1] was an article by Dunham and Lipinski [36], and the two studies share some important concepts related with the model and numerical algorithm. The mentioned paper focuses on an energy analysis of two distinct solar stand-alone models: one that is a single Brayton cycle, and another that is a combined cycle (quite similar to model 1 of Rodrigues [1], with the only difference being the lack of a combustor). Results show that the single Brayton cycle´s maximum 1st law efficiency of 15.31 % is reached with CO_2 as the working fluid, while the combined cycle potentially achieves a global efficiency of 21.06 % with the fluid pair CO_2 and R-245fa. The different results achieved by the previously mentioned studies are mainly due to distinct model considerations, as concluded by Rodrigues [1].

In his PhD thesis, Spelling [26] conducted a thorough thermoeconomic analysis of different solar tower hybrid power plant designs. For this matter, a complex software tool named DYESOPT (Dynamic Energy System OPTimizer) was developed. This powerful integrated algorithm is capable of computing the steady-state and transient performance of a power plant, as well as the associated costs. Additionally, it incorporates an evolutionary algorithm multi-objective optimization tool that enables the identification of Pareto-optimal designs (see figure 2.1). Obtained results favor the use of combined cycle configurations with integrated thermal energy storage (TES). The incorporation of TES systems allowed for a higher annual solar share and consequently reductions on CO_2 emissions of up to 34 %, and the addition of a bottoming cycle resulted in a decrease on electricity generation cost of up to 22 % comparing to equivalent conventional power generation technologies.

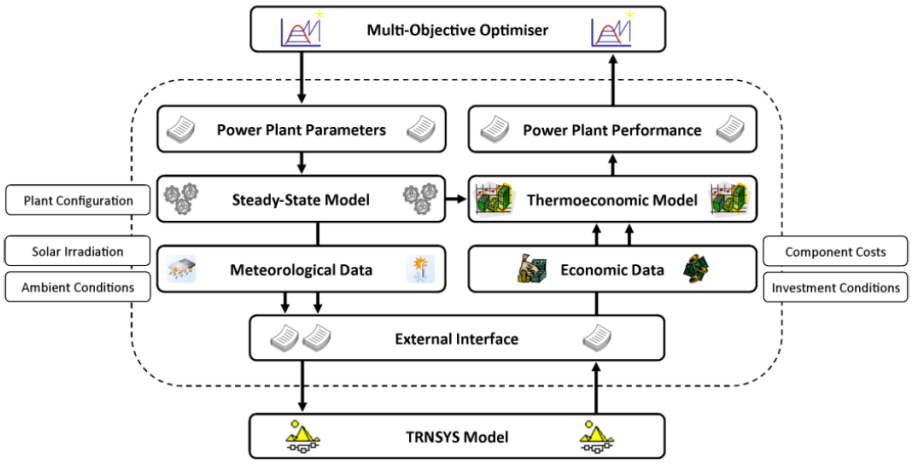

Figure 2. 1 DYESOPT algorithm diagram [26]

Baghernejad and Yaghoubi published three reports showcasing the results of exergoeconomic analyses and optimizations of two different hybrid solar-thermal power plants located in Iran. Genetic algorithms were used to conduct single [37,38] or multi-objective optimizations [39], with interesting outcomes. Similarly, Ameri et al. [40,41] analyzed the energy, exergy and economic performance of existent gas and steam turbine power plants under different conditions. The thermodynamic / costing models and analysis methods presented in these studies were used as a reference throughout the current thesis.

Pihl et al. [42] conducted a thermoeconomic optimization in order to study the feasibility of retrofitting a set of parabolic trough collectors to an existent combined cycle power plant, turning the system into an integrated solar combined cycle plant (ISCC). The idealized model proposes that part of the heat delivered to the Rankine cycle comes from the new solar unit, comprising a PTC field plus thermal energy storage tanks. Evolutionary algorithms were employed to conduct a MOO with the goal of finding the system optimal performance and costs. Results reveal that the integration of TES is not an attractive solution for the given design, and that annual solar shares are limited to 1.2 % (4 % nominal share). However, the minimum achieved costs of generated electricity are close to 0.10 €/kWh, as opposed to the 0.17–0.19 €/kWh achieved by an equivalent stand-alone solar power plant.

2.3 Description of the model

The model under study consists of a Brayton-Rankine combined cycle with a solar receiver and a combustor working in series as heat sources to the topping cycle. It proposes the addition of a regenerator after the compressor that recovers part of the heat discharged by the gas turbine (see figure 2.2). The heat exchanger (HEX) and condenser are responsible for discharging heat from the system, and water at 15 ºC and 1 bar was chosen as the cold fluid for both. The model assumes that this water is captured from a nearby river, and thus its cost is neglected. Pressure drops within the system were defined in accordance with the paper of Dunham and Lipinski [36]: 5 % inside the solar receiver, an estimation based on the work of Pye et al. [43], and 2 % for each heat exchanger as well as the combustor. Loss of pressure inside the transmission pipes is neglected. The minimum temperature and pressure are set to $T_1 = 308\ K$ and $p_1 = 1\ bar$.

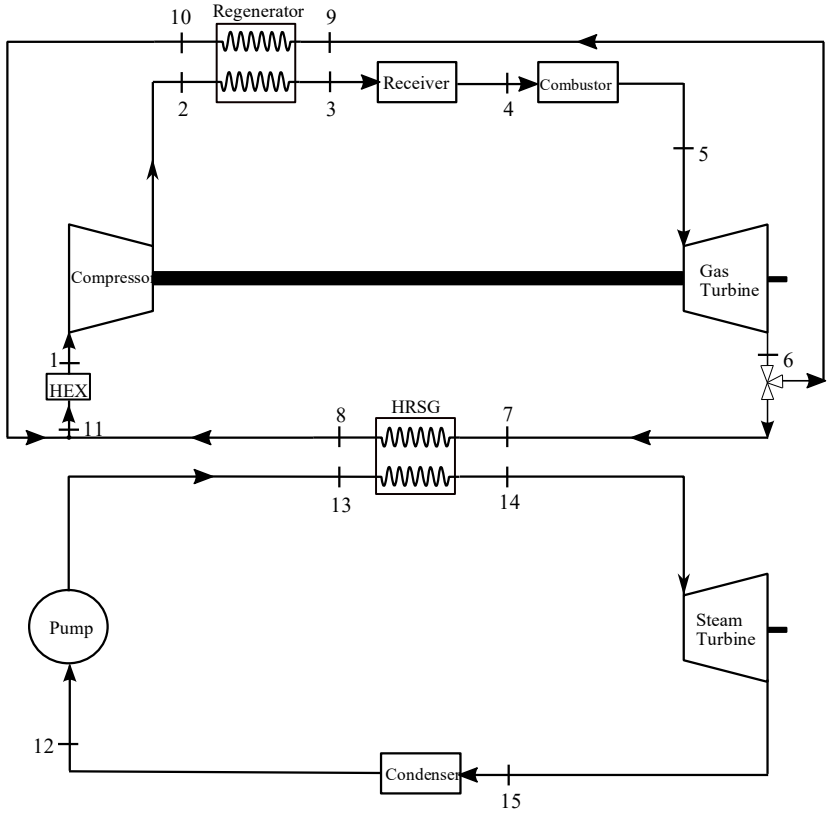

Figure 2. 2 Proposed model [1]

The main difference between the bottoming cycle idealized in this work and the one studied by Dunham and Lipinski [36] is that the heating fluid comes directly from the gas turbine outlet, reaching the HRSG with a much higher temperature. For this reason, it is possible to increase the evaporation temperature and consequently the steam turbine inlet temperature (T_{14}), boosting the thermodynamic performance of the cycle. However, this high temperature heat source may originate some thermal stability issues, thus special attention must be taken during the working fluid selection process. Cyclohexane and n-Pentane are hydrocarbons with relatively low auto ignition temperatures - approximately 533.15 K - and so these fluids were not considered for safety reasons. Previous studies

have shown that fluid degradation occurs for regular refrigerants at high temperatures. The work of Angelino and Invernizzi [44] concludes that R-245fa exhibits excellent thermal stability up to temperatures of 573 K, while Calderazzi and Paliano [45] refers that R-141b exhibits some signs of decomposition for temperatures as low as 363 K. These refrigerants employed in the works of Dunham and Lipinski [36] and Rodrigues [1] are suited for low temperature heat source applications, given their lower evaporation temperature in comparison to water, but they are not good solutions for high temperature cycles.

As previously mentioned, a computational software was used to obtain the thermodynamic properties of the fluids in specific states. This software, which will be described later on, employs equations of state (EOS) for that matter. These EOS are available for a limited range of temperatures and pressures for each substance. Table 2.1 summarizes some limitative properties of the fluids mentioned above, namely, the critical temperatures and pressures ($T_{critical}$ and $p_{critical}$), the auto-ignition temperatures (T_{AI}), and the maximum temperatures and pressures that are considered by the EOS of the given fluid ($T_{max\ EOS}$ and $p_{max\ EOS}$).

Table 2. 1 Limitative properties of bottoming cycle fluids considered in Rodrigues's work [1]

	$T_{critical}[K]$	$p_{critical}[bar]$	$T_{AI}[K]$	$T_{max\ EOS}[K]$	$p_{max\ EOS}[bar]$
R-245fa	427.01	36.5	685.15	440	2000
R-141b	477.5	42.15	823	500	4000
Cyclohexane	533.6	40.82	533.15	700	2500
n-Pentane	469.7	33.68	533.15	650	7800
Water	647.096	220.6	X	2000	10000

According to Lai [46], "(…) existing high-temperature ORC plants use mainly siloxanes and some few also toluene" as working fluids due to their good performance and thermal stability under these conditions. Many other studies refer the advantages of employing such substances as well as some specific hydrocarbons [44,47–53]. For these reasons, the current work considered the following bottoming cycle fluids: Water, Toluene (C_7H_8), Cyclopentane (C_5H_{10}), Octamethyltrisiloxane ($C_8H_{24}O_2Si_3$) and Hexamethyldisiloxane ($C_6H_{18}OSi_2$), commonly known as MDM and MM, respectively. Cyclopentane, MDM and MM exhibit the lowest maximum operating temperatures at around 575 K [51], thus this value was set as an upper limit for the simulations. Table 2.2 summarizes some limitative properties of the fluids mentioned above. The topping cycle fluids studied by Rodrigues [1] were kept in the current analysis: CO_2, air, N_2, He and H_2.

Table 2. 2 Limitative properties of employed bottoming cycle fluids

	$T_{critical}[K]$	$p_{critical}[bar]$	$T_{AI}[K]$	$T_{max\ EOS}[K]$	$p_{max\ EOS}[bar]$
Toluene	591.75	41.26	753	700	5000
Cyclopentane	511.72	45.71	634	550	2500
MDM	564.09	14.10	691	575	1300
MM	518.75	19.39	613	673	300

The criteria for selection of the pump inlet and outlet pressures (p_{12} and p_{13}) was the same as that of the works of Dunham and Lipinski [36] as well as Rodrigues [1]. At the pump inlet, the fluid temperature is fixed at 308 K, and its pressure is either the saturation or ambient pressure, whichever is greater, assuring that it is either in saturated liquid or compressed liquid phase. At the pump outlet, the fluid pressure is set to the value between p_{12} and 20 bar that yields the highest net power for the Rankine cycle, considering the imposed thermodynamic restrictions. As higher temperatures for the HRSG outlet (T_{14}) are considered, higher evaporation temperatures become feasible and p_{13} assumes higher values. The fluids MDM and MM boast a relatively low critical pressure. The current work focuses on a subcritical Rankine cycle, thus for these two cases the higher-pressure limit of the bottoming cycle (evaporation pressure) is set to 1 bar lower than the critical pressure, as suggested by Drescher and Brüggemann [52].

2.4 Description of the algorithm

The MatLab® algorithm employed in the current work is divided in two parts: the first is responsible for computing the energy streams flowing through each component and it is similar to Rodrigues's program [1]. The second part calculates the flows of exergy and the system costs, which is completely new with regard to Rodrigues's work [1]. The ability to run the simulations under different ambient conditions was also added to the program. For the MOO conducted in chapter 4, the developed algorithm and the optimization routine interact with each other as illustrated in figure 2.3.

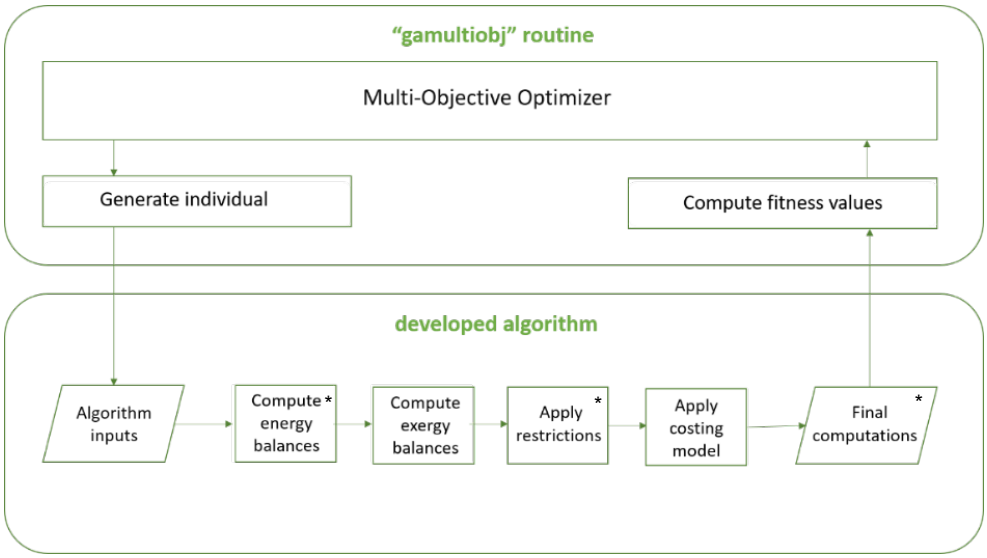

Figure 2. 3 Algorithm flowchart

*Section taken or adapted from [1]

2.4.1 Energy streams

The algorithm starts off by setting specific thermodynamic properties to key points (or states) of the system. Most of these properties are inherent to the model itself and were previously described. However, varying values were considered for some other properties, which are program inputs (see table 2.3). It then goes on calculating additional properties for each state by means of the energy and mass balances of each component (eqs. (2.10) and (2.11)) coupled with thermodynamic computational software. As previously stated, according to the Gibb's phase rule, it is possible to retrieve all thermodynamic properties of the fluids given that a set of independent properties is known. For this purpose, the program employs polynomial functions presented in the work of McBride et al. [54] for calculations referring to the topping cycle, and CoolProp for calculations referring to the bottoming cycle. CoolProp is a C++ library that computes the thermodynamic properties of a large variety of fluids employing the state-of-the-art Helmholtz-energy-explicit EOS.

Table 2. 3 MatLab® program inputs

	Input variable	Symbol
Ambient cond.	Nominal solar influx	$G_0[W/m^2]$
	Ambient temperature	$T_{amb}\ [K]$
Operating conditions	Compression ratio	$p_r = p_2/p_1$
	Mass flow ratio	$r = \dot{m}_9/\dot{m}_1$
	Gas turbine inlet temperature	$T_5[K]$
	Regenerator heat transfer area	$A_{reg}[m^2]$
	Steam turbine inlet temperature	$T_{14}\ [K]$
	Solar collector area	$A_{col}[m^2]$
	Compressor isentropic efficiency	$\eta_{comp}[\%]$
	Gas turbine isentropic efficiency	$\eta_{GT}[\%]$
	Steam turbine isentropic efficiency	$\eta_{ST}[\%]$
	Pump's isentropic efficiency	$\eta_{pump}[\%]$

Since the energy and mass balances of all the components have already been thoroughly described in a previous thesis [1], only the models for the solar receiver and HRSG are presented here.

Solar receiver

For the computation of the temperature at the solar receiver outlet (T_4), the methodology presented in the work of Dunham and Lipinski [36] was employed. The authors compute the operating temperature of the solar receiver ($T_{receiver}$) as a function of the system efficiency. As a simplification of the heat transfer process between the receiver surface and the working fluid, the outlet temperature of the solar receiver (T_4) is assumed to be 50 K lower than $T_{receiver}$.

Considering the cost and maturity of currently available solar thermal technologies, a parabolic trough collector (PTC) was chosen as the most suitable for this system, and the following receiver parameters were set accordingly:

- Absorptivity of the receiver's tubes surface, $\alpha = 0.9$
- Emissivity of the receiver's tubes surface, $\varepsilon = 0.2$
- Overall heat transfer coefficient, $U_{conv} = 10\ [W/m^2K]$
- Concentration ratio, $C = 70$

Heat Recovery Steam Generator

The HRSG cold side outlet temperature is the steam turbine inlet temperature T_{14} (see figure 2.2) and so it is initially defined by the user as an algorithm input. The HRSG cold side inlet pressure (p_{13}) is also pre-defined, and the outlet pressure (p_{14}) is calculated according to the pressure losses considerations. Since the bottoming cycle fluid is undergoing a phase change inside the HRSG, a pinch point analysis is conducted in order to compute the mass flow of stream ($\dot{m}_b$) and the HRSG hot side outlet enthalpy (h_8). The pinch point is the location where the minimum temperature difference between the hot side fluid and the cold side fluid is achieved, which is the evaporator inlet in the present case, *i.e.*, where the bottoming cycle fluid is at saturated liquid state (see fig. 2.4). This minimum temperature difference is denominated pinch point temperature difference ($\Delta T_{pinch\ point}$) and is set to 10 K based on typical practical values identified by Ganapathy [55].

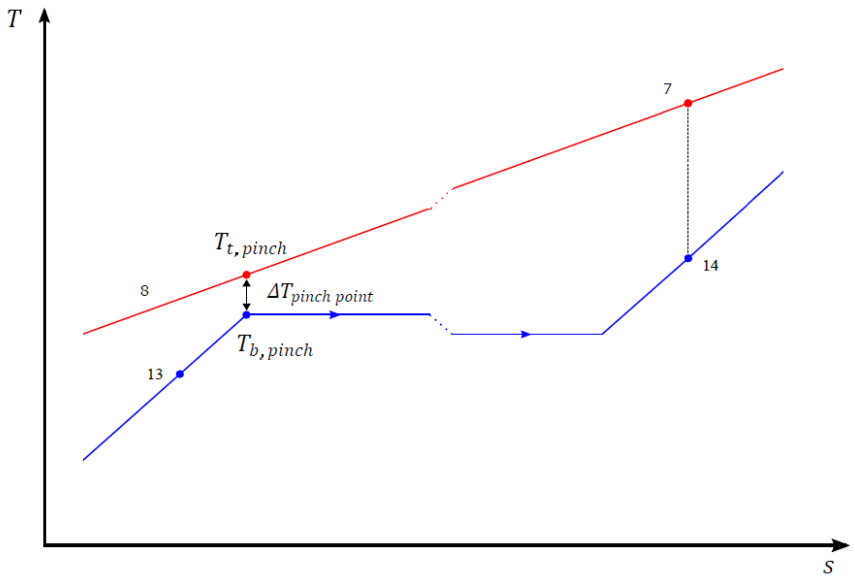

Figure 2. 4 HRSG T-s diagram

The saturation pressure is set to p_{13}, and so the temperature and enthalpy of the cold side fluid at the pinch point ($T_{b,pinch}$ and $h_{b,pinch}$) can be directly retrieved from CoolProp library. Once these properties are known, equation 2.14 is employed to calculate the temperature of the hot side fluid at the pinch point ($T_{t,pinch}$), and subsequently its enthalpy ($h_{t,pinch}$).

$$T_{t,pinch} = T_{b,pinch} + \Delta T_{pinch\ point} \tag{2.14}$$

Neglecting losses, the same amount of heat is discharged by the hot side fluid from state 7 to state 8 and absorbed by the cold side fluid from point 13 to point 14 (eq. 2.15). The same statement can be made regarding the heat discharged from state 7 until the pinch point on the hot side, and the heat absorber from the pinch point until state 14 in the cold side (eq. 2.16). Solving this system of equations, one gets the topping cycle fluid outlet enthalpy (h_8) and bottoming cycle fluid mass flow rate ($\dot{m}_b$).

$$\dot{m}_7(h_7 - h_8) = \dot{m}_b(h_{14} - h_{13}) \tag{2.15}$$

$$\dot{m}_7\left(h_7 - h_{t,pinch}\right) = \dot{m}_b\left(h_{14} - h_{b,pinch}\right) \tag{2.16}$$

2.4.2 Exergy streams and Exergy costing

Once all the thermodynamic states and energy streams are fully defined, the second part of the algorithm kicks in. The program employs equations (2.8) and (2.13) to compute the specific flow exergy at each state and the exergy destruction inside each component. The exergy balances for each component are summarized on table 2.4.

Table 2. 4 Exergy destruction by component

Component	***Exergy destruction ($\dot{E}_{x_{d,k}}$)***
Compressor	$\dot{E}_{x_{d,comp}} = T_0\dot{m}_1(s_2 - s_1)$
Regenerator	$\dot{E}_{x_{d,reg}} = T_0[\dot{m}_1(s_3 - s_2) + \dot{m}_9(s_{10} - s_9)]$
Solar Receiver	$\dot{E}_{x_{d,rec}} = T_0\dot{m}_1\left[(s_4 - s_3) + \frac{h_3 - h_4}{T_{rec}}\right]$
Combustor	$\dot{E}_{x_{d,comb}} = \dot{E}_{x_{fuel}} - \dot{E}_{x_{f.g.}} + \dot{m}_1[h_4 - h_5 - T_0(s_4 - s_5)] - \left(1 - \frac{T_0}{T_{sur}}\right)\dot{Q}_{sur}$ $\dot{Q}_{sur} = 0.01\dot{m}_f LHV$ [56] $T_{sur} = 40\ °C$
Gas Turbine	$\dot{E}_{x_{d,GT}} = T_0\dot{m}_1(s_6 - s_5)$
Stream Splitter / Valve	$\dot{E}_{x_{d,SS}} = T_0[\dot{m}_7(s_7 - s_6) + \dot{m}_9(s_9 - s_6)]$
HRSG	$\dot{E}_{x_{d,HRSG}} = T_0[\dot{m}_7(s_8 - s_7) + \dot{m}_b(s_{14} - s_{13})]$
Stream Bifurcation	$\dot{E}_{x_{d,SB}} = T_0[\dot{m}_9(s_{11} - s_{10}) + \dot{m}_7(s_{11} - s_8)]$
HEX	$\dot{E}_{x_{d,HEX}} = T_0\left[\dot{m}_1(s_1 - s_{11}) + \dot{m}_{w_{HEX}}(s_{wo} - s_{wi})_{HEX}\right]$
Steam Turbine	$\dot{E}_{x_{d,ST}} = T_0\dot{m}_b(s_{15} - s_{14})$
Condenser	$\dot{E}_{x_{d,cond}} = T_0\left[\dot{m}_b(s_{12} - s_{15}) + \dot{m}_{w_{cond}}(s_{wo} - s_{wi})_{cond}\right]$
Pump	$\dot{E}_{x_{d,pump}} = T_0\dot{m}_b(s_{13} - s_{12})$

After all the exergy streams are computed, the program applies the SPECO method to calculate the associated costs, which consists of a three steps methodology:

Step 1: Identification of exergy streams

To begin with, every single exergy stream flowing in and out of each component must be identified and quantified. Then, a decision must be made if the analysis of each stream is going to be conducted considering separate forms of exergy (mechanical, thermal, chemical, etc.) or the total exergy. The current work focuses on a system with relatively simple components, so the total exergy of each stream was studied as a whole. The proposed model is composed of 12 components and 25 streams in total: 20 for mass (15 internal streams and 5 external), 1 for heat and 4 for work (see fig. 2.5).

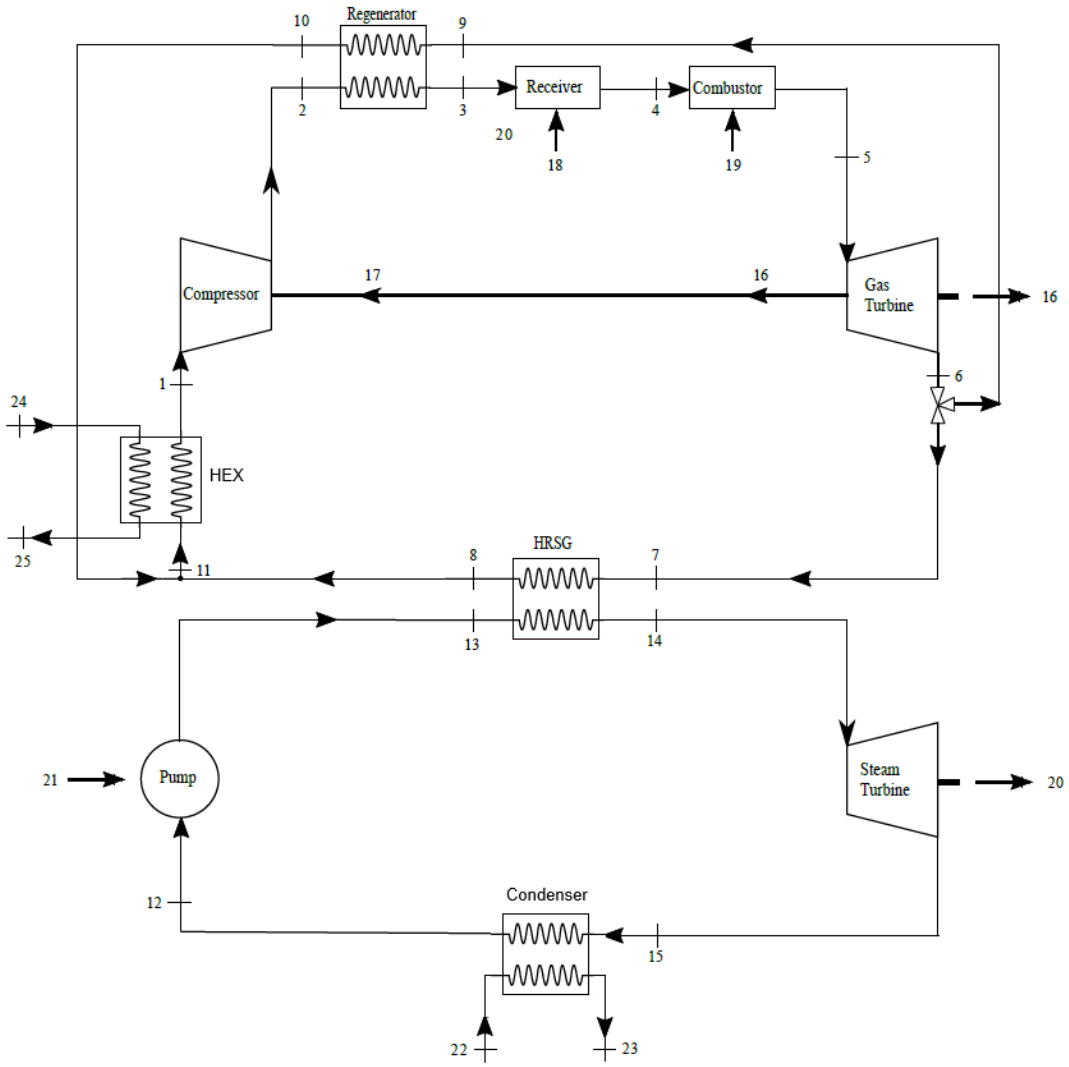

Figure 2. 5 Exergy costing model

Step 2: Definition of fuel and product

The second step is to break the exergy streams in two categories: fuel and product. The product represents the desired products yielded by each component, while the fuel represents all the resources expended to generate such product.

Table 2. 5 Fuel / Product stream definition

Component	Fuel	Product
Compressor	$\dot{W}_c$	$\dot{E}_{x_2} - \dot{E}_{x_1}$
Regenerator	$\dot{E}_{x_{f9}} - \dot{E}_{x_{f10}}$	$\dot{E}_{x_{f3}} - \dot{E}_{x_{f2}}$
Solar Receiver	$\left(1 - \frac{T_0}{T_b}\right) \cdot \dot{Q}_{receiver}$ *	$\dot{E}_{x_{f4}} - \dot{E}_{x_{f3}}$
Combustor	$\dot{E}_{x_{fuel}}$	$\dot{E}_{x_{f5}} - \dot{E}_{x_{f4}}$
Gas Turbine	$\dot{E}_{x_{f5}} - \dot{E}_{x_{f6}}$	$\dot{W}_{gt}$
HRSG	$\dot{E}_{x_{f7}} - \dot{E}_{x_{f8}}$	$\dot{E}_{x_{f14}} - \dot{E}_{x_{f13}}$
Stream Bifurcation	$\dot{E}_{x_{f8}} + \dot{E}_{x_{f10}}$	$\dot{E}_{x_{f11}}$
HEX	$\dot{E}_{x_{f11}} - \dot{E}_{x_{f1}}$	$[\dot{E}_{x_{fwo}} - \dot{E}_{x_{fwi}}]_{HEX}$
Steam Turbine	$\dot{E}_{x_{f14}} - \dot{E}_{x_{f15}}$	$\dot{W}_{st}$
Condenser	$\dot{E}_{x_{f15}} - \dot{E}_{x_{f12}}$	$[\dot{E}_{x_{fwo}} - \dot{E}_{x_{fwi}}]_{cond}$
Pump	$\dot{W}_p$	$\dot{E}_{x_{f13}} - \dot{E}_{x_{f12}}$

*$\dot{Q}_{receiver} = \dot{m}_1 \cdot (h_4 - h_3)$

Step 3: Cost equations

Finally, a specific cost rate ($\dot{C}_f$, in €/s) is assigned to each exergy stream as follows:

$$\dot{C}_f = c_f \dot{E}_{x_f} \tag{2.17}$$

where c_f represents the cost per unit of exergy (in € per kJ, for example), and $\dot{E}_{x_f}$ is the associated flow exergy, in kW. The sum of the cost rates of exergy streams entering a component plus cost rates of input exergy in the form of heat or work is equal to the sum of the cost rates of exergy streams exiting that component plus cost rates of output exergy plus the cost rate due to capital investment plus operation and maintenance of that component. Thus, one may write the following CV balance:

$$\sum_e^N \left(c_e \dot{E}_{x_{fe}}\right)_k + c_{w,k} \dot{W}_k = c_{q,k} \dot{E}_{x_{q,k}} + \sum_i^N \left(c_i \dot{E}_{x_{fi}}\right)_k + \dot{Z}_k \tag{2.18}$$

where $c_i \dot{E}_{x_{fi}}$ and $c_e \dot{E}_{x_{fe}}$ are the inlet and outlet stream cost rates, $c_{w,k} \dot{W}_k$ and $c_{q,k} \dot{E}_{x_{q,k}}$ represent the net cost rates associated with mechanical and thermal exergy transfers and $\dot{Z}_k$ is the cost rate due to capital investment plus operation and maintenance expenses of each component. This exergy costing balance is applied to each component as summarized in table 2.6 in order to find the costs per unit of exergy (c_f) at each state.

Table 2. 6 Exergy costing equations for different components

Component	Exergy costing equation(s)
Boundary conditions	
Compressor	$c_2 \dot{E}_{x_{f2}} = c_1 \dot{E}_{x_{f1}} + c_{17} \dot{W}_c + \dot{Z}_c$
Regenerator	$c_3 \dot{E}_{x_{f3}} + c_{10} \dot{E}_{x_{f10}} = c_2 \dot{E}_{x_{f2}} + c_9 \dot{E}_{x_{f9}} + \dot{Z}_{reg}$ $c_9 = c_{10}$
Solar Receiver	$c_4 \dot{E}_{x_{f4}} = c_{19} \dot{E}_{x_{f19}} + c_3 \dot{E}_{x_{f3}} + \dot{Z}_{rec}$
Combustor	$c_5 \dot{E}_{x_{f5}} = c_{18} \dot{E}_{x_{f18}} + c_4 \dot{E}_{x_{f4}} + \dot{Z}_{comb}$
Gas Turbine	$c_6 \dot{E}_{x_{f6}} + c_{16} \dot{W}_{gt} = c_5 \dot{E}_{x_{f5}} + \dot{Z}_{gt}$ $c_5 = c_6$
Stream Splitter / Valve	$c_9 \dot{E}_{x_{f9}} + c_7 \dot{E}_{x_{f7}} = c_6 \dot{E}_{x_{f6}}$ $c_9 = c_7$
HRSG	$c_{14} \dot{E}_{x_{f14}} + c_8 \dot{E}_{x_{f8}} = c_7 \dot{E}_{x_{f7}} + c_{13} \dot{E}_{x_{f13}} + \dot{Z}_{HRSG}$ $c_7 = c_8$
Stream Bifurcation	$c_{11} \dot{E}_{x_{f11}} = c_8 \dot{E}_{x_{f8}} + c_{10} \dot{E}_{x_{f10}}$
HEX	$c_1 \dot{E}_{x_{f1}} + c_{25} \dot{E}_{x_{f25}} = c_{11} \dot{E}_{x_{f11}} + c_{24} \dot{E}_{x_{f24}} + \dot{Z}_{HEX}$ $c_{24} = c_{25}$
Steam Turbine	$c_{15} \dot{E}_{x_{f15}} + c_{20} \dot{W}_{st} = c_{14} \dot{E}_{x_{f14}} + \dot{Z}_{st}$ $c_{14} = c_{15}$
Condenser	$c_{12} \dot{E}_{x_{f12}} + c_{23} \dot{E}_{x_{f23}} = c_{15} \dot{E}_{x_{f15}} + c_{22} \dot{E}_{x_{f22}} + \dot{Z}_{cond}$ $c_{22} = c_{23}$
Pump	$c_{13} \dot{E}_{x_{f13}} = c_{12} \dot{E}_{x_{f12}} + c_{21} \dot{W}_p + \dot{Z}_p$
Auxiliary equations	
$\boldsymbol{c_{19} = 0}$	
$\boldsymbol{c_{24} = 0}$	
$\boldsymbol{c_{22} = 0}$	
$\boldsymbol{c_{16} = c_{17}}$	
$\boldsymbol{c_{20} = c_{21}}$	
$\boldsymbol{c_{18} = c_f = 0.0401\ €/kWh}$	

The cost rate due to capital investment plus operation and maintenance expenses of each component ($\dot{Z}_k$) is estimated using the following equation:

$$\dot{Z}_k = \frac{C_k f \varphi}{H} \tag{2.19}$$

where φ and H are the maintenance factor and annual system operating time assumed to be 1.06 [41,57] and 4015 h/year, respectively, and f is the annuity factor,

$$f = \frac{i(1+i)^n}{(1+i)^n - 1} \tag{2.20}$$

where the interest rate (i) and lifetime of the plant (n) are assumed to be 8 % and 25 years, respectively. The annual operating time is defined according to the number of solar hours available throughout the year (see chapter 3.2). The direct capital cost of purchase of each component (C_k) was approximated by costing equations available in the literature as function of their main thermodynamic parameters (Table 2.7). Most of these equations are outdated, thus the cost index method was applied in order to account for monetary inflation and market fluctuations. The Chemical Engineering Plant Cost Index (CEPCI) was used for this matter.

Table 2. 7 Costing equations for different components

Component	Capital cost of the equipment, C_k [USD]	Ref.
Compressor	$71.1\left(\frac{\dot{m}_1}{0.9-\eta_C}\right)\left(\frac{p_2}{p_1}\right)\ln\left(\frac{p_2}{p_1}\right)$	[32]
*Regenerator **	$2143\left(A_{reg}^{0.514}\right)$	[58]
*Solar Receiver ***	$295A_{col}$	[42]
Combustor	$46.08\left(\frac{\dot{m}_1}{0.995-\frac{p_5}{p_4}}\right)(1+exp(0.018T_5-26.4))$	[32]
Gas turbine	$479.34\left(\frac{\dot{m}_1}{0.93-\eta_{GT}}\right)\ln\left(\frac{p_5}{p_6}\right)(1+exp(0.036T_5-54.4))$	[32]
HRSG	$6570\left[\left(\frac{\dot{Q}_{economizer}}{\Delta T_{lm,ec}}\right)^{0.8}+\left(\frac{\dot{Q}_{evaporator}}{\Delta T_{lm,ev}}\right)^{0.8}\right]+21276\dot{m}_b+1184.4{\dot{m}_7}^{1.2}$	[32]
*Heat exchanger **	$2143(A_{HEX}^{0.514})$	[58]
Steam Turbine	$538\cdot10^3\cdot1.9781\dot{m}_b\left(\frac{T_{14}}{p_{14}}\right)^{0.05}{p_{15}}^{-0.75}\left(\frac{\eta_{ST}}{1-\eta_{ST}}\right)^{0.9}$	[59]
Condenser	$430\cdot0.582\frac{\dot{Q}_{cond}}{\Delta T_{lm}}\Delta p_t^{-0.01}\Delta p_s^{-0.1}$	[59]
Pump	$32\cdot0.435\,{\dot{m}_b}^{0.55}\Delta P^{0.55}\left(\frac{\eta_p}{1-\eta_p}\right)^{1.05}$	[59]

* Shell and Tube (CS)-CS Heat Exchanger

** In accordance with the price of the EuroTrough models

As proposed by Zhou et al. [58], the cost of heat exchangers is typically proportional to the surface heat transfer area, which is calculated as follows:

$$A = \frac{\dot{Q}}{U \cdot \Delta T_{lm}} \tag{2.21}$$

where ΔT_{lm} and U represent the logarithmic mean temperature differences and overall heat transfer coefficients of each heat exchanger. The overall heat transfer coefficients of the regenerator and the heat exchanger were assumed to be 140 $W/(m^2K)$ and 200 $W/(m^2K)$, respectively [1].

Once the cost rates of the fluids at each state are defined, it is possible to compute important performance indicators. The work of Bejan et al. [32] describes a specially usefull one, the cost rate of exergy destruction $\dot{C}_{D,k}$, which is calculated as follows:

$$\dot{C}_{D,k} = c_{f,k}\dot{E}_{x_{D,k}} \tag{2.22}$$

where $c_{f,k}$ and $\dot{E}_{x_{D,k}}$ stand for the cost of exergy destruction and the rate of exergy destruction of component k, respectively.

2.4.3 Thermodynamic restrictions

The algorithm was developed in MatLab®, a software which is not particularly dedicated to energy systems modelling. Consequently, practical impossible solutions that violate the laws of thermodynamics are a possibility and must be controlled. For this matter, a set of restrictions were implemented to ensure feasibility of the system. Any simulation that does not meet these criteria will be discarded, and the respective results will be labeled as “NaN” (Not a Number).

For each component, the program checks the difference between the enthalpies of the inlet and outlet streams to ensure that energy streams are flowing through the components in the right direction. For example, in the regenerator, the following conditions must be met: $h_3 > h_2$ and $h_9 > h_{10}$. The algorithm also ensures that the mass flow rates of the topping and bottoming cycle fluids are a positive number: $\dot{m}_1 > 0$ and $\dot{m}_b > 0$.

As previously mentioned, the pinch point method is employed in the computation of the HRSG operating conditions. Thus, special attention must be taken to avoid temperature cross-over inside this component, and so the following conditions must be met:

$$T_8 - \Delta T_{pinch\ point} > T_{13}$$
$$T_7 - \Delta T_{pinch\ point} > T_{14}$$

The current work is highly motivated by sustainability, and so a high degree of hybridization is set as one of the optimization goals. Hence, it was defined as an algorithm restriction that the total heat produced by the combustion of fuel should be lower or equal than the amount being absorbed by the

solar receiver: $\dot{Q}_s \geq \dot{Q}_c$. It should be noted that the MOO conducted in chapter 4, which employed this restriction, assumed average ambient conditions, and for this reason it is possible for some Pareto-optimal designs to yield solar shares lower than 50 % during Winter.

As previously mentioned, the temperatures of the bottoming cycle fluids are taken from the CoolProp thermodynamic library, and so the range of acceptable values is controlled by this computational routine. However, the temperatures of the topping cycle fluids are computed from polynomial functions, and so the acceptable range of values must be defined to avoid unwanted phenomenon such as condensation happening outside the condenser. The lower acceptable temperatures for the fluids were taken from the work of Rodrigues [1] and Dunham and Lipinski [36], and correspond to the triple point temperatures for all fluids except CO_2. As Rodrigues stated in his work, "in the CO_2 case (…), because its triple point temperature is too high comparing to the others (216.6 K), its restriction is pushed down to 195 K in order to increase the span of results" [1].

Table 2. 8 Topping cycle fluid temperature limits

Topping cycle fluid	Lower temperature limit [K]
CO_2	195.00
Air	60.00
N_2	63.15
He	2.18
H_2	13.96

2.4.4 Final computations

Finally, the algorithm computes critical parameters of the global cycle such as the 1st and 2nd Thermodynamics law efficiencies, net work output, electrical power output, solar share, and total exergy destruction, as follows:

$$\eta_{global} = \eta^{1^{st}\,law} = \frac{\dot{W}_{net}}{\dot{Q}_{in}} \tag{2.23}$$

$$\varepsilon_{global} = \eta^{2^{nd}\,law} = \frac{\dot{W}_{net}}{\dot{E}_{x_{fuel}} + \dot{m}_1 \left(1 - \frac{T_{amb}}{T_{receiver}}\right)(h_4 - h_3)} \tag{2.24}$$

$$\dot{W}_{net} = \dot{W}_{topping} + \dot{W}_{bottoming} = \dot{m}_b[(h_{14} - h_{15}) - (h_{13} - h_{12})] + \dot{m}_1 \left[(h_5 - h_6) - \frac{(h_2 - h_1)}{0.9797}\right] \tag{2.25}$$

$$\dot{P}_{el} = \eta_{generator} \cdot \dot{W}_{net} = 0.96 \cdot \dot{W}_{net} \tag{2.26}$$

$$f_{sol} = \frac{\dot{Q}_{receiver}}{\dot{Q}_{receiver} + \dot{Q}_{combustor}} \tag{2.27}$$

$$\dot{E}_{x_{d,system}} = \sum \dot{E}_{x_{d,k}} \tag{2.28}$$

Chapter 3

Preliminary analysis

At an early stage of this work, a strictly thermodynamic analysis of the model was conducted using the MatLab® algorithm. The system was initially simulated for fixed ambient conditions and then for varying ambient conditions, in order to study the impact of seasonal fluctuations on its performance. The aim of this preliminary analysis is to define a reference case for comparison with the optimized case resulting from the multi-objective optimization developed in chapter 4.

3.1 Standard conditions

The thermodynamic model was applied to every fluid combination with incremental values of compression ratio, mass flow ratio and HRSG outlet temperature. These variables were restricted to the following ranges of values:

- $p_r = \frac{p_2}{p_1} = [1{,}20]$, with increments of 0.01
- $r = \frac{\dot{m}_9}{\dot{m}_1} = [0.01{,}0.99]$, with increments of 0.01
- $T_{14} = [500\ \mathrm{K}\,, 575\ \mathrm{K}]$, with increments of $25\ \mathrm{K}$

All the remaining inputs were fixed according to the work of Rodrigues [1] as follows:

- $T_5 = 825\ K$
- $A_{reg} = 6\ m^2$
- $A_{col} = 200\ m^2$
- $\eta_{comp} = 79.6\ \%$
- $\eta_{GT} = 85.8\ \%$
- $\eta_{ST} = 68.0\ \%$
- $\eta_{pump} = 60.0\%$

The standard ambient conditions proposed by Dunham and Lipinski [36] ($G_0 = 1000\ W/m^2$ and $T_{amb} = 303\ K$) were used for this initial simulation. For each fluid combination, mass flow ratio (r) and HRSG outlet temperature the model was simulated with incrementing compression ratios, retrieving values for the global efficiencies (1st and 2nd law), net work output and exergy destruction rate of the system with respect to each incrementation. For each value of T_{14} simulated, the obtained results reveal that the optimum fluid combination, *i.e.*, the one that yields the highest peak efficiencies and net work output, varies with the mass flow ratio. For the initial simulations (T_{14} equal to 500 K and 525 K), CO_2 and Cyclopentane boast optimal performance for lower values of r, followed by H_2 and Cyclopentane at intermediate values and finally CO_2 and Water for higher values. However, for higher values of T_{14} (550 K and 575 K), the fluid pair CO_2 and Cyclopentane is superior for virtually all the simulated mass flow ratios. Figures 3.1-3.4 illustrate the behaviour of the peak efficiencies and net work outputs (maximum values achieved for the considered range of compression ratios) of these three fluid pairs with r.

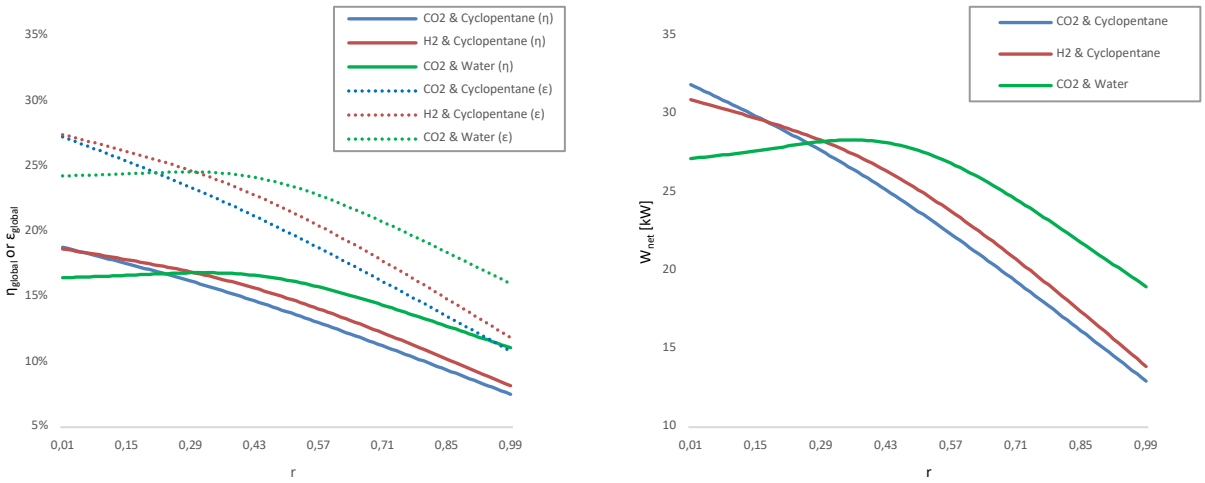

Figure 3. 1 System 1st and 2nd law peak efficiencies and net work outputs for $T_{14} = 500$ K

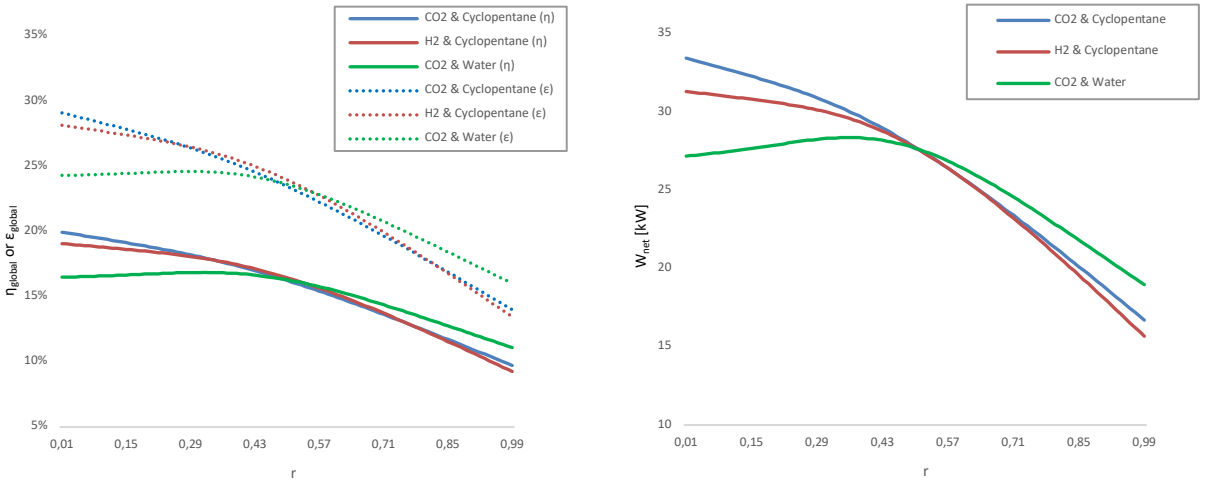

Figure 3. 2 System 1st and 2nd law peak efficiencies and net work outputs for $T_{14} = 525$ K

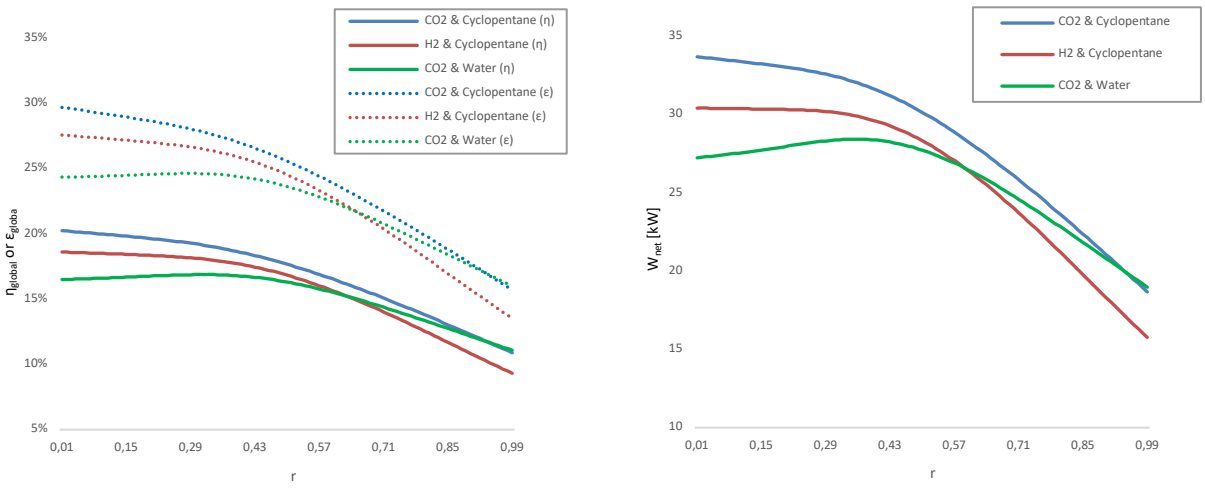

Figure 3. 3 System 1st and 2nd law peak efficiencies and net work outputs for $T_{14} = 550$ K

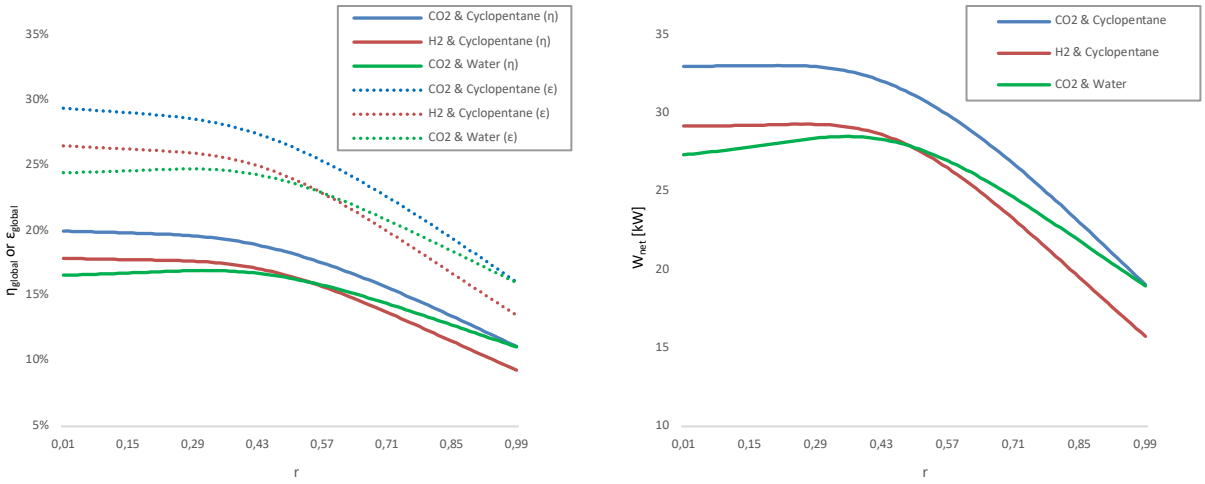

Figure 3. 4 System 1st and 2nd law peak efficiencies and net work outputs for $T_{14} = 575$ K

It is notable that, independently of the values assumed for T_{14}, the best overall performance is achieved by the pair CO_2 and Cyclopentane at $r = 0.01$, which suggests that for the specified ambient and operating conditions the regenerator should not be in operation. The system thermodynamic performance is maximized if the entirety of the gas turbine outlet gases is directed towards the HRSG, and none is, therefore, directed towards the regenerator.

As the mass flow ratio (r) increases, so does the regenerator outlet temperature and enthalpy, T_3 and h_3, due to more heat being transferred within this component. However, the amount of heat being absorbed by the solar receiver, $\dot{Q}_s = G_0 \cdot A_{col} \cdot \eta_{receiver}$, as well as its outlet temperature and enthalpy, T_4 and h_4, remain unchanged for the same ambient conditions. As a result, the mass flow rate of the topping fluid, which is calculated as $\dot{m}_1 = \dot{Q}_s/(h_4 - h_3)$, increases with r, which ultimately leads to an increase on the Brayton cycle net work output ($\dot{W}_{topping}$), but at the same time an increase on the amount of heat being delivered by the combustor, $\dot{Q}_c = \dot{m}_1(h_5 - h_4)$, which has to keep up with the greater mass

flow rate. At the same time, greater values of r lead to lesser mass flow rates for the fluids flowing through the HRSG, $\dot{m}_7$ and $\dot{m}_b$, resulting in a reduction of the Rankine cycle work output ($\dot{W}_{bottoming}$). For the specified conditions, these relations, which are summarized on figure 3.5, ultimately result in a reduction of the global efficiencies and net work output for increasing values of r. Further analysis will be conducted in the following chapters to confirm if this is indeed a better solution for the system under more realistic conditions.

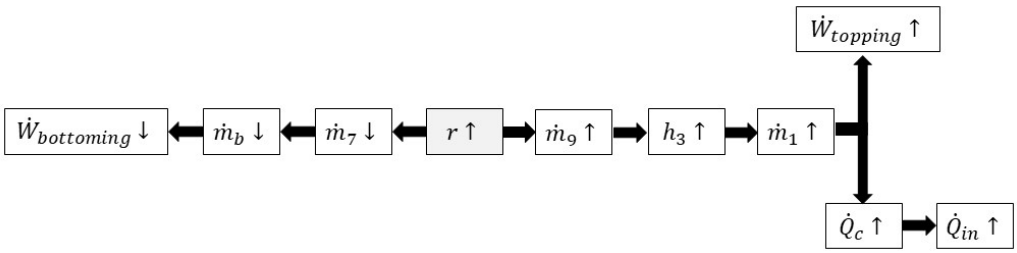

Figure 3. 5 Representation of the relations between system parameters

Increasing the HRSG outlet temperature results in a higher enthalpy drop inside the steam turbine, but also in a lower mass stream flowing through the bottoming cycle ($\dot{m}_b$). The consequence is that for the same p_r, a higher T_{14} results in a worse thermodynamic performance. However, increasing T_{14} also broadens the range of acceptable results, as lower compression ratios are possible without temperature crossover occurring inside the HRSG, allowing the system to achieve better performances. This ultimately results in a growing trend of the system overall peak efficiencies and work output from $T_{14} = 500\ \text{K}$ to $550\ \text{K}$ that reaches its maximum at this last value.

Figures 3.6-3.9 show the evolution of the system efficiencies and net work output when employing the three fluid combinations mentioned above for the different values of p_r considered and for $r = 0.01$. Only acceptable solutions, *i.e.*, those that meet the pre-defined thermodynamic criteria/restrictions, are presented.

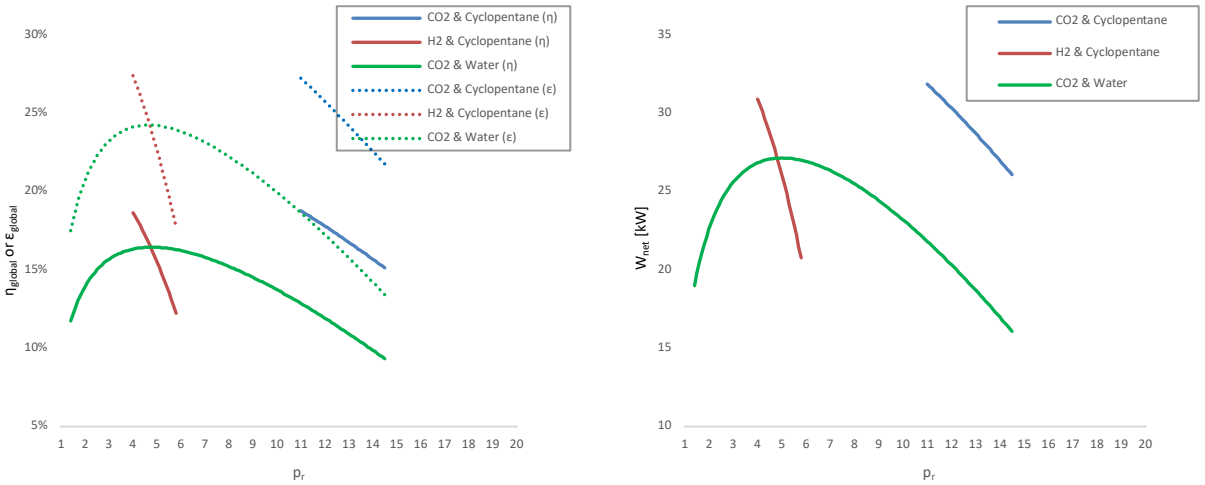

Figure 3. 6 System 1st and 2nd law efficiencies and net work output for $r = 0.01$ and $T_{14} = 500\ \text{K}$

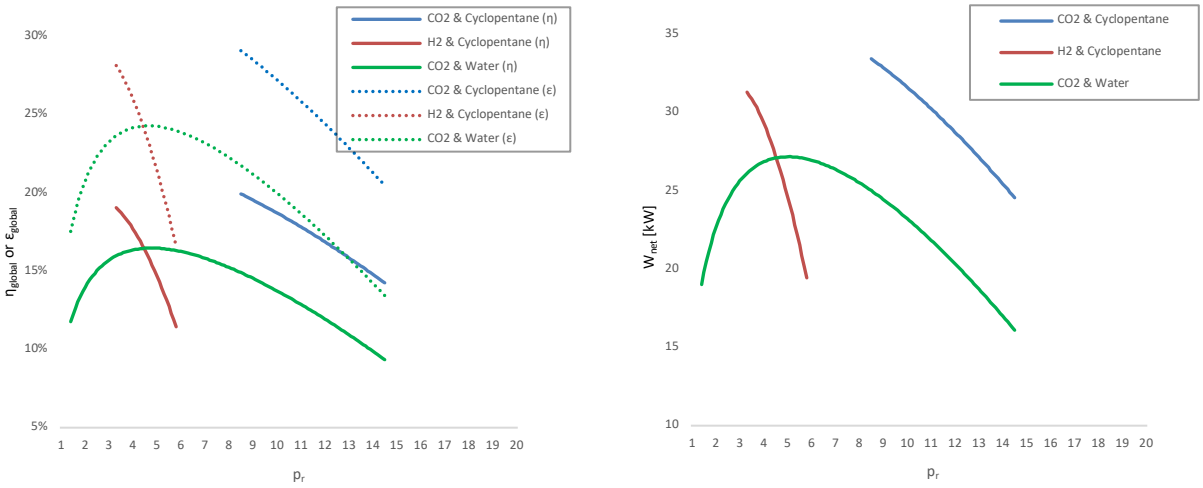

Figure 3. 7 System 1st and 2nd law efficiencies and net work output for $r = 0.01$ and $T_{14} = 525$ K

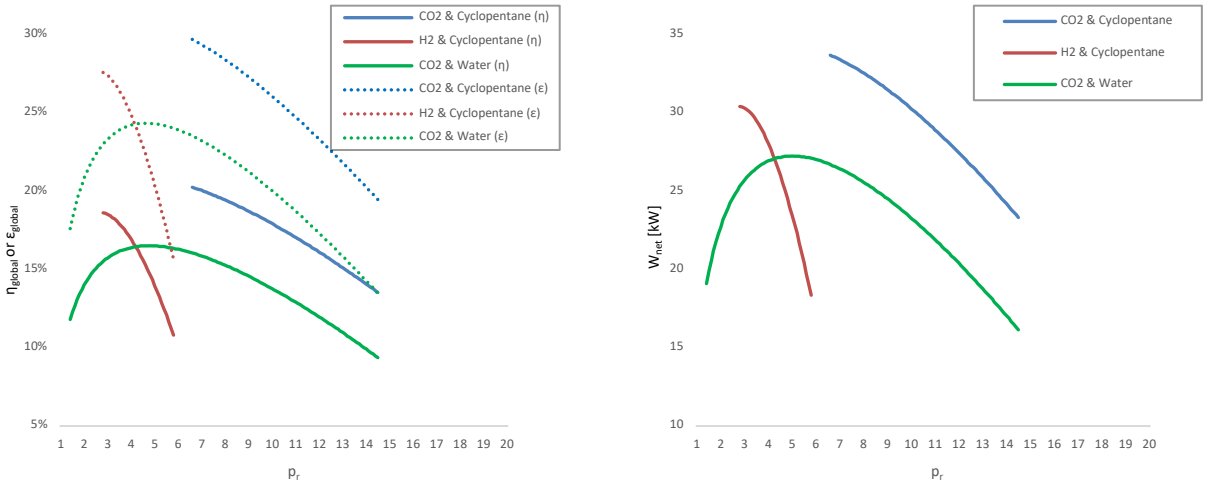

Figure 3. 8 System 1st and 2nd law efficiencies and net work output for $r = 0.01$ and $T_{14} = 550$ K

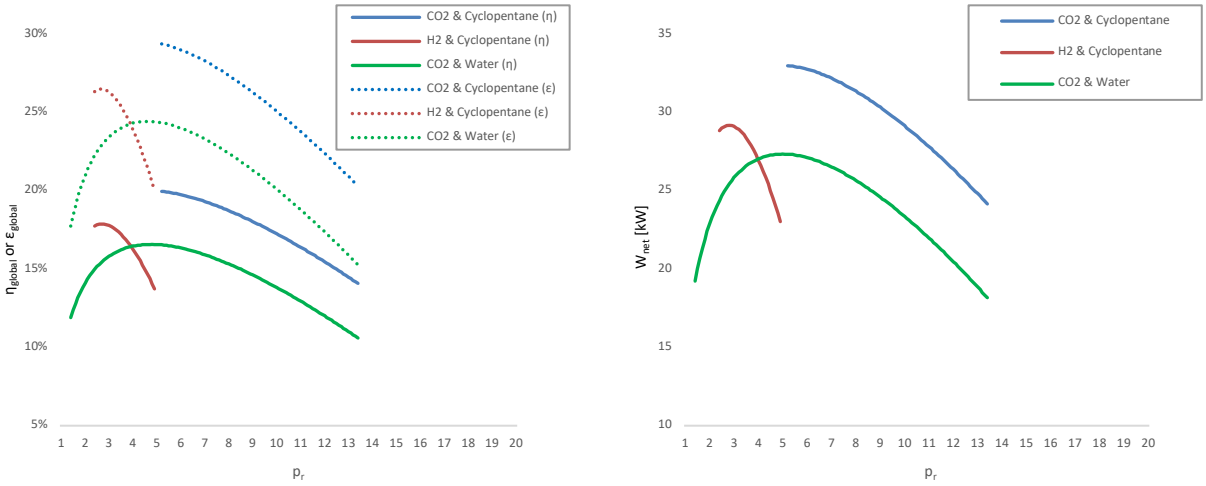

Figure 3. 9 System 1st and 2nd law efficiencies and net work output for r = 0.01 and T_{14} = 575 K

The simulations conducted in this chapter expose CO_2 and Cyclopentane as the optimal fluid combination overall for $T_{14} = 550\ \mathrm{K}$ and $r = 0.01$. Thus, this fluid pair and operating conditions will be used for the seasonal analysis that follows. As seen in fig. 3.8, the peak efficiencies and work output are reached for $p_r = 6.6$, and assume the values presented on tables 3.1 and 3.2. More detailed data regarding the thermodynamic state of the fluids at each point can be found on Appendix A.

Table 3. 1 Thermodynamic performance of the system

p_r	6.6
r	0.01
T_{14} $[K]$	550
η_{global} [%]	20.26
ε_{global} [%]	29.17
$\dot{W}_{net}$ [kW]	35.13
$\dot{E}_{x_{d,system}}$ [kW]	80.52
$\dot{Q}_{input}$ [kW]	173.44
f_{sol} [%]	86.15

Table 3. 2 Exergy destruction by component

Component (k)	$\dot{E}_{x_{d,k}}$ [kW]	$\frac{\dot{E}_{x_{d,k}}}{\dot{E}_{x_{d,system}}}$ [%]
Compressor	10.46	12.99
Regenerator	0.61	0.76
Solar Receiver	18.99	23.58
Combustor	9.88	12.27
Gas Turbine	7.63	9.48
HRSG	9.30	0.00
Stream Bifurcation	0.14	11.55
HEX	1.02	0.17
Steam Turbine	6.43	1.27
Condenser	15.73	7.99
Pump	0.32	19.54
Total	80.52	100

3.2 Seasonal conditions

The ambient temperature and direct normal irradiance of a specific geographic location change considerably throughout the day and year. A simplifying seasonal analysis of the thermodynamic model was conducted in order to quantify the effects of such fluctuations on the system. The chosen location for this generation unit was Évora, Portugal, given the high insolation values of this southern region. Daily profiles where taken from a typical meteorological year (TMY) data file, available in EnergyPlus™ database. According to the file, the yearly DNI of the area is close to 1600 $\mathrm{kWh/m^2 \cdot yr}$, which is a significant value even though it cannot compete with standard locations for large-scale CSP power plants such as the Sahara desert where values of over 2500 $\mathrm{kWh/m^2 \cdot yr}$ are common.

The seasonal analysis presented in this work considers one representative day for each season: 26th of January (Winter), 26th of March (Spring), 12th of July (Summer) and 5th of October (Fall). For the sake of coherence, four days with similar daily clearness indexes (K_t) were chosen, and an effort was made to meet the clear sky day condition ($0.7 < K_t < 0.9$) [60] when possible. This index is defined as the ratio between the daily radiation and the daily extra-terrestrial radiation, and so it compares the amount of solar radiation that actually reaches an horizontal plane located on Earth crust, H , with the amount that reaches an horizontal plane outside the atmosphere, H_0 ($K_t = H/H_0$).

Table 3. 3 Daily profile of the representative days in Évora (38.57º N, 7.91º W)

Season	Summer		Fall		Winter		Spring	
Representative day	12/07		05/10		26/01		26/03	
Kt	0.71		0.69		0.65		0.70	
Time	T_{amb} [ºC]	DNI [W/m²]	T_{amb} [ºC]	DNI [W/m²]	T_{amb} [ºC]	DNI [W/m²]	T_{amb} [ºC]	DNI [W/m²]
1:00	17.9	0	19.3	0	6.4	0	9.8	0
2:00	17.2	0	18.7	0	6	0	9.8	0
3:00	16.5	0	18.2	0	5.6	0	9.8	0
4:00	15.9	0	17.5	0	5.2	0	8.9	0
5:00	15.4	0	16.9	0	4.7	0	8	0
6:00	14.8	0	16.2	0	4.3	0	7.1	0
7:00	16.7	194	16.7	0	4.3	0	7.9	0
8:00	18.7	431	17.1	265	4.4	0	8.8	217
9:00	20.6	670	17.6	516	4.4	171	9.6	496
10:00	23.1	773	19.7	715	6	459	10.8	686
11:00	25.7	828	21.9	819	7.6	657	12.1	795
12:00	28.2	871	24	870	9.2	810	13.3	902
13:00	29.7	883	24.8	880	9.9	849	14	909
14:00	31.3	896	25.6	872	10.7	841	14.7	884
15:00	32.8	859	26.4	840	11.4	793	15.4	624
16:00	33.1	822	25.5	720	10.7	648	15.3	760
17:00	33.3	725	24.5	499	10.1	338	15.3	605
18:00	33.6	530	23.6	104	9.4	0	15.2	280
19:00	30.7	256	21.7	0	8.5	0	14.1	0
20:00	27.7	0	19.7	0	7.7	0	13.1	0
21:00	24.8	0	17.8	0	6.8	0	12	0
22:00	22.9	0	16.3	0	6.9	0	10.9	0
23:00	21.1	0	14.7	0	6.9	0	9.9	0
24:00	19.2	0	13.2	0	7	0	8.8	0
Average (sun hours only)	27.50	672.15	22.79	645.45	8.89	618.44	13.14	650.73
No. sun hours	13		11		9		11	

As a simplification, it was assumed that the solar collectors are always normal to the sun rays, thus the incident nominal solar influx (G_0) is equal to the DNI. The daily average values of the DNI and ambient temperature for each of the representative days were introduced in the MatLab® program, and the model was simulated once again. As previously stated, this simulation assumed the fluid pair CO_2 and Cyclopentane and $T_{14} = 550$ K, as well as the compression and mass flow ratios of interest. All the remaining input variables were kept unchanged. Results from these simulations were used as a reference to compare with the optimal designs that came from the MOO conducted in chapter 4.

The first conclusion directly arises from the TMY weather file, which reveals that the initially assumed values for the solar flux and ambient temperature, $G_0 = 1000\ \mathrm{W/m^2}$ and $T_{amb} = 303$ K, are quite optimistic and not representative of the considered location. In reality, the daily average solar radiation values in Évora fluctuate from 500 to 700 W/m^2 throughout the year, which strongly influences the performance of the system. Two major consequences arise from the consideration of real values for G_0 and T_{amb}: the optimal mass flow ratio (r) now assumes two different values depending on the optimization objective – efficiency or net work output, while the optimal compression ratio remains unchanged (see table 3.4); and the solar share (f_{sol}) is considerably reduced, from around 86 % for standard conditions to 50 – 60 %, depending on the season and optimization goal.

Table 3. 4 Thermodynamic performance of the system for each seasonal representative day, T_{14}=550 K

Season	**Summer**		**Fall**		**Winter**		**Spring**	
Maximization objective	**Max. η and ε**	**Max. $\dot{W}_{net}$**	**Max. η and ε**	**Max. $\dot{W}_{net}$**	**Max. η and ε**	**Max. $\dot{W}_{net}$**	**Max. η and ε**	**Max. $\dot{W}_{net}$**
p_r	6.6	6.6	6.6	6.6	6.6	6.6	6.6	6.6
r	0.01	0.33	0.01	0.34	0.01	0.36	0.01	0.34
η_{global} [%]	20.26	19.08	20.26	19.00	20.26	18.81	20.26	18.98
ε_{global} [%]	26.22	23.85	25.70	23.21	24.71	22.00	25.22	22.75
$\dot{W}_{net}$ [kW]	31.32	32.59	31.74	33.54	33.80	36.82	33.30	35.49
$\dot{E}_{x_{d,system}}$[kW]	81.15	96.61	82.54	100.76	86.68	111.33	84.77	104.71
$\dot{Q}_{input}$ [kW] *	154.62	170.83	156.68	176.48	166.85	195.67	164.37	186.98
f_{sol} [%]	62.95 %	56.97 %	59.55 %	52.87 %	53.70 %	45.79 %	57.51 %	50.56 %

*$\dot{Q}_{input} = \dot{Q}_{rec} + \dot{Q}_{comb}$

From the analysis of table 3.4 one can infer that if the objective is to maximize the system efficiencies the optimal conditions are always $r = 0.01$ and $p_r = 6.6$, but if the goal is to maximize the system work output, a common practice for small systems with size limitation, the mass flow ratio r assumes values between 0.33 and 0.36, depending on the season. There is also the possibility of designing a system with variable mass flow ratio that can adapt to different scenarios, maximizing $\dot{W}_{\mathrm{net}}$ during peak demand periods, for example. Thus, the system could eventually benefit from the possibility to control r. More detailed data regarding the thermodynamic state of the fluids at each point for each of the representative days can be found in Appendix A.

The algorithm was developed in such a way that the 1st law efficiency is directly constrained by the user-defined gas turbine inlet temperature (T_5) and compression ratio (p_r), so in the colder months

when the gas temperature at the receiver outlet is lower, the system will compensate by burning more fuel in order to achieve the desired T_5. This is the reason why η_{global} does not change seasonally. On the other hand, exergetic efficiency peaks during Summer due to a higher ambient temperature, while the net power output peaks during Winter. The behaviour of this last property is also related to the functioning of the algorithm: a colder day results in a lower solar receiver outlet temperature (T_4), which in turn results in higher mass flow ratios for the topping and bottoming cycle fluids and consequently higher power outputs. The amount of exergy destroyed in each component varies throughout the year, especially in the combustor and solar receiver (see tables 3.5 and 3.6 and figures 3.10 and 3.11). This is because the solar share is also changing considerably. As previously explained, the lower DNI and T_{amb} values during the cold months result in a reduction of the solar energy absorbed by the receiver and a greater need for heat generation in the combustor. As expected, a similar trend is followed by the exergy destruction inside these components, with the solar receiver's and combustor's exergy destruction peaking during the Summer and Winter, respectively. Furthermore, the total rate of exergy destruction and exergetic efficiency of the system reach their maximum and minimum during Winter, respectively.

Table 3. 5 Exergy destruction by component (maximum efficiency scenario)

Season	**Summer**		**Fall**		**Winter**		**Spring**	
Component (k)	$\dot{E}_{x_{d,k}}$ **[kW]**	$\frac{\dot{E}_{x_{d,k}}}{\dot{E}_{x_{d,system}}}$ **[%]**	$\dot{E}_{x_{d,k}}$ **[kW]**	$\frac{\dot{E}_{x_{d,k}}}{\dot{E}_{x_{d,system}}}$ **[%]**	$\dot{E}_{x_{d,k}}$ **[kW]**	$\frac{\dot{E}_{x_{d,k}}}{\dot{E}_{x_{d,system}}}$ **[%]**	$\dot{E}_{x_{d,k}}$ **[kW]**	$\frac{\dot{E}_{x_{d,k}}}{\dot{E}_{x_{d,system}}}$ **[%]**
Compressor	9.25	11.40	9.23	11.18	9.36	10.80	9.36	11.05
Regenerator	0.54	0.67	0.54	0.66	0.55	0.63	0.55	0.65
Solar Receiver	11.80	14.54	11.06	13.40	10.01	11.55	10.80	12.74
Combustor	23.66	29.16	25.90	31.39	30.42	35.10	27.72	32.70
Gas Turbine	6.75	8.32	6.73	8.16	6.83	7.89	6.83	8.06
HRSG	8.22	10.13	8.20	9.94	8.33	9.60	8.33	9.82
Stream Bifurcation	0.12	0.15	0.12	0.15	0.13	0.15	0.13	0.15
HEX	0.91	1.12	0.90	1.09	0.92	1.06	0.92	1.08
Steam Turbine	5.69	7.01	5.68	6.88	5.76	6.65	5.76	6.80
Condenser	13.92	17.15	13.88	16.82	14.09	16.25	14.09	16.62
Pump	0.28	0.35	0.28	0.34	0.29	0.33	0.29	0.34
Total	81.15	100	82.54	100	86.68	100	84.77	100

Table 3. 6 Exergy destruction by component (maximum work output scenario)

Season	Summer		Fall		Winter		Spring	
Component (k)	$\dot{E}_{x_{d,k}}$ [kW]	$\frac{\dot{E}_{x_{d,k}}}{\dot{E}_{x_{d,system}}}$ [%]	$\dot{E}_{x_{d,k}}$ [kW]	$\frac{\dot{E}_{x_{d,k}}}{\dot{E}_{x_{d,system}}}$ [%]	$\dot{E}_{x_{d,k}}$ [kW]	$\frac{\dot{E}_{x_{d,k}}}{\dot{E}_{x_{d,system}}}$ [%]	$\dot{E}_{x_{d,k}}$ [kW]	$\frac{\dot{E}_{x_{d,k}}}{\dot{E}_{x_{d,system}}}$ [%]
Compressor	11.87	12.28	12.11	12.02	12.86	11.55	12.39	11.84
Regenerator	2.40	2.48	2.49	2.47	2.75	2.47	2.56	2.45
Solar Receiver	10.01	10.36	9.36	9.29	8.47	7.61	9.16	8.75
Combustor	30.36	31.42	34.00	33.75	41.77	37.52	36.70	35.05
Gas Turbine	8.66	8.97	8.84	8.77	9.38	8.43	9.05	8.64
HRSG	7.14	7.39	7.18	7.12	7.39	6.64	7.35	7.02
Stream Bifurcation	3.34	3.46	3.50	3.47	3.95	3.55	3.62	3.46
HEX	5.56	5.76	5.92	5.87	6.89	6.19	6.11	5.83
Steam Turbine	4.94	5.12	4.97	4.93	5.11	4.59	5.08	4.86
Condenser	12.08	12.51	12.15	12.05	12.50	11.23	12.43	11.87
Pump	0.25	0.25	0.25	0.24	0.25	0.23	0.25	0.24
Total	96.61	100	100.76	100	111.33	100	104.71	100

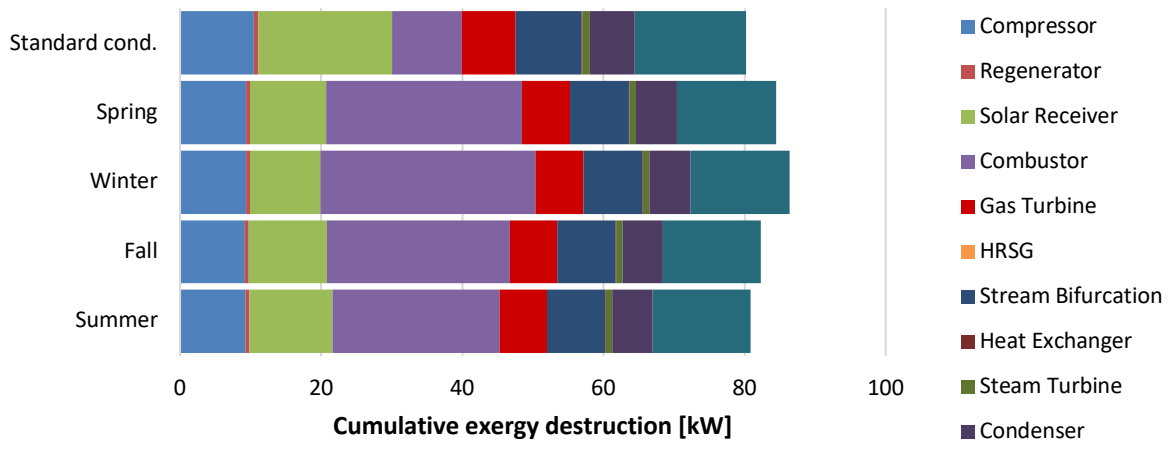

Figure 3. 10 Exergy destruction by component, maximum efficiency scenario

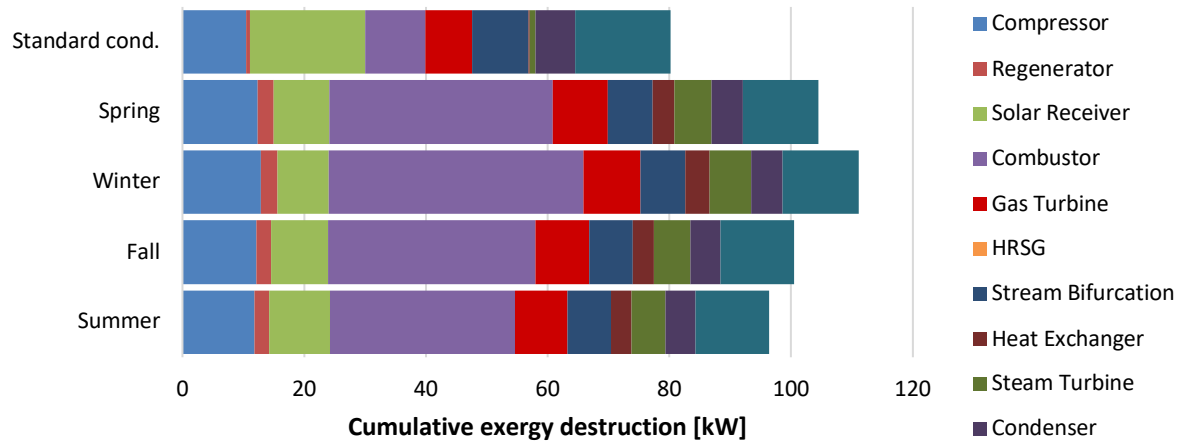

Figure 3. 11 Exergy destruction by component, maximum work output scenario

Chapter 4

Multi-Objective Optimization

Results presented in chapter 3 reveal that the proposed model achieves higher efficiencies if the regenerator is removed from the system, while yielding a lower work output. In this chapter, a multi-objective optimization analysis is conducted focusing on two goals: understand in which scenarios and conditions does the model without regenerator outperform the model with regenerator; interpret the resultant set of Pareto-optimal solutions and chose a set of optimal designs to compare with the base design. Therefore, the MOO considers both models (with and without regenerator).

4.1 Objective functions

The main targets of the current optimization analysis are to maximize the system thermodynamic performance, increasing revenue, while minimizing associated costs. Therefore, total investment cost (C_{inv}) minimization and net present value (NPV) maximization were chosen as objective functions.

4.1.1 Total investment cost

The total initial monetary investment was computed as the sum of three contributions: equipment, land, and civil engineering related costs. This approach was based on the methodology used by Pihl et al. [42].

$$C_{inv} = C_{eqp} + C_{land} + C_{civil}\ [€] \tag{4.1}$$

4.1.1.1 Investment in equipment

The total investment in equipment represents the sum of the costs of purchase of each of the model components:

$$C_{eqp} = \sum_{k} C_k\ [€] \tag{4.2}$$

For this matter, the costing equations exposed in table 2.7 were used.

4.1.1.2 Investment in land

Investment associated with land purchase was assumed to represent 3.5 % of the total investment in equipment as proposed by Turchi [61]. It is evident that expenses related to land ownership are much greater for a system with a vast field of solar collectors, thus this approach is only acceptable since the investment in equipment is highly dependent on the size of the collector field.

4.1.1.3 Investment related to civil engineering

Investment related with power electronics, construction and civil engineering was assumed to represent 15 % of the total investment in equipment [61].

4.1.2 Net Present Value

The net present value (NPV) is an indicator of the value that an investor confers to the investment and reflects the weight of the system revenue over the cash-flows during the lifetime of the plant. It reflects both the regular expenses of the system and its thermodynamic performance on the form of yearly revenues.

$$NPV = -C_{inv} + \sum_{t=1}^{n} \frac{R - C_{O\&M}}{(1+i)^t} \, [€] \tag{4.3}$$

where n and i are the plant expected lifetime and interest rate, assumed to be 25 years and 8%, respectively. In equation (4.3), R is the revenue and $C_{O\&M}$ stands for the operation and maintenance costs.

4.1.2.1 Yearly operation and maintenance costs

The yearly operation and maintenance costs of the system were divided into two categories – equipment associated costs ($C_{O\&M_{eqp}}$) and fuel cost ($C_{O\&M_{fuel}}$) - and were calculated as follows:

$$C_{O\&M_{eqp}} = C_{eqp} \cdot f \cdot (\varphi - 1) \, [€/y] \tag{4.4}$$

$$C_{O\&M_{fuel}} = \dot{m}_{fuel} \cdot C_{fuel} \cdot LHV_{fuel} \cdot H \, [€/y] \tag{4.5}$$

In equation (4.4), the assigned values for the maintenance factor (φ) and annuity factor (f) were the same as those of the exergy costing model. In equation (4.5), $\dot{m}_{fuel}$ and C_{fuel} represent the mass flow (in kg/s) and specific cost (in €/kWh) of the natural gas burnt in the combustor, respectively. The parameter H accounts for the yearly operating time of the system, in hours. The specific cost of natural gas was assumed to follow an increasing trend of 0.3 % (average inflation in Portugal, 2019) for each year of operation, taking on the initial value of 40.1 €/MWh (average cost of natural gas for industrial users in 2019, accounting for all service expenses such as transmission, distribution, etc.). These two values were taken from statistics published by PORDATA on their webpage [62]**.** Natural gas is mainly composed of Methane (CH_4), with typical molar fractions of over 90 % for this hydrocarbon. For this reason, the lower heating value of the fuel (LHV_{fuel}) was assumed to be equal to that of CH_4, taking on the value of 50 020 kJ/kg [10].

4.1.2.2 Yearly revenue

The yearly revenue (R) was computed under the assumption that the system would supply a small community, working as an auto-consumption unit (in Portuguese *Unidade de Produção para Auto Consumo* or UPAC*)* that may or may not be connected to the main grid. Therefore, it was calculated as the savings that such a community would sustain if all its electricity came free of charge directly from the system instead of the main grid. This scenario implies that the initial investor would either be the community itself or a private investor that would close some sort of trade deal with the community. The specific cost of electricity ($C_{electricity}$) was assumed to follow an increasing trend of 0.3 % (average inflation in Portugal, 2019) for each year of operation, taking on the initial value of 215 €/MWh (average cost of electricity for domestic users in 2019, accounting for all service expenses such as transmission, distribution, etc.). These two values were taken from statistics published by PORDATA [62].

$$R = C_{electricity} \cdot \dot{P}_{el} \cdot H \ [€/y] \tag{4.6}$$

4.2 Decision variables

The program inputs exhibited on table 2.3 were considered as decision variables, with the exception of those that determine the ambient conditions, G_0 and T_{amb}, which assumed fixed average values during the MOO. The efficiencies of the compressor, turbines, and pump were considered as decision variables with the goal of quantifying the respective impacts on the system cost and net present value. Investing more capital in a component with a higher isentropic efficiency might ultimately result in a higher NPV, and an increase in η_{comp} of 1 % might be more valuable than the same increase in η_{pump}, for example. The following ranges of values were considered:

1) $\mathrm{p_r} \in [1, 20]$

2) $r \in [0.01, 0.99]$

3) $T_5 \in [800\ K, 900\ K]$

4) $A_{reg} \in [2\ m^2, 10\ m^2]$

5) $T_{14} \in [500\ K, 575\ K]$

6) $\mathrm{A_{col}} \in [200\ m^2, 400\ m^2]$

7) $\eta_{comp} \in [75\ \%, 90\ \%]$

8) $\eta_{GT} \in [75\ \%, 90\ \%]$

9) $\eta_{ST} \in [60\ \%, 75\ \%]$

10) $\eta_{pump} \in [60\ \%, 75\ \%]$

4.3 Performance indicators

For each Pareto-optimal solution, the algorithm computes a set of performance indicators to be used as references for the measurement of its performance. The global cycle 1st (η_{global}) and 2nd law efficiencies (ε_{global}), electrical power output ($\dot{P}_{el}$) and total heat input ($\dot{Q}_{input}$) quantify the thermodynamic performance of the system, while the payback period (*PBP*), the internal rate of return (*IRR*) and the levelized electricity cost (*LEC*) quantify the economic performance of the system[2]. The calculation of the *PBP* is straightforward and requires no explanation, the *IRR* is computed using a MatLab® function, and the *LEC* is calculated in a simplifying manner as follows:

$$LEC = \frac{f \cdot C_{inv} + C_{O\&M}}{\dot{P}_{el} \cdot H}\ [€/\mathrm{kWh}] \tag{4.7}$$

where f, C_{inv}, $C_{O\&M}$, $\dot{P}_{el}$, and H stand for the previously defined annuity factor, investment cost, operation and maintenance costs, electrical power output, and yearly operating time, respectively. Finally, the solar share (f_{sol}), mass of $\mathrm{CO_2}$ emissions and savings ($m_{CO_2\ emitted}\ and\ m_{CO_2\ saved}$) quantify the environmental performance of the system and are calculated as explained bellow. The carbon dioxide emissions savings correspond to the additional mass of $\mathrm{CO_2}$ that would be released into the atmosphere if the same system was entirely powered by the combustion chamber.

$$\dot{m}_{CO_2\ emitted} = \dot{m}_{fuel} \cdot \frac{M_{CO_2}}{M_{CH_4}}\ [\mathrm{kg/s}] \tag{4.8}$$

$$\dot{m}_{CO_2\ saved} = \frac{f_{sol} \cdot m_{CO_2\ emitted}}{1 - f_{sol}}\ [\mathrm{kg/s}] \tag{4.9}$$

[2] The *PBP* is the amount of time in years necessary for the net present value to be nil and the project to become profitable, the *IRR* is the interest rate that makes the *NPV* calculated for the whole operation time nil, and the *LEC* quantifies the amount of capital expended per kWh of generated electricity.

In equation (4.6), M_{CO_2} and M_{CH_4} stand for the molecular weights of carbon dioxide and methane, respectively. This equation assumes stoichiometric combustion of the fuel, which is considered to be methane (CH_4) as an approximation.

4.4 Results and discussion

When analyzing the model without regenerator, only 8 optimization variables were considered, excluding the mass flow ratio and regenerator area. For the ambient conditions, an average of the four representative days was considered ($G_0 = 646.7\ \mathrm{W/m^2}$ and $T_{amb} = 18.08\ ºC$). The result of each optimization was a Pareto front composed of 70 solutions (a.k.a. individuals or subjects), as illustrated in figure 4.1. The dashed line represented in the figure will be contextualized in section 4.4.1. Complete tables showcasing the 70 subjects and their respective genes, fitness values and performance indicators can be found in Appendix B.

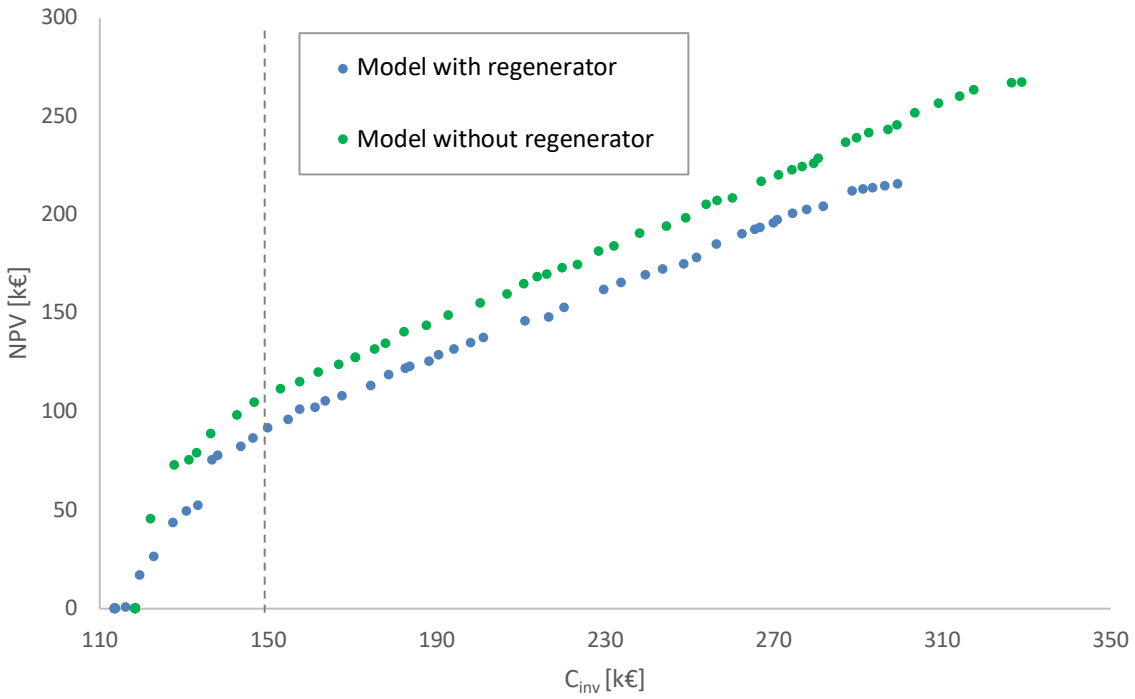

Figure 4. 1 Resultant Pareto fronts

Looking at the two Pareto fronts in fig. 4.1, it is possible to conclude that the results from the MOO of the model without regenerator dominate those of the model with regenerator throughout most of the considered domain, with the exception of the very low NPV subjects, which are not very interesting from the economical perspective. This is a strong evidence that the system thermoeconomical performance is indeed stronger if the regenerator is eliminated. The truth is that without this component the model exergy destruction is decreased, and a larger amount of heat is transferred to the bottom cycle,

increasing its power output (see fig. 3.5). Additionally, with the elimination of the regenerator it is possible to have a greater area of solar collectors as well as more efficient components for the same investment cost. Therefore, the further analysis refers to the model without regenerator, which was considered to be a more interesting design. Let us now find the optimized designs.

It is important to point out that all of the 70 solutions are optimal solutions, in a sense that it is impossible to improve one of the objective functions without hurting the other, thus it is the designer's task to consider all the solutions and chose the one(s) that better fit the purpose of the system. For this matter, the genes, fitness values, and performance indicators of each subject were organized on tables B.1 and B.2 and analyzed. The search for the most favorable solution(s) was divided in three steps: analysis of the behaviour of the decision variables/genes, fitness values and performance indicators interpretation, and decision making.

4.4.1 Decision variables behaviour

It is crucial for the decision making to identify what is happening with each optimization variable as the investment cost is increased. The results are displayed in figures 4.2 - 4.4. One conclusion that immediately arises is that the steam turbine's inlet temperature (T_{14}) assumes the maximum value of 575 K for all the subjects (see fig. 4.2). The second obvious conclusion is that the Pareto front can be divided into two distinct regions: the first region, composed of the first 27 subjects (although only 8 are actually distinguishable in fig. 4.1), where the local derivative of the plot keeps changing ($f'(i) = (NPV_i - NPV_{i-1})/(C_{inv_i} - C_{inv_{i-1}})$), and the second region, composed of the last 43 subjects, where such derivative assumes a more steady close to unit value. The transition between regions is marked with a dashed line on the plots presented in this chapter. This behaviour is related to the evolution of the components efficiencies and the solar receiver area A_{col}, which keeps a close-to-constant value of around 200 m^2 for the initial subjects and then starts increasing at a continuous pace throughout the second region until it reaches the maximum value of 400 m^2 (fig. 4.2). The last two subjects are outliers within the second region because they have reached the maximum value for A_{col}, which results in similar NPVs. The gas turbine's inlet temperature (T_5) and compression ratio (p_r) follow an increasing trend for the first 36 subjects and then stabilize at around 864.01 K and 7.63, respectively (fig. 4.3). The behaviour of the four efficiencies considered as optimization variables is illustrated in fig. 4.4. The compressor, gas and steam turbines efficiencies assume an increasing trend throughout the first region and then stabilize at around 85.45 %, 88.60 % and 74.67 %, respectively, while the behaviour of the pump efficiency is more chaotic and takes on values within the entire considered range (60 to 75 %).

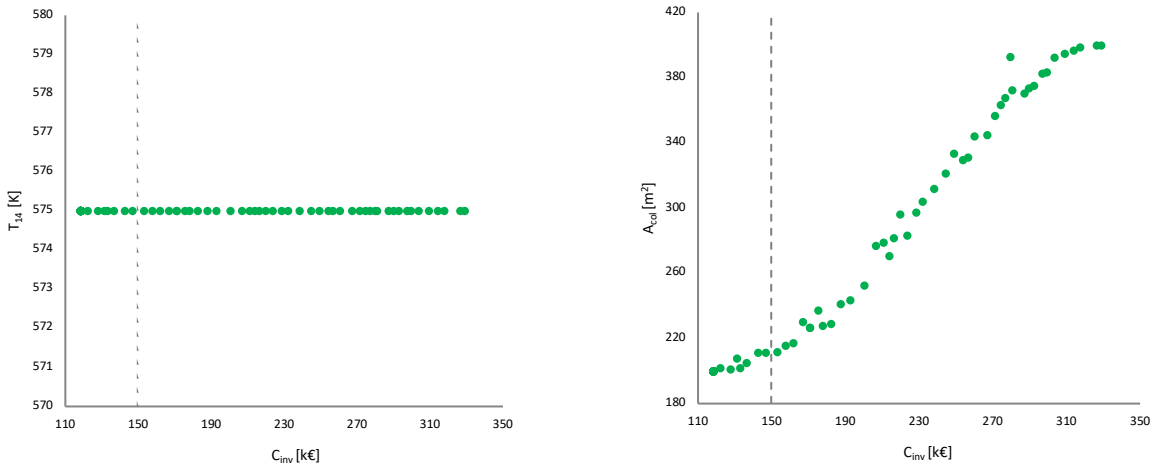

Figure 4. 2 Decision variables of Pareto-optimal solutions: T_{14} and A_{col}

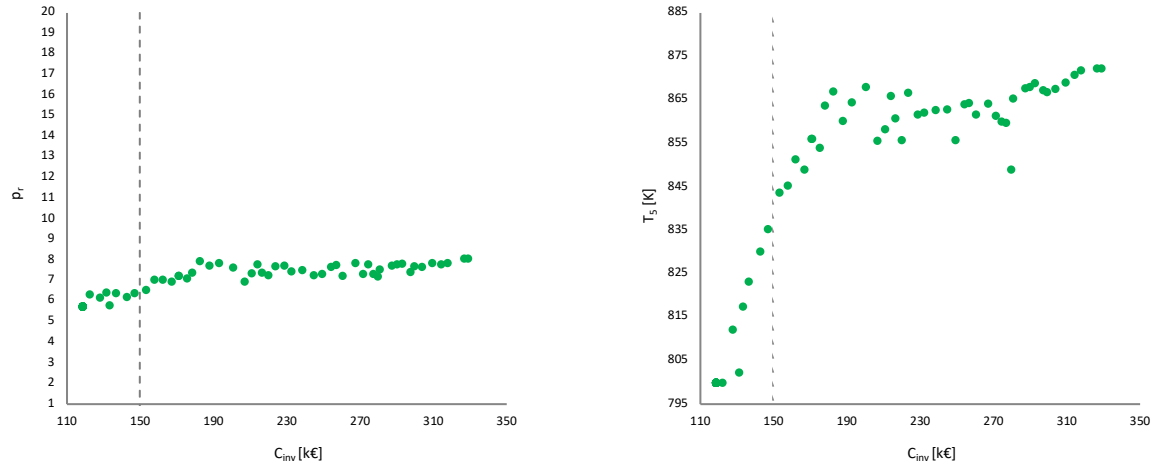

Figure 4. 3 Decision variables of Pareto-optimal solutions: p_r and T_5

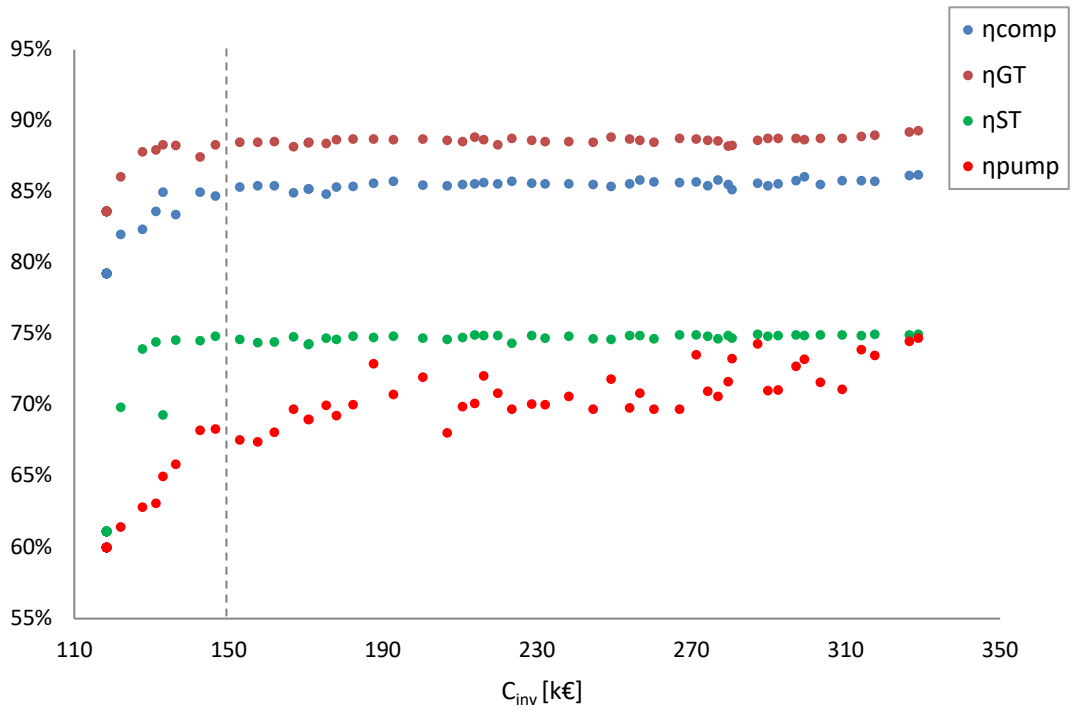

Figure 4. 4 Decision variables of Pareto-optimal solutions: components efficiencies

4.4.2 Fitness values and Performance indicators behaviour

The NPV increases with C_{inv} throughout the Pareto front, thus a higher initial investment results in a higher profit in the future. The fitness values of Pareto-optimal solutions go from investment costs of 118,264 € with near zero NPV values, to 328,706 € worth of investment for a net present value of 267,373 € (see figure 4.1). As previously mentioned, the resultant NPV/C_{inv} curve is quite steep throughout the 1st region, with constant variations of the local derivative, and assumes a more smooth and steady inclination after transitioning to the 2nd region. Similar conclusions can be drawn from the payback period and levelized electricity cost, which decrease with C_{inv}, and the internal rate of return, which increases with C_{inv} (see figs. 4.5 and 4.6). Resultant Pareto-optimal solutions boast LECs on the order of 0.159 – 0.221 €/kWh, which corresponds to 0.179 – 0.248 USD/kWh according to the considered conversion rate. These results show that the optimized system can yield similar or lower costs of electricity generation than conventional stand-alone CSP systems, which take on global average LEC values of 0.182 USD/kWh according to IRENA [11]. However, from a strictly economic point of view, it clearly falls behind when compared to standard natural gas fired combined cycle power plants, whose LEC typically falls on the 0.044 – 0.073 USD/kWh range according to Lazard's data [63].

Both efficiencies (1st and 2nd law) follow an increasing trend along the first region, and then begin to stabilize after the transition to the second region at around 26.9 % and 32.6 %, respectively (see fig. 4.5). These values, which fall within the range of 16.46 % – 27.97 % and 21.49 % – 33.53 %, represent a valuable improvement comparing to the base case design, which boasts maximum 1st and 2nd law efficiencies of 20.26 % and 26.22 % respectively (see table 3.4). Resultant isentropic efficiencies are higher than those of typical stand-alone PTC power plants (10-16 %) but quite lower than typical values for natural-gas-fired CCPPs (50-60 %). This is due to the constraints imposed to the gas turbine inlet temperature and compression ratios, which were set to maximums of 900 K and 20:1, respectively, quite low numbers when compared to standard CCPPs that often yield values of over 1500 K and 35:1 [9]. However, without these limitative constraints the solar shares would greatly decrease, and the cost of the system would increase. Moreover, these CCPP reference values presented by Boyce refer to large-scale power plants, and so this comparison is not fair. Overall, the LECs and efficiencies of Pareto-optimal designs are quite interesting for this type of microgeneration unit. On the other hand, the system net electrical power output increases almost linearly throughout both regions. This proves that the second is the optimal efficiency region, where the main variation from one subject to another is the increase of the collector field area accompanied by an increase on the system size and power output (economy of scale), see fig. 4.5.

The solar share (f_{sol}) is the highest for the first subject (~ 65 %), and then assumes a decreasing trend until the 36th subject, where it stabilizes at around 51 %. This behaviour is highly related to the evolution of p_r, T_5 and A_{col}. The first two variables initially increase with C_{inv}, leading to greater heat outputs from the combustor, and then also stabilize at the 36th subject (see fig. 4.3), while the last variable's growth rate also increases along the lower investment cost subjects and then stabilizes at the same point (see fig. 4.2). Furthermore, the employed algorithm invalidates any solution with a solar share under 50 % so this is the minimum acceptable value. As a reference, if we look at the Pareto-

optimal solution with the closest NPV to that of the base case (13,420 €) and compare the solar shares of both solutions, we see that the optimized design yields a solar share of almost 65 %, which represents an increase of roughly 6.5 % (depending on the season), for an investment cost that is 20 % lower. These results reveal the clear superiority of the optimized designs from an environmental point of view. Since the system power output and input are increasing with investment cost, it is expected that the annual mass of saved CO_2 emissions also increases with C_{inv}, but the same trend does not apply to the solar share (see fig. 4.6). For a design with the maximum considered solar collector area of 400 m^2, the amount of CO_2 that is not discharged to the environment due to solar hybridization is over 150 tons per year.

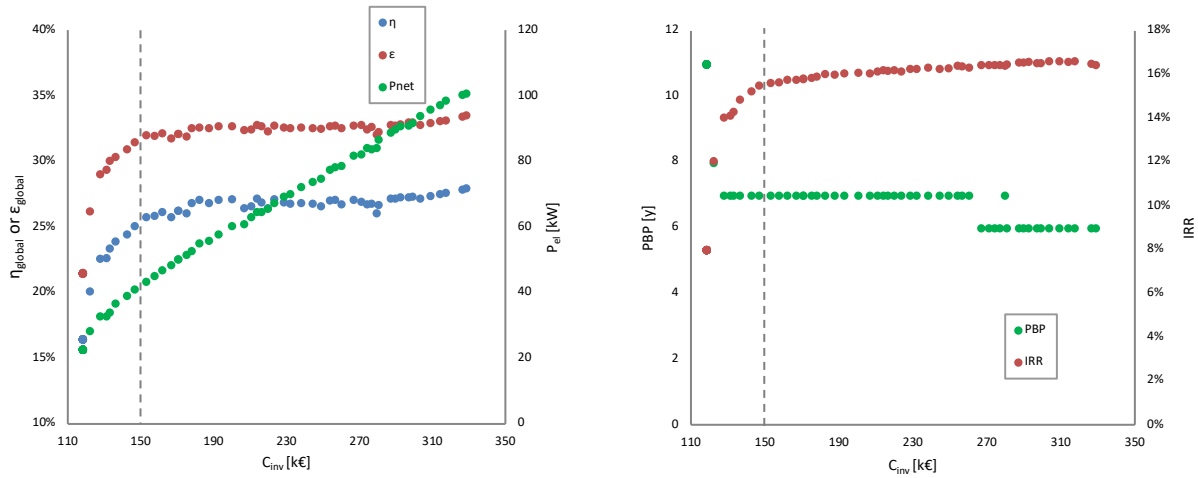

Figure 4. 5 Performance indicators of Pareto-optimal solutions: thermodynamic and economic

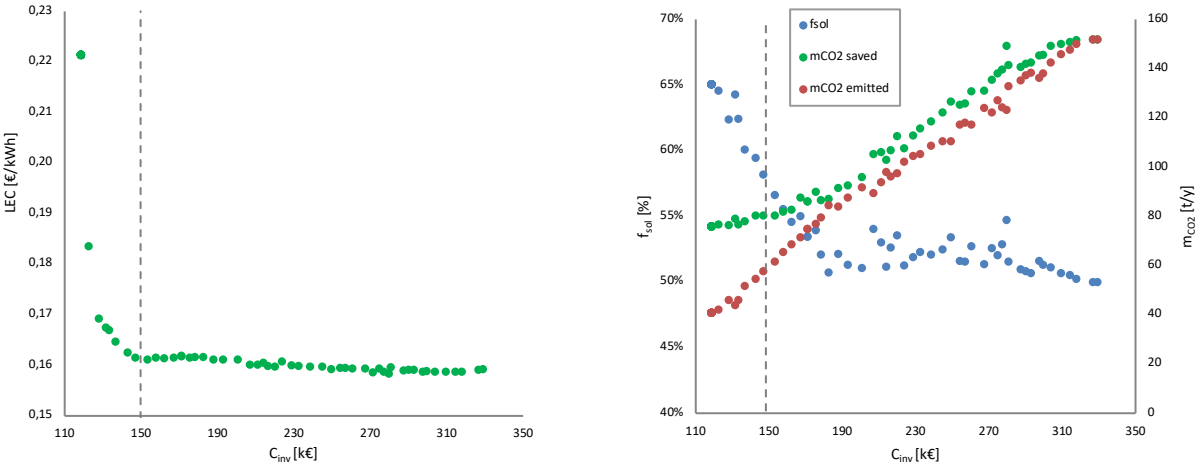

Figure 4. 6 Performance indicators of Pareto-optimal solutions: economic and environmental

4.4.3 Decision making

The fact that the NPV consistently increases with C_{inv} implies that the last subject yields the greatest profit, which might suggest that it is the best choice. However, two factors must be carefully considered:

- In a real-life situation, the amount of money available for investment is limited, as well as the acceptable time for the return of such investment (payback period). The decision maker must weigh the benefits resulting from injecting more capital into a certain project in opposition to applying it elsewhere.

- In a realistic scenario, there is a specific energy demand that must be met, and in a case where surplus electricity is being produced the system would either have to sell it to the grid or require some kind of thermal energy storage technology. Either way, considering the consequential additional costs would probably result in a stabilization of the NPV/C_{inv} curve at some point (as happens in the work of Pihl et al. [42]).

None of these factors is considered in the model, so the author of the present work considered three different scenarios/criteria to select suitable designs for the given system. Any of these scenarios might be a good solution, depending on the specific goals of the decision maker. In addition to the performance indicators, the exergy costing model was applied to each solution to provide a more thorough comparison between the base design and the optimized designs. The respective specific cost rates can be found in Annex B. For each scenario, the performance of the chosen Pareto-optimal design was compared to that of the base case design corresponding to the results showcased on chapter 3.2 with respect to the "maximize efficiency" goal (see table 3.4). This design was chosen as the base case given that the one corresponding to the "maximize power output" goal yields a negative NPV, as it is not a profitable investment. At the end of this section, figure 4.9 and table 4.19 are presented in order to facilitate comparison between each scenario.

4.4.3.1 Scenario #1 – Economical criteria

Although the LEC and IRR of the project follow a decreasing and increasing trend with C_{inv}, respectively, the differences from one subject to another (ΔLEC and ΔIRR) after the transition to the second region are almost neglectable, as clearly seen in figures 4.5 and 4.6. Therefore, it was considered that the most interesting solution from a strictly economic point of view would be the first individual of the second region (**# 28**), as it yields close to peak LEC and IRR values for a relatively low C_{inv}. Tables 4.1 – 4.6 compare the performance of the base case with the optimized case designs.

Table 4. 1 Genes, fitness value and economical performance indicators – base design vs subject # 28

	Base case	***Optimized case***
Decision variables / Genes		
p_r	6.6	6.58
r	0.01	X
T_5 $[K]$	825	843.72
A_{reg} $[m^2]$	6	X
T_{14} $[K]$	550	575
A_{col} $[m^2]$	200	211.78
η_{comp} [%]	79.6 %	85.34 %
η_{GT} [%]	85.8 %	88.53 %
η_{ST} [%]	68 %	74.66 %
η_{pump} [%]	60 %	67.56 %
Objective functions / Fitness values		
C_{inv} [€]	153,192.7	152,858.1 (- 334.6)
NPV [€]	13,420.4	111,584.9 (+ 98,164.5)
Performance indicators		
PBP [y]	10	7 (-3)
IRR [%]	8.99 %	15.66% (+ 6.66%)
LEC [€/kWh]	0.211	0.161 (- 0.05)

Table 4. 2 Seasonal comparison of performance indicators - base design vs subject # 28

	Summer		**Fall**		**Winter**		**Spring**	
	Base case	Optimized case	Base case	Optimized case	Base case	Optimized case	Base case	Optimized case
η_{global} [%]	20.26%	25.76% (+5.5%)	20.26%	25.76% (+5.5%)	20.26%	25.76% (+5.5%)	20.26%	25.76% (+5.5%)
ε_{global} [%]	26.22%	32.91% (+6.68%)	25.70%	32.31% (+6.61%)	24.71%	31.18% (+6.47%)	25.22%	31.76% (+6.54%)
$\dot{P}_{el}$ [kW]	30.07	41.96 (+11.9)	30.47	42.39 (+11.92)	32.45	44.86 (+12.42)	31.96	44.38 (+12.42)
$\dot{Q}_{input}$ $[kW]$	154.62	169.72 (+15.1)	156.68	171.45 (+14.77)	166.85	181.44 (+14.59)	164.37	179.50 (+15.13)
f_{sol} [%]	62.95%	60.72% (-2.22%)	59.55%	57.63% (-1.93%)	53.70%	52.29% (-1.41%)	57.51%	55.76% (-1.75%)
$m_{co_2\ emitted}$ [kg/h]	11.58	13.47 (+1.89)	12.81	14.68 (+1.87)	15.61	17.50 (+1.88)	14.12	16.05 (+1.93)
$m_{co_2\ saved}$ [kg/h]	19.67	20.83 (+1.16)	18.86	19.97 (+1.11)	18.11	19.17 (+1.07)	19.10	20.23 (+1.13)

Table 4. 3 System cost rates, Summer season – base design vs subject # 28

Component (k)	$\dot{E}_{x_{d,k}}$ [kW]		$\dot{E}_{x_{d,k}}/\dot{E}_{x_{d,syst}}$ [%]		$\dot{C}_{D,k}$ [€/h]		$\dot{Z}_k$ [€/h]		$\dot{C}_{D,k} + \dot{Z}_k$ [€/h]	
	Base case	Optimized case	Base case	Optimized case	Base case	Optimized case	Base case	Optimized case	Base case	Optimized case
Compressor	9.25	6.27	11.40	7.70	0.67	0.44	0.13	0.28	0.80	0.72
Regenerator	0.54	X	0.67	X	0.04	X	0.13	X	0.16	X
Solar Receiver	11.80	13.07	14.54	16.05	0.00	0.00	1.30	1.38	1.30	1.38
Combustor	23.66	27.15	29.16	33.33	0.95	1.09	0.05	0.05	0.99	1.13
Gas Turbine	6.75	5.54	8.32	6.80	0.44	0.35	0.20	0.36	0.64	0.71
HRSG	8.22	8.58	10.13	10.54	0.54	0.53	1.26	0.97	1.80	1.51
Stream Bifurcation	0.12	X	0.15	X	0.00	X	0.00	X	0.00	X
HEX	0.91	1.30	1.12	1.59	0.00	0.00	0.05	0.06	0.05	0.06
Steam Turbine	5.69	4.25	7.01	5.22	1.08	0.74	0.01	0.01	1.09	0.75
Condenser	13.92	15.10	17.15	18.54	0.00	0.00	0.01	0.01	0.01	0.01
Pump	0.28	0.19	0.35	0.23	0.07	0.04	0.02	0.02	0.09	0.06
Total	81.15	81.46 (+0.31)	100	100	3.79	3.19 (-0.6)	3.14	3.14 (=)	6.93	6.33 (-0.6)

Table 4. 4 System cost rates, Fall season – base design vs subject # 28

Component (k)	$\dot{E}_{x_{d,k}}$ [kW]		$\dot{E}_{x_{d,k}}/\dot{E}_{x_{d,syst}}$ [%]		$\dot{C}_{D,k}$ [€/h]		$\dot{Z}_k$ [€/h]		$\dot{C}_{D,k} + \dot{Z}_k$ [€/h]	
	Base case	Optimized case	Base case	Optimized case	Base case	Optimized case	Base case	Optimized case	Base case	Optimized case
Compressor	9.23	6.24	11.18	7.56	0.69	0.45	0.13	0.28	0.82	0.73
Regenerator	0.54	X	0.66	X	0.04	X	0.13	X	0.16	X
Solar Receiver	11.06	12.26	13.40	14.85	0.00	0.00	1.30	1.38	1.30	1.38
Combustor	25.90	29.29	31.39	35.48	1.04	1.17	0.05	0.05	1.08	1.22
Gas Turbine	6.73	5.51	8.16	6.67	0.45	0.35	0.20	0.36	0.65	0.72
HRSG	8.20	8.54	9.94	10.34	0.55	0.55	1.27	0.98	1.82	1.52
Stream Bifurcation	0.12	X	0.15	X	0.00	X	0.00	X	0.00	X
HEX	0.90	1.29	1.09	1.56	0.00	0.00	0.05	0.06	0.05	0.06
Steam Turbine	5.68	4.23	6.88	5.12	1.12	0.77	0.01	0.01	1.13	0.78
Condenser	13.88	15.02	16.82	18.19	0.00	0.00	0.01	0.01	0.01	0.01
Pump	0.28	0.19	0.34	0.23	0.07	0.04	0.02	0.02	0.09	0.06
Total	82.54	82.56 (+0.02)	100	100	3.96	3.33 (-0.63)	3.16	3.16 (=)	7.13	6.48 (-0.65)

Table 4. 5 System cost rates, Winter season – base design vs subject # 28

Component (k)	$\dot{E}_{x_{d,k}}$ [kW]		$\dot{E}_{x_{d,k}}/\dot{E}_{x_{d,syst}}$ [%]		$\dot{C}_{D,k}$ [€/h]		$\dot{Z}_k$ [€/h]		$\dot{C}_{D,k} + \dot{Z}_k$ [€/h]	
	Base case	Optimized case	Base case	Optimized case	Base case	Optimized case	Base case	Optimized case	Base case	Optimized case
Compressor	9.36	6.29	10.80	7.31	0.70	0.45	0.14	0.30	0.84	0.75
Regenerator	0.55	X	0.63	X	0.04	X	0.13	X	0.16	X
Solar Receiver	10.01	11.09	11.55	12.89	0.00	0.00	1.30	1.38	1.30	1.38
Combustor	30.42	33.64	35.10	39.07	1.22	1.35	0.05	0.05	1.27	1.40
Gas Turbine	6.83	5.56	7.89	6.46	0.46	0.36	0.22	0.39	0.68	0.74
HRSG	8.33	8.61	9.60	10.00	0.56	0.56	1.34	1.03	1.91	1.58
Stream Bifurcation	0.13	X	0.15	X	0.00	X	0.00	X	0.00	X
HEX	0.92	1.30	1.06	1.51	0.00	0.00	0.05	0.06	0.05	0.06
Steam Turbine	5.76	4.27	6.65	4.96	1.22	0.83	0.01	0.01	1.23	0.84
Condenser	14.09	15.15	16.25	17.59	0.00	0.00	0.01	0.01	0.01	0.01
Pump	0.29	0.19	0.33	0.22	0.08	0.04	0.02	0.02	0.10	0.07
Total	86.68	86.10 (-0.58)	100	100	4.29	3.59 (-0.7)	3.26	3.25 (-0.01)	7.54	6.84 (-0.7)

Table 4. 6 System cost rates, Spring season – base design vs subject # 28

Component (k)	$\dot{E}_{x_{d,k}}$ [kW]		$\dot{E}_{x_{d,k}}/\dot{E}_{x_{d,syst}}$ [%]		$\dot{C}_{D,k}$ [€/h]		$\dot{Z}_k$ [€/h]		$\dot{C}_{D,k} + \dot{Z}_k$ [€/h]	
	Base case	Optimized case	Base case	Optimized case	Base case	Optimized case	Base case	Optimized case	Base case	Optimized case
Compressor	9.36	6.32	11.05	7.47	0.68	0.44	0.13	0.29	0.81	0.74
Regenerator	0.55	X	0.65	X	0.04	X	0.13	X	0.16	X
Solar Receiver	10.80	11.97	12.74	14.15	0.00	0.00	1.30	1.38	1.30	1.38
Combustor	27.72	31.10	32.70	36.76	1.11	1.25	0.05	0.05	1.16	1.29
Gas Turbine	6.83	5.58	8.06	6.60	0.45	0.35	0.21	0.38	0.66	0.73
HRSG	8.33	8.65	9.82	10.22	0.55	0.54	1.33	1.02	1.87	1.56
Stream Bifurcation	0.13	X	0.15	X	0.00	X	0.00	X	0.00	X
HEX	0.92	1.30	1.08	1.54	0.00	0.00	0.05	0.06	0.05	0.06
Steam Turbine	5.76	4.28	6.80	5.06	1.17	0.80	0.01	0.01	1.18	0.81
Condenser	14.09	15.21	16.62	17.98	0.00	0.00	0.01	0.01	0.01	0.01
Pump	0.29	0.19	0.34	0.23	0.07	0.04	0.02	0.02	0.09	0.07
Total	84.77	84.60 (-0.17)	100	100	4.07	3.42 (-0.65)	3.24	3.23 (-0.01)	7.30	6.65 (-0.65)

According to table 4.1, the optimized design takes on higher values for all the decision variables, except for the compression ratio, which remains almost unchanged, even though the respective investment cost is marginally lower (-0.2 %) and the NPV is substantially higher (+731.5%). This is due to the elimination of the regenerator associated costs. Likewise, the resultant PBP, IRR and LEC are far more interesting than those of the base design.

From table 4.2 one can infer that the system efficiencies (1st and 2nd law) and electrical power output are also superior, with increases of approximately 5.5 %, 6.58 % and 38.94 %, respectively, on an annual average basis. The first two indicators achieve greater values during the warmer seasons, as expected, while $\dot{P}_{el}$ follows the opposite trend. This seasonal behaviour has been previously explained

on chapter 3.2. On the other hand, the total heat input increases 9.27 % and the solar share decreases 1.83 % on an annual average basis, thus the evident increase on the CO_2 emissions (14.01 %).

Tables 4.3 - 4.6 reveal that the total exergy destruction within the optimized system is quite similar to that of the base case, with a slight increase during Summer and Fall and a slight decrease during Winter and Spring due to the ambient temperature fluctuations throughout the year. This means the optimized case is able to generate more power for the same exergy destruction. As expected, the higher isentropic efficiency of the compressor, turbines, and pump results in lower values of exergy destruction as well as higher investment plus operation and maintenance cost rates ($\dot{Z}_k$). However, the cost rates due to exergy destruction ($\dot{C}_{D,k}$) decrease simultaneously. The decrease of $\dot{C}_{D,k}$ typically overcompensates the increase of $\dot{Z}_k$, ultimately resulting in a reduction of the total cost rates of most of these components, except for the gas turbine. The exergy destruction inside the HRSG is higher for the optimized case due to the increase of T_{14}, and its total cost rate decreases due to the reduction of $\dot{Z}_k$ associated with the changes in $\dot{m}_7$, $\dot{m}_b$, $\dot{Q}_{economizer}$ and $\dot{Q}_{evaporator}$. At the same time, there is more fuel being burned inside the combustor, so it is consequent upon that the exergy destruction and associated cost rate increases for this component. Finally, the exergy destruction inside the solar receiver is also increasing due to the higher solar collector area. At a global level, the optimized design results in a reduction of the system total cost rate of up to 9.3 %.

4.4.3.2 Scenario #2 – Thermodynamic criteria

The analysis conducted in chapter 3.2 concluded that the maximum net work output for the initially considered model is achieved for an r around 0.35, fluctuating seasonally. However, the MOOs conducted in the present chapter revealed that with the model without regenerator ($r = 0$ and $A_{reg} = 0\ m^2$) it is possible to have a larger area of solar collectors for the same investment cost, which ultimately results in a greater work output for this design. This conclusion was based on the previously described optimization analysis and reinforced by the results of a second MOO in which the "maximize NPV" objective function was replaced with "maximize $\dot{P}_{el}$", and whose results are illustrated in Annex B.

Small-scale power plants are usually limited by two key factors: investment budget and available space (especially for the solar collector field in this case). Accordingly, the current scenario represents the probable choice of an investor whose decision making is constrained by funds and available land, and whose objective is to maximize generation power ($\dot{P}_{el}$).

The generation power relative to investment cost and collector field area ($\dot{P}_{el}/C_{inv}$ and $\dot{P}_{el}/A_{col}$) follow a trend that is quite similar to that of the 1st and 2nd law efficiencies (see figure 4.7). Both variables rapidly increase in value along the initial subjects and then stabilize at subject # 36. This behaviour proves that once the system gets to the maximum efficiency region (# 36 - # 70), every additional euro invested results in a fixed increase in generated power. Thus, it was considered that subject **# 36** is the most interesting solution for the given scenario, as it is the individual within the "stabilization region" that yields the lowest C_{inv}. The tables that follow (tables 4.7 – 4.12) provide a comparison between the performance of the base case design and the optimized case design.

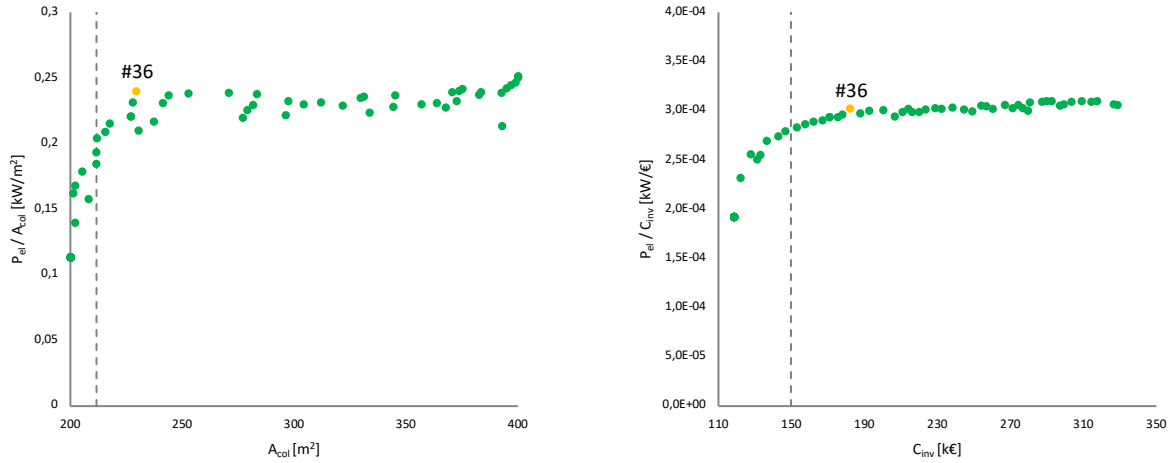

Figure 4. 7 Relative electrical power output of Pareto-optimal solutions

Table 4. 7 Genes, fitness value and economical performance indicators – base design vs subject # 36

	Base case	***Optimized case***
Optimization variables / Genes		
p_r	6.6	7.97
r	0.01	**X**
T_5 $[K]$	825	867.04
A_{reg} $[m^2]$	6	**X**
T_{14} $[K]$	550	575
A_{col} $[m^2]$	200	229.36
η_{comp} [%]	79.6 %	85.39 %
η_{GT} [%]	85.8 %	88.72 %
η_{ST} [%]	68 %	74.88 %
η_{pump} [%]	60 %	70.05 %
Objective functions / Fitness values		
C_{inv} [€]	153,192.7	182,221 (+ 29,028.3)
NPV [€]	13,420.4	140,483.9 (+127,063.5)
Performance indicators		
PBP [y]	10	7 (- 3)
IRR [%]	8.99%	16.06% (+ 7.06%)
LEC [€/kWh]	0.211	0.162 (- 0.05)

Table 4. 8 Seasonal comparison of performance indicators - base design vs subject # 36

	Summer		Fall		Winter		Spring	
	Base case	Optimized case	Base case	Optimized case	Base case	Optimized case	Base case	Optimized case
η_{global} [%]	20.26%	27.08% (+6.83%)	20.26%	27.08% (+6.83%)	20.26%	27.08% (+6.83%)	20.26%	27.08% (+6.83%)
ε_{global} [%]	26.22%	33.44% (+7.22%)	25.70%	32.87% (+7.17%)	24.71%	31.79% (+7.08%)	25.22%	32.35% (+7.13%)
$\dot{P}_{el}$ [kW]	30.07	52.98 (+22.91)	30.47	53.77 (+23.3)	32.45	57.45 (+25)	31.96	56.46 (+24.5)
$\dot{Q}_{input}$ [kW]	154.62	203.77 (+49.15)	156.68	206.81 (+50.13)	166.85	220.93 (+54.08)	164.37	217.19 (+52.82)
f_{sol} [%]	62.95%	54.77% (-8.17%)	59.55%	51.74% (-7.81%)	53.70%	46.51% (-7.19%)	57.51%	49.91% (-7.6%)
$m_{co_2\ emitted}$ [kg/h]	11.58	18.63 (+7.05)	12.81	20.17 (+7.36)	15.61	23.88 (+8.27)	14.12	21.98 (+7.87)
$m_{co_2\ saved}$ [kg/h]	19.67	22.56 (+2.89)	18.86	21.63 (+2.77)	18.11	20.77 (+2.66)	19.10	21.91 (+2.80)

Table 4. 9 System cost rates, Summer season - base design vs subject # 36

Component (k)	$\dot{E}_{x_{d,k}}$ [kW]		$\dot{E}_{x_{d,k}}/\dot{E}_{x_{d,syst}}$ [%]		$\dot{C}_{D,k}$ [€/h]		$\dot{Z}_k$ [€/h]		$\dot{C}_{D,k} + \dot{Z}_k$ [€/h]	
	Base case	Optimized case	Base case	Optimized case	Base case	Optimized case	Base case	Optimized case	Base case	Optimized case
Compressor	9.25	7.96	11.40	7.96	0.67	0.59	0.13	0.44	0.80	1.03
Regenerator	0.54	X	0.67	X	0.04	X	0.13	X	0.16	X
Solar Receiver	11.80	13.26	14.54	13.26	0.00	0.00	1.30	1.49	1.30	1.49
Combustor	23.66	36.92	29.16	36.94	0.95	1.48	0.05	0.05	0.99	1.53
Gas Turbine	6.75	7.21	8.32	7.21	0.44	0.48	0.20	0.50	0.64	0.97
HRSG	8.22	10.13	10.13	10.13	0.54	0.67	1.26	1.12	1.80	1.79
Stream Bifurcation	0.12	X	0.15	X	0.00	X	0.00	X	0.00	X
HEX	0.91	1.50	1.12	1.50	0.00	0.00	0.05	0.07	0.05	0.07
Steam Turbine	5.69	4.98	7.01	4.98	1.08	0.90	0.01	0.01	1.09	0.91
Condenser	13.92	17.80	17.15	17.81	0.00	0.00	0.01	0.02	0.01	0.02
Pump	0.28	0.20	0.35	0.20	0.07	0.04	0.02	0.03	0.09	0.07
Total	81.15	99.95 (+18.8)	100	100	3.79	4.16 (+0.37)	3.14	3.73 (+0.59)	6.93	7.88 (+0.95)

Table 4. 10 System cost rates, Fall season - base design vs subject # 36

Component (k)	$\dot{E}_{x_{d,k}}$ [kW]		$\dot{E}_{x_{d,k}}/\dot{E}_{x_{d,syst}}$ [%]		$\dot{C}_{D,k}$ [€/h]		$\dot{Z}_k$ [€/h]		$\dot{C}_{D,k} + \dot{Z}_k$ [€/h]	
	Base case	Optimized case	Base case	Optimized case	Base case	Optimized case	Base case	Optimized case	Base case	Optimized case
Compressor	9.23	7.95	11.18	7.81	0.69	0.60	0.13	0.45	0.82	1.05
Regenerator	0.54	X	0.66	X	0.04	X	0.13	X	0.16	X
Solar Receiver	11.06	12.43	13.40	12.21	0.00	0.00	1.30	1.49	1.30	1.49
Combustor	25.90	39.61	31.39	38.92	1.04	1.59	0.05	0.05	1.08	1.64
Gas Turbine	6.73	7.20	8.16	7.08	0.45	0.49	0.20	0.50	0.65	0.99
HRSG	8.20	10.12	9.94	9.94	0.55	0.68	1.27	1.13	1.82	1.82
Stream Bifurcation	0.12	X	0.15	X	0.00	X	0.00	X	0.00	X
HEX	0.90	1.50	1.09	1.47	0.00	0.00	0.05	0.07	0.05	0.07
Steam Turbine	5.68	4.97	6.88	4.89	1.12	0.93	0.01	0.01	1.13	0.95
Condenser	13.88	17.78	16.82	17.47	0.00	0.00	0.01	0.02	0.01	0.02
Pump	0.28	0.20	0.34	0.20	0.07	0.05	0.02	0.03	0.09	0.07
Total	82.54	101.74 (+19.2)	100	100	3.96	4.33 (+0.37)	3.16	3.76 (+0.6)	7.13	8.09 (+0.96)

Table 4. 11 System cost rates, Winter season - base design vs subject # 36

Component (k)	$\dot{E}_{x_{d,k}}$ [kW]		$\dot{E}_{x_{d,k}}/\dot{E}_{x_{d,syst}}$ [%]		$\dot{C}_{D,k}$ [€/h]		$\dot{Z}_k$ [€/h]		$\dot{C}_{D,k} + \dot{Z}_k$ [€/h]	
	Base case	Optimized case	Base case	Optimized case	Base case	Optimized case	Base case	Optimized case	Base case	Optimized case
Compressor	9.36	8.09	10.80	7.56	0.70	0.61	0.14	0.48	0.84	1.09
Regenerator	0.55	X	0.63	X	0.04	X	0.13	X	0.16	X
Solar Receiver	10.01	11.24	11.55	10.50	0.00	0.00	1.30	1.49	1.30	1.49
Combustor	30.42	45.21	35.10	42.23	1.22	1.81	0.05	0.06	1.27	1.87
Gas Turbine	6.83	7.33	7.89	6.85	0.46	0.50	0.22	0.54	0.68	1.04
HRSG	8.33	10.30	9.60	9.62	0.56	0.70	1.34	1.20	1.91	1.90
Stream Bifurcation	0.13	X	0.15	X	0.00	X	0.00	X	0.00	X
HEX	0.92	1.53	1.06	1.43	0.00	0.00	0.05	0.07	0.05	0.07
Steam Turbine	5.76	5.06	6.65	4.73	1.22	1.02	0.01	0.01	1.23	1.03
Condenser	14.09	18.10	16.25	16.91	0.00	0.00	0.01	0.02	0.01	0.02
Pump	0.29	0.20	0.33	0.19	0.08	0.05	0.02	0.03	0.10	0.08
Total	86.68	107.08 (+20.4)	100	100	4.29	4.69 (+0.4)	3.26	3.89 (+0.63)	7.54	8.58 (+1.04)

Table 4. 12 System cost rates, Spring season - base design vs subject # 36

Component (k)	$\dot{E}_{x_{d,k}}$ [kW]		$\dot{E}_{x_{d,k}}/\dot{E}_{x_{d,syst}}$ [%]		$\dot{C}_{D,k}$ [€/h]		$\dot{Z}_k$ [€/h]		$\dot{C}_{D,k} + \dot{Z}_k$ [€/h]	
	Base case	Optimized case	Base case	Optimized case	Base case	Optimized case	Base case	Optimized case	Base case	Optimized case
Compressor	9.36	8.08	11.05 %	7.72 %	0.68	0.60	0.13	0.47	0.81	1.07
Regenerator	0.55	X	0.65 %	X	0.04	X	0.13	X	0.16	X
Solar Receiver	10.80	12.13	12.74 %	11.60 %	0.00	0.00	1.30	1.49	1.30	1.49
Combustor	27.72	41.93	32.70 %	40.10 %	1.11	1.68	0.05	0.06	1.16	1.74
Gas Turbine	6.83	7.32	8.06 %	7.00 %	0.45	0.48	0.21	0.53	0.66	1.01
HRSG	8.33	10.28	9.82 %	9.83 %	0.55	0.68	1.33	1.18	1.87	1.86
Stream Bifurcation	0.13	X	0.15 %	X	0.00	X	0.00	X	0.00	X
HEX	0.92	1.52	1.08 %	1.46 %	0.00	0.00	0.05	0.07	0.05	0.07
Steam Turbine	5.76	5.05	6.80 %	4.83 %	1.17	0.98	0.01	0.01	1.18	0.99
Condenser	14.09	18.06	16.62 %	17.27 %	0.00	0.00	0.01	0.02	0.01	0.02
Pump	0.29	0.20	0.34 %	0.19 %	0.07	0.05	0.02	0.03	0.09	0.08
Total	84.77	104.57 (+ 19.8)	100 %	100 %	4.07	4.47 (+ 0.4)	3.24	3.86 (+ 0.62)	7.30	8.32 (+1.02)

According to Table 4.7, the optimized design takes on higher values for all the decision variables, resulting in a greater investment cost (+18.9 %) and NPV (+946.8 %). Likewise, the resultant PBP, IRR and LEC are far more interesting than those of the base design.

From table 4.8 one can infer that the system efficiencies (1st and 2nd law) and electrical power output are also superior, with increases of 6.83 %, 7.15 % and 76.6 % on an annual average basis. On the other hand, the heat input increases by 32.09 % and the solar share decreases by 7.69 %, thus the increase on the CO_2 emissions is quite significant (up to 60.9 % during Summer), which reveals the poor environmental performance of this design.

Similarly to what occurred in scenario #1, the higher isentropic efficiencies of the compressor, turbines, and pump result in lower values of exergy destruction and associated costs ($\dot{C}_{D,k}$) for these components. However, there is a substantial increase in the correspondent investment plus operation and maintenance cost rates ($\dot{Z}_k$), which ultimately results in higher total cost rates for the compressor and gas turbine. At the same time, there is more heat being absorbed by the solar receiver and generated by the combustor, and so more exergy is being destroyed within these two components. The global trend is that the system exergy destruction and total cost rate increase by up to 23.4 % and 14 %, respectively. This is due to the higher scale of the optimized design, with its greater compression ratio, components isentropic efficiencies, gas turbine temperature inlet, solar collector area, heat input and electrical power output.

4.4.3.3 Scenario #3 – Environmental criteria

As previously mentioned, sustainability is a major motivation of this work. Therefore, a third MOO was conducted to understand which model (with or without regenerator) could possibly achieve a better environmental performance, *i.e.*, less pollutant emissions. For this matter, the "maximize NPV" objective function was replaced with "maximize $m_{co_2\ saved}$". The results, which can be consulted in Annex B, reveal that the model with regenerator can achieve greater CO_2 emissions savings under specific operating conditions, implying that it can be a "greener" design. However, this environmental superiority is not extremely significant: up to 8 % greater savings for the same investment cost. Furthermore, these specific operating conditions are far from optimal from the thermoeconomical point of view ($r{\sim}0.7$), resulting in lesser net present values without practical interest. Under more interesting operating conditions, the difference between the CO_2 emissions savings for both models becomes irrelevant, and so this should not be a selection criterion between models. For this reason, the focus on the model without regenerator was maintained, given its proven superiority for the already studied criteria.

As previously described, the system solar share assumes a steep decreasing trend for the initial subjects (see fig. 4.6) down to the minimum value of 50 %, where it stabilizes since solutions with lower f_{sol} are automatically discarded by the algorithm. Similarly, the behaviour of $m_{co_2\ saved}/C_{inv}$ reveals that the first individuals yield a larger yearly amount of CO_2 savings relatively to its investment cost (see fig. 4.8). It is interesting to realize that for the first 24 subjects, the Net Present Value greatly increases while the amount of CO_2 emitted and respective savings do not change much (see fig. 4.8). This last behaviour is strongly related to the evolution of A_{col}. Looking at figures 4.6 and 4.8, subject **# 23** was selected as the optimized design for this scenario, given that it boasts a great environmental performance for an interesting net present value and investment cost.

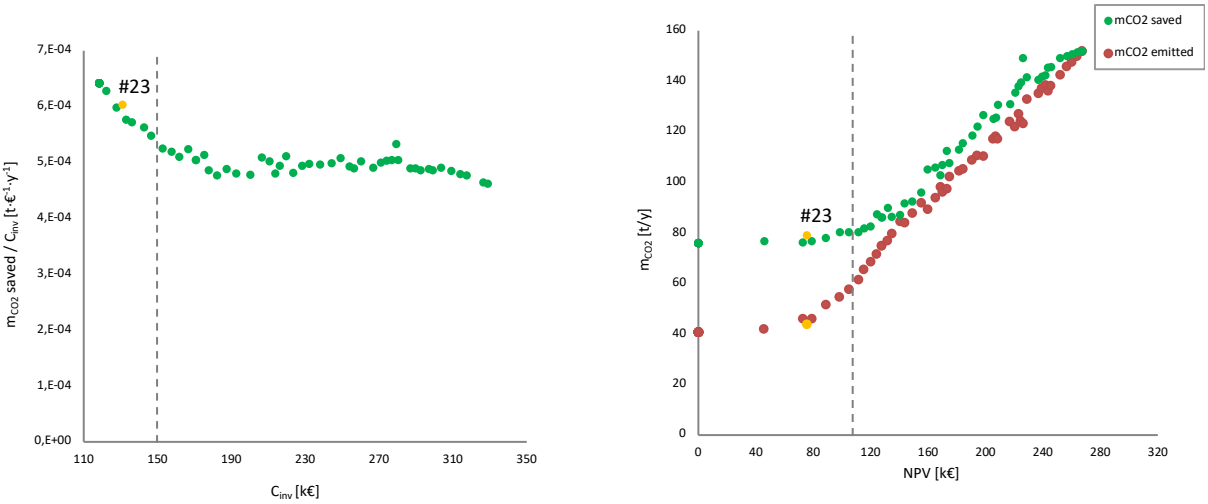

Figure 4. 8 Relative CO_2 emissions of Pareto-optimal solutions

Table 4. 13 Genes, fitness value and economical performance indicators – base design vs subject #23

	Base case	***Optimized case***
Optimization variables / Genes		
p_r	6.6	6.44
r	0.01	X
T_5 $[K]$	825	802.44
A_{reg} $[m^2]$	6	X
T_{14} $[K]$	550	575
A_{col} $[m^2]$	200	208.04
η_{comp} [%]	79.6 %	83.64 %
η_{GT} [%]	85.8 %	87.98 %
η_{ST} [%]	68 %	74.47 %
η_{pump} [%]	60 %	63.12 %
Objective functions / Fitness values		
C_{inv} [€]	153,192.7	131,102.5 (- 22,090.2)
NPV [€]	13,420.4	75,690.7 (+ 62,270.3)
Performance indicators		
PBP [y]	10	7 (- 3)
IRR [%]	8.99 %	14.14 % (+ 5.15%)
LEC [€/kWh]	0.211	0.168 (- 0.043)

Table 4. 14 Seasonal comparison of performance indicators - base design vs subject # 23

	Summer		Fall		Winter		Spring	
	Base case	Optimized case	Base case	Optimized case	Base case	Optimized case	Base case	Optimized case
η_{global} [%]	20.26%	22.63% (+2.37%)	20.26%	22.63% (+2.37%)	20.26%	22.63% (+2.37%)	20.26%	22.63% (+2.37%)
ε_{global} [%]	26.22%	30.37% (+4.15%)	25.70%	29.72% (+4.02%)	24.71%	28.48% (+3.77%)	25.22%	29.11% (+3.89%)
$\dot{P}_{el}$ [kW]	30.07	31.89 (+1.82)	30.47	32.23 (+1.76)	32.45	34.12 (+1.67)	31.96	33.75 (+1.78)
$\dot{Q}_{input}$ [kW]	154.62	146.83 (-7.78)	156.68	148.36 (-8.31)	166.85	157.08 (-9.77)	164.37	155.36 (-9.02)
f_{sol} [%]	62.95%	68.95% (+6%)	59.55%	65.42% (+5.87%)	53.70%	59.33% (+5.63%)	57.51%	63.29% (+5.78%)
$m_{co_2\ emitted}$ [kg/h]	11.58	9.22 (-2.36)	12.81	10.37 (-2.44)	15.61	12.91 (-2.70)	14.12	11.53 (-2.59)
$m_{co_2\ saved}$ [kg/h]	19.67	20.46 (+0.79)	18.86	19.62 (+0.76)	18.11	18.83 (+0.73)	19.10	19.87 (+0.77)

Table 4. 15 System cost rates, Summer season - base design vs subject # 23

Component (k)	$\dot{E}_{x_{d,k}}$ [kW]		$\dot{E}_{x_{d,k}}/\dot{E}_{x_{d,syst}}$ [%]		$\dot{C}_{D,k}$ [€/h]		$\dot{Z}_k$ [€/h]		$\dot{C}_{D,k} + \dot{Z}_k$ [€/h]	
	Base case	Optimized case	Base case	Optimized case	Base case	Optimized case	Base case	Optimized case	Base case	Optimized case
Compressor	9.25	6.96	11.40	9.89	0.67	0.49	0.13	0.19	0.80	0.68
Regenerator	0.54	X	0.67	X	0.04	X	0.13	X	0.16	X
Solar Receiver	11.80	12.80	14.54	18.20	0.00	0.00	1.30	1.35	1.30	1.35
Combustor	23.66	19.18	29.16	27.29	0.95	0.77	0.05	0.04	0.99	0.81
Gas Turbine	6.75	5.66	8.32	8.04	0.44	0.35	0.20	0.30	0.64	0.66
HRSG	8.22	7.12	10.13	10.13	0.54	0.44	1.26	0.69	1.80	1.13
Stream Bifurcation	0.12	X	0.15	X	0.00	X	0.00	X	0.00	X
HEX	0.91	2.54	1.12	3.62	0.00	0.00	0.05	0.08	0.05	0.08
Steam Turbine	5.69	3.50	7.01	4.98	1.08	0.59	0.01	0.01	1.09	0.60
Condenser	13.92	12.35	17.15	17.57	0.00	0.00	0.01	0.01	0.01	0.01
Pump	0.28	0.19	0.35	0.27	0.07	0.04	0.02	0.02	0.09	0.06
Total	81.15	70.30 (-10.85)	100	100	3.79	2.69 (-1.1)	3.14	2.70 (-0.44)	6.93	5.39 (-1.54)

Table 4. 16 System cost rates, Fall season - base design vs subject # 23

Component (k)	$\dot{E}_{x_{d,k}}$ [kW]		$\dot{E}_{x_{d,k}}/\dot{E}_{x_{d,syst}}$ [%]		$\dot{C}_{D,k}$ [€/h]		$\dot{Z}_k$ [€/h]		$\dot{C}_{D,k} + \dot{Z}_k$ [€/h]	
	Base case	Optimized case	Base case	Optimized case	Base case	Optimized case	Base case	Optimized case	Base case	Optimized case
Compressor	9.23	6.92	11.18	9.68	0.69	0.50	0.13	0.20	0.82	0.70
Regenerator	0.54	X	0.66	X	0.04	X	0.13	X	0.16	X
Solar Receiver	11.06	12.00	13.40	16.79	0.00	0.00	1.30	1.35	1.30	1.35
Combustor	25.90	21.35	31.39	29.87	1.04	0.86	0.05	0.05	1.08	0.90
Gas Turbine	6.73	5.62	8.16	7.87	0.45	0.36	0.20	0.31	0.65	0.67
HRSG	8.20	7.08	9.94	9.91	0.55	0.46	1.27	0.69	1.82	1.15
Stream Bifurcation	0.12	X	0.15	X	0.00	X	0.00	X	0.00	X
HEX	0.90	2.53	1.09	3.54	0.00	0.00	0.05	0.08	0.05	0.08
Steam Turbine	5.68	3.48	6.88	4.87	1.12	0.62	0.01	0.01	1.13	0.63
Condenser	13.88	12.29	16.82	17.19	0.00	0.00	0.01	0.01	0.01	0.01
Pump	0.28	0.19	0.34	0.26	0.07	0.04	0.02	0.02	0.09	0.06
Total	82.54	71.46 (-11.08)	100	100	3.96	2.84 (-1.12)	3.16	2.71 (-0.45)	7.13	5.55 (-1.58)

Table 4. 17 System cost rates, Winter season - base design vs subject # 23

Component (k)	$\dot{E}_{x_{d,k}}$ [kW]		$\dot{E}_{x_{d,k}}/\dot{E}_{x_{d,syst}}$ [%]		$\dot{C}_{D,k}$ [€/h]		$\dot{Z}_k$ [€/h]		$\dot{C}_{D,k} + \dot{Z}_k$ [€/h]	
	Base case	Optimized case	Base case	Optimized case	Base case	Optimized case	Base case	Optimized case	Base case	Optimized case
Compressor	9.36	6.98	10.80	9.32	0.70	0.52	0.14	0.21	0.84	0.72
Regenerator	0.55	X	0.63	X	0.04	X	0.13	X	0.16	X
Solar Receiver	10.01	10.86	11.55	14.50	0.00	0.00	1.30	1.35	1.30	1.35
Combustor	30.42	25.58	35.10	34.15	1.22	1.03	0.05	0.05	1.27	1.07
Gas Turbine	6.83	5.68	7.89	7.58	0.46	0.38	0.22	0.32	0.68	0.70
HRSG	8.33	7.15	9.60	9.54	0.56	0.47	1.34	0.73	1.91	1.20
Stream Bifurcation	0.13	X	0.15	X	0.00	X	0.00	X	0.00	X
HEX	0.92	2.55	1.06	3.41	0.00	0.00	0.05	0.08	0.05	0.08
Steam Turbine	5.76	3.51	6.65	4.69	1.22	0.68	0.01	0.01	1.23	0.69
Condenser	14.09	12.40	16.25	16.55	0.00	0.00	0.01	0.01	0.01	0.01
Pump	0.29	0.19	0.33	0.25	0.08	0.04	0.02	0.02	0.10	0.06
Total	86.68	74.90 (-11.78)	100	100	4.29	3.11 (-1.17)	3.26	2.78 (-0.48)	7.54	5.90 (-1.64)

Table 4. 18 System cost rates, Spring season - base design vs subject # 23

Component (k)	$\dot{E}_{x_{d,k}}$ [kW]		$\dot{E}_{x_{d,k}}/\dot{E}_{x_{d,syst}}$ [%]		$\dot{C}_{D,k}$ [€/h]		$\dot{Z}_k$ [€/h]		$\dot{C}_{D,k} + \dot{Z}_k$ [€/h]	
	Base case	Optimized case	Base case	Optimized case	Base case	Optimized case	Base case	Optimized case	Base case	Optimized case
Compressor	9.36	7.01	11.05	9.55	0.68	0.50	0.13	0.21	0.81	0.71
Regenerator	0.55	X	0.65	X	0.04	X	0.13	X	0.16	X
Solar Receiver	10.80	11.72	12.74	15.97	0.00	0.00	1.30	1.35	1.30	1.35
Combustor	27.72	23.03	32.70	31.39	1.11	0.92	0.05	0.05	1.16	0.97
Gas Turbine	6.83	5.70	8.06	7.77	0.45	0.36	0.21	0.32	0.66	0.68
HRSG	8.33	7.18	9.82	9.78	0.55	0.46	1.33	0.72	1.87	1.18
Stream Bifurcation	0.13	X	0.15	X	0.00	X	0.00	X	0.00	X
HEX	0.92	2.56	1.08	3.50	0.00	0.00	0.05	0.08	0.05	0.08
Steam Turbine	5.76	3.53	6.80	4.81	1.17	0.65	0.01	0.01	1.18	0.66
Condenser	14.09	12.45	16.62	16.97	0.00	0.00	0.01	0.01	0.01	0.01
Pump	0.29	0.19	0.34	0.26	0.07	0.04	0.02	0.02	0.09	0.06
Total	84.77	73.36 (-11.41)	100	100	4.07	2.93 (-1.14)	3.24	2.77 (-0.47)	7.30	5.70 (-1.6)

According to table 4.13, the optimized case takes on higher values for most decision variables, except for the compression ratio and gas turbine inlet temperature which decrease, even though the respective investment cost is lower (-14.4 %) and the *NPV* is substantially higher (+464 %). This is due to the elimination of the regenerator associated costs. Likewise, the resultant PBP, IRR and LEC are far more interesting than those of the base design.

From table 4.14 one can infer that the system efficiencies (1st and 2nd law) are also superior, with respective increases of 2.37 % and 3.96 %, on an annual average basis. The gas turbine inlet temperature is minimized, greatly reducing the need for heat generation inside the combustor, which results in solar shares of up to 69 % during Summer. A reduction of 20.4 % in CO_2 emissions is achieved

for this season, evidencing the superior environmental performance of the design. Lower heat generation inside the combustor is compensated by a larger area of solar collectors, as well as higher steam turbine inlet temperature and components isentropic efficiencies, ultimately resulting in an even higher electrical power output (by roughly 5.63 %), for a total heat input that is 5.43 % lower, on an annual average basis.

In this scenario, the reduction of the cost rates due to exergy destruction ($\dot{C}_{D,k}$) of the compressor, turbines, and pump tend to overcompensate the increase of the respective cost rates due to capital investments plus operation and maintenance ($\dot{Z}_k$), similarly to what occurred in scenario #1. The outcome is a reduction of the total cost rate for most of these components, except for the gas turbine. At the same time, the solar receiver is absorbing more heat while the combustor is generating less heat, so it is expected that the exergy destruction and total cost rate of these components increase and decrease, respectively. Globally, the optimized design results in a reduction of the system exergy destruction and total cost rate by up to 13.6 % and 22.2 %, respectively.

4.4.3.4 Comparative remarks

Figure 4.9 and table 4.19 summarize the results of each scenario. In figure 4.9, the parameters have been normalized to facilitate comparison, and the thermodynamic/environmental indicators, which change seasonally, have been averaged over the four representative days. As one can clearly see, scenario #2 is the most costly by a large amount, but it also yields the greatest thermodynamic performance, as expected. However, its environmental performance is quite poor. Comparing to the base design, scenario #1 yields a similar investment cost for a far better thermodynamic and economic performance, even though its environmental performance is worse. Finally, scenario #3 is the only one that outperforms the base design in every parameter, with a remarkably better environmental performance.

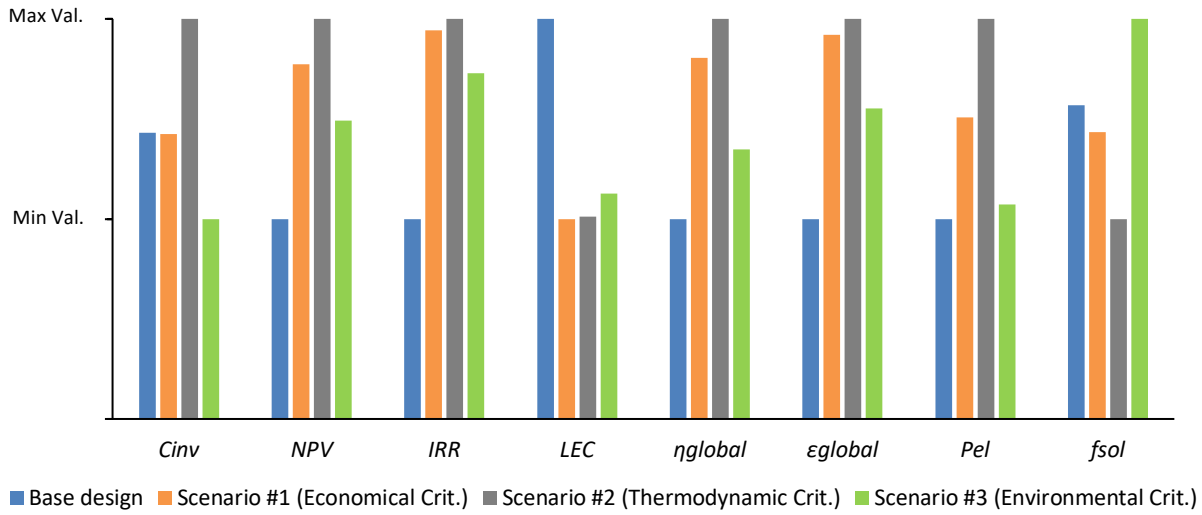

Figure 4. 9 Comparison of different scenarios regarding normalized fitness values and performance indicators

Table 4. 19 Genes, fitness values and performance indicators of different scenarios

		Optimized designs		
	Base design	***Scenario #1 (Economic criteria)***	***Scenario #2 (Thermodynamic criteria)***	***Scenario #3 (Environmental criteria)***
Decision variables / Genes				
p_r	6.6	6.58	7.97	6.44
r	0.01		X	
T_5 $[K]$	825	843.72	867.04	802.44
A_{reg} $[m^2]$	6		X	
T_{14} $[K]$	550	575	575	575
A_{col} $[m^2]$	200	211.78	229.36	208.04
η_{comp} [%]	79.6	85.34	85.39	83.64
η_{GT} [%]	85.8	88.53	88.72	87.98
η_{ST} [%]	68	74.66	74.88	74.47
η_{pump} [%]	60	67.56	70.05	63.12
Objective functions / Fitness values				
C_{inv} [€]	153,192.7	152,858.1	182,221	131,102.5
NPV [€]	13,420.4	111,584.9	140,483.9	75,690.7
Performance indicators				
PBP [y]	10	7	7	7
IRR [%]	8.99	15.66	16.06	14.14
LEC [€/kWh]	0.211	0.161	0.162	0.168
η_{global} [%] *	20.26	25.76	27.08	22.63
ε_{global} [%] *	25.46	32.04	32.61	29.42
$\dot{P}_{el}$ [kW] *	31.24	43.40	55.16	33.00
$\dot{Q}_{input}$ [kW] *	160.63	175.53	212.18	151.91
f_{sol} [%] *	58.43	56.60	50.73	64.25
$\dot{m}_{co_2\ emitted}$ [kg/h] *	13.53	15.42	21.17	11.01
$\dot{m}_{co_2\ saved}$ [kg/h] *	18.93	20.05	21.71	19.70
$\dot{E}_{x_{d,system}}$[kW] *	83.79	83.68	103.52	72.51
$\dot{C}_{D,system} + \dot{Z}_{k,system}$ [€/h]*	7.23	6.58	8.22	5.64

*Annual average basis

Chapter 5

Concluding remarks

5.1 Conclusions

A thermoeconomical model for a hybrid solar-thermal power plant was developed in a MatLab® environment and used to conduct a multi-objective optimization of the system. The initially proposed model consisted of a combined cycle with a solar receiver and a natural-gas-fired combustor coupled in series, and a regenerator pre-heating the topping cycle fluid after the compressor.

A preliminary analysis was conducted in order to analyze the system thermodynamic performance under different conditions. Results revealed that a bottoming high temperature organic Rankine cycle is an interesting solution, with the fluid pair CO_2 and Cyclopentane emerging as the best option. Furthermore, the system appears to achieve maximum 1st and 2nd law efficiencies for a mass flow ratio of $r = 0.01$ ($\eta = 20.26\,\%$ and $\varepsilon = 26.22\,\%$ during Summer), while yielding peak net work outputs for mass flow ratios of around 0.35 ($\dot{W}_{net} = 36.82\ \mathrm{kW}$ during Winter and for a solar collector area of $200\ \mathrm{m^2}$), depending on the season. This was the first indication that the valve and regenerator might be dispensable depending on the system's objective. The 1st law efficiency is directly constrained by the user-defined gas turbine inlet temperature and compression ratio, so it does not vary seasonally, while the 2nd law efficiency peaks during Summer and the net work output during Winter. Additionally, this initial study provided a basis of comparison with the optimized designs resulting from the multi-objective optimization that followed.

Succeeding this simplifying analysis, a MOO was conducted in order to find a set of Pareto-optimal solutions. Results provide evidence that the performance of the system would benefit from the complete elimination of the valve and regenerator, redirecting the entirety of the topping cycle turbine outlet gas to the HRSG. Optimized designs yield 1st and 2nd law efficiencies within the ranges of 16.46 - 27.97 % and 21.49 - 33.53 %, respectively, which represents a great improvement comparing to the peak values achieved with the base design: 20.26 % and 26.22 %, respectively. Additionally, resultant electricity generation costs fall within the range of 0.159 – 0.221 €/kWh, which corresponds to 0.179 – 0.248 USD/kWh according to the considered conversion rate. These results reveal that the optimized system can yield similar or lower costs of electricity generation than conventional stand-alone CSP systems, which take on typical LEC values of 0.182 USD/kWh [11]. However, from a strictly economic

point of view, it clearly falls behind when compared to standard natural-gas-fired combined cycle power plants, whose LEC characteristically falls within the range of 0.044 – 0.073 USD/kWh [63]. The environmental performance of Pareto-optimal designs can be considerably better, with average solar shares between 50 % and 65 % as opposed to roughly 58.4 % for the base design, and saved CO_2 emissions of up to 152 tons/year for the most expensive solution.

In the decision-making process, three optimized designs were selected, each of them corresponding to the most suitable solution for three different scenarios. The first consists of a solution based on economic criteria and represents an interesting choice for an investor who is focused on financial return. The chosen design yields a Net Present Value of 111,585 €, which comparing to the base design represents an increase of 98,165 € (731.5 %), for an initial investment that is 0.2 % lower (152,858 €). Furthermore, the project becomes profitable after 7 years, which is 3 years earlier than the base design, the Internal Rate of Return is 6.66 % higher and the LEC assumes the competitive value of 0.161 €/kWh. Even with a significantly higher power output, the total exergy destruction of the system remains virtually unchanged and its total cost rates are reduced by up to 9.3 %, depending on the season. The biggest downside of this solution is the lower solar share (1.83 % reduction on an annual average basis) and consequential higher CO_2 emissions (annual average increase of 14.01 %) comparing to the base case.

The second scenario focuses on thermodynamic criteria and idealizes a probable option for an investor whose decision making is highly constrained by funds and available land, and whose objective is to maximize generation power ($\dot{P}_{el}$). The resultant investment cost is almost 19 % higher (182,221 €), but the Net Present Value and generated power are also much greater, with respective percentual increases of 946.8 % (140,484 €) and 76.6 % (55.16 kW) on an annual average basis. The economic performance of this design is generally good, but the system exergy destruction and cost rates are up to 23.4 % and 14 % greater (depending on the season) than those of the base case, respectively. This is due to the higher scale of the system, with its remarkably higher compression ratio, components isentropic efficiencies, gas turbine temperature inlet, and solar collector area, which also explains the much greater electrical power output. At the same time, it assumes a quite poor environmental performance, with solar shares as low as 46.5 % and CO_2 emissions as high as 23.88 kg/h during Winter, representing deviations from the base case of -7.2 % and +53 %, respectively.

The third scenario emphasizes environmental criteria, prioritizing a greener design. Results reveal that the chosen solution is better than the base case for all the thermodynamic, economic, and environmental indicators considered in this work. The Net Present Value of 75,691 €, representing an increase of 464 %, is achieved for a lower investment cost of 131,103 € (-14.4 %). The gas turbine inlet temperature is minimized, greatly reducing the mass of burnt fuel and thus achieving solar shares of up to 69 % in Summer. A reduction of 20.4 % in CO_2 emissions is achieved for this season, evidencing the superior environmental performance of the design. Lower heat generation inside the combustor is compensated by a larger area of solar collectors, as well as higher steam turbine inlet temperature and component isentropic efficiencies, ultimately resulting in an even higher electrical power output. Globally, the system exergy destruction and total cost rate are reduced by up to 13.6 % and 22.2 %, respectively, depending on the season.

Results of this thesis reinforce the already established idea that CSP and fossil fuel hybrid electricity generation units offer great advantages for systems of large and small scale. The optimized system could have important applications such as providing reliable, dispatchable, and partially green electricity to off-grid communities.

5.2 Future work

This study provided interesting results regarding the system performance under different conditions. However, some pertinent simplifications were considered for the development of the energy/exergy, seasonal and costing models. A more in-depth analysis of the proposed model would be relevant. The author presents the following suggestions for future work around this or similar models:

- A more realistic analysis of the system would require a thorough thermodynamic and economic model for the solar receiver, considering diverse operating conditions and parameters such as the concentration ratio, receiver surface characteristics and heat transfer process between the receiver and working medium. Additionally, other CSP technologies capable of achieving higher temperature solar heat such as solar towers and parabolic dish collectors should be considered.

- This thesis lacks a transient hourly analysis of the system. Such study would provide important results that could serve as powerful tools for comparison with real systems, including operating stand-alone solar power plants.

- The MOOs conducted in the current work employ economical indicators as objective functions, while other important thermodynamic, economical, and environmental indicators are only considered in the post-computation phase. Interesting results could be taken from different approaches such as a joint thermoeconomic and environmental optimization by internalizing CO_2 emissions in the costing model, for example.

References

[1] J.A.M. Rodrigues, "Hybrid Solar Thermal Power Plants", Msc. thesis, Dept. Mech. Eng., Instituto Superior Técnico, Lisbon, Portugal, 2019.

[2] S. Leahy, "Climate change driving entire planet to dangerous 'tipping point'", Natl. Geogr. Mag. (2019). https://www.nationalgeographic.com/science/2019/11/earth-tipping-point/ (accessed Nov. 3, 2020).

[3] NASA, Global Temperature, (2019). https://climate.nasa.gov/vital-signs/global-temperature/ (accessed November 23, 2020).

[4] IEA, "Our World in Data". https://ourworldindata.org/ (accessed November 3, 2020).

[5] IEA, "World Energy Outlook 2019", 2019. https://www.iea.org/reports/world-energy-outlook-2019 (accessed November 3, 2020).

[6] IEA, CO2 emissions by sector, (n.d.). https://www.iea.org/data-and-statistics?country=WORLD&fuel=CO2 emissions&indicator=CO2BySector (accessed November 23, 2020).

[7] F. Martins, C. Felgueiras, M. Smitkova, N. Caetano, "Analysis of fossil fuel energy consumption and environmental impacts in european countries", Energies 12 (2019) 1–11.

[8] IEA, "Electricity generation by fuel and scenario", (n.d.). https://www.iea.org/data-and-statistics/charts/electricity-generation-by-fuel-and-scenario-2018-2040 (accessed June 24, 2020).

[9] M.P. Boyce, "Combined cycle power plants", in *Combined Cycle Systems for near-Zero Emission Power Generation*, Woodhead publishing, 2012, ch. 1, pp. 1–43.

[10] M.B.B. Michael J. Moran, Howard N. Shapiro, Daisie D. Boettner," Fundamentals Of Engineering Thermodynamics", John Wiley & Sons, 8th ed., 2014.

[11] IRENA, "Solar Energy" (n.d.). https://www.irena.org/solar (accessed June 24, 2020).

[12] G.J. Nathan, M. Jafarian, B.B. Dally, W.L. Saw, P.J. Ashman, E. Hu, A. Steinfeld, "Solar thermal hybrids for combustion power plant: A growing opportunity", Progress in Energy and Combustion Science 64 (2018) 4–28.

[13] Renewable Energy World, "How solar PV is winning over CSP", (2013). https://www.renewableenergyworld.com/2013/03/12/how-solar-pv-is-winning-over-csp/#gref (accessed January 19, 2021).

[14] SolarPACES, "CSP projects around the world", (n.d.). https://www.solarpaces.org/csp-technologies/csp-projects-around-the-world/ (accessed June 30, 2020).

[15] J. Reca-Cardena, R. López-Luque, "Design Principles of Photovoltaic Irrigation Systems", Advanced Renewable Energies Power Technologies 1 (2018) 295–333.

[16] S. Dabiri, M.F. Rahimi, "Basic introduction of solar collectors and energy and exergy analysis of a heliostat plant", The 3rd International Conference and Exhibition of Solar Energy. (2016).

[17] X. Xu, K. Vignarooban, B. Xu, K. Hsu, A.M. Kannan, "Prospects and problems of concentrating solar power technologies for power generation in the desert regions", Renewable and Sustainable Energy Reviews 53 (2016) 1106–1131.

[18] E.Z. Moya, "Parabolic-trough concentrating solar power (CSP) systems", in: *Concentrating Solar Power Technology - Principles, Developments and Applications*, Woodhead publishing, 2012, ch. 7, pp. 197–239.

[19] M. Geyer, E. Lüpfert, R. Osuna, P. Nava, J. Langenkamp, E. Mandelberg, "EUROTROUGH - Parabolic Trough Collector Developed for Cost Efficient Solar Power Generation", presented at: 11th SolarPACES International Symposium on Concentrating Solar Power Chemical Energy Technologies, Zurich, Switzerland, Sep. 4-6, 2002.

[20] E. Bellos, C. Tzivanidis, K.A. Antonopoulos, I. Daniil, "The use of gas working fluids in parabolic trough collectors – An energetic and exergetic analysis", Applied Thermal Engineering 109 (2016) 1–14.

[21] H. Olia, M. Torabi, M. Bahiraei, M.H. Ahmadi, M. Goodarzi, M.R. Safaei, "Application of nanofluids in thermal performance enhancement of parabolic trough solar collector: State-of-the-art", Appl. Sci. 9 (2019).

[22] L.L. Vant-Hull, "Central tower concentrating solar power (CSP) systems", in: *Concentrating Solar Power Technology - Principles, Developments and Applications*, Woodhead publishing, 2012, ch. 8, pp. 240–283.

[23] MI-NET, "New Methods and Results for the Optimisation of Solar Power Tower Plants", (2017). https://mi-network.org/2017/08/21/new-methods-and-results-for-the-optimisation-of-solar-power-tower-plants/ (accessed June 30, 2020).

[24] D.R. Mills, "Linear Fresnel Reflector (LFR) technology", in: *Concentrating Solar Power Technology - Principles, Developments and Applications*, Woodhead publishing, 2012 pp. 153–196.

[25] T.K. W. Schiel, "Parabolic dish concentrating solar power (CSP) systems", in: *Concentrating Solar Power Technology - Principles, Developments and Applications*, Woodhead publishing, 2012, ch.9, pp. 284–322.

[26] J. Spelling, "Hybrid Solar Gas-Turbine Power Plants - A Thermoeconomic Analysis", Phd. thesis, Dept. En. Tech., KTH Royal Institute of Technology, Stockholhm, Sweden, 2013.

[27] M. Livshits, A. Kribus, "Performance and water consumption of the solar steam-injection gas turbine cycle", J. Sol. Energy Eng. Trans. ASME. 135 (2013) 1–7.

[28] R. Buck, T. Bräuning, T. Denk, M. Pfänder, P. Schwarzbözl, F. Tellez, "Solar-hybrid gas turbine-based power tower systems (REFOS)", J. Sol. Energy Eng. Trans. ASME. 124 (2002) 2–9.

[29] K.M. Powell, K. Rashid, K. Ellingwood, J. Tuttle, B.D. Iverson, "Hybrid concentrated solar thermal power systems: A review", Renew. Sustain. Energy Rev. 80 (2017) 215–237.

[30] L. Aichmayer, J. Spelling, B. Laumert, "Preliminary design and analysis of a novel solar receiver for a micro gas-turbine based solar dish system", Solar Energy 114 (2015) 378–396.

[31] H. G. Jin, H. Hong, "Hybridization of concentrating solar power (CSP) with fossil fuel power plants", in: *Concentrating Solar Power Technology - Principles, Developments and Applications*, Woodhead publishing, 2012, ch. 12, pp. 395–420.

[32] A. Bejan, G. Tsatsaronis, M. Moran, "Thermal Design and Optimization", John Wiley & Sons , 1996.

[33] A. Lazzaretto, G. Tsatsaronis, "SPECO: A systematic and general methodology for calculating efficiencies and costs in thermal systems", Energy 31 (2006) 1257–1289.

[34] G. Leyland, "Multi-objective optimisation applied to industrial energy problems", Phd. thesis, Dept. Mech. Eng., *École Polytechnique Fédérale de Lausanne,* Switzerland, 2002.

[35] E. Zitzler, K. Deb, L. Thiele, "Comparison of multiobjective evolutionary algorithms: empirical results"., Evoutionary Computation 8 (2000) 173–195.

[36] M.T. Dunham, W. Lipiński, "Thermodynamic analyses of single Brayton and combined Brayton-Rankine cycles for distributed solar thermal power generation", J. Sol. Energy Eng. Trans. ASME. 135 (2013).

[37] A. Baghernejad, M. Yaghoubi, "Exergoeconomic analysis and optimization of an Integrated Solar Combined Cycle System (ISCCS) using genetic algorithm", Energy Convers. Manag. 52 (2011) 2193–2203.

[38] A. Baghernejad, M. Yaghoubi, "Thermoeconomic methodology for analysis and optimization of a hybrid solar thermal power plant", Int. J. Green Energy. 10 (2013) 588–609.

[39] A. Baghernejad, M. Yaghoubi, "Multi-objective exergoeconomic optimization of an Integrated Solar Combined Cycle System using evolutionary algorithms", Int. J. Energy Res. 35 (2011) 601–615.

[40] J.Q. Wu, D.F. Zhu, H. Wang, Y. Zhu, "Exergetic analysis of a solar thermal power plant", Adv. Mater. Res. 724–725 (2013) 156–162.

[41] M. Ameri, P. Ahmadi, A. Hamidi, "Energy, exergy and exergoeconomic analysis of a steam power plant: A case study", Int. J. Energy Res. 33 (2009) 499–512.

[42] E. Pihl, J. Spelling, F. Johnsson, "Thermo-economic optimization of hybridization options for

solar retrofitting of combined-cycle power plants", J. Sol. Energy Eng. Trans. ASME. 136 (2014) 1–9.

[43] J. Pye, G. Morrison, M. Behnia, "Pressure drops for direct steam generation in line-focus solar thermal systems", Aust. New Zeal. Sol. Energy Soc. Conf. (2006).

[44] G. Angelino, C. Invernizzi, "Experimental investigation on the thermal stability of some new zero ODP refrigerants", Int. J. Refrig. 26 (2003) 51–58.

[45] L. Calderazzi, P. Colonna di Paliano, "Thermal stability of R-134a, R-141b, R-13I1, R-7146, R-125 associated with stainless steel as a containing material", Int. J. Refrig. 20 (1997) 381–389.

[46] N.A. Lai, M. Wendland, J. Fischer, "Working fluids for high-temperature organic Rankine cycles", Energy. 36 (2011) 199–211.

[47] R. Rayegan, Y.X. Tao, "A procedure to select working fluids for Solar Organic Rankine Cycles (ORCs)", Renewable Energy 36 (2011) 659-670.

[48] A. Algieri, P. Morrone, "Comparative energetic analysis of high-temperature subcritical and transcritical Organic Rankine Cycle (ORC). A biomass application in the Sibari district", Appl.Therm. Eng. 36 (2012) 236–244.

[49] C.M. Invernizzi, P. Iora, G. Manzolini, S. Lasala, "Thermal stability of n-pentane, cyclo-pentane and toluene as working fluids in organic Rankine engines", Appl. Therm. Eng. 121 (2017) 172–179.

[50] D. Maraver, J. Uche, J. Royo, "Assessment of high temperature organic Rankine cycle engine for polygeneration with MED desalination: A preliminary approach", Energy Convers. Manag. 53 (2012) 108–117.

[51] R. Vescovo, E. Spagnoli, "High Temperature ORC Systems", Energy Procedia. 129 (2017) 82–89.

[52] U. Drescher, D. Brüggemann, "Fluid selection for the Organic Rankine Cycle (ORC) in biomass power and heat plants", Appl. Therm. Eng. 27 (2007) 223–228.

[53] P. Garg, P. Kumar, K. Srinivasan, P. Dutta, "Evaluation of isopentane, R-245fa and their mixtures as working fluids for organic Rankine cycles", Appl. Therm. Eng. 51 (2013) 292–300.

[54] B. J. McBride, M. J. Zehe, S. Gordon, "NASA Glenn coefficients for calculating thermodynamic properties of individual species", Glenn Research Center, Cleveland OH, USA, NASA/TP—2002-211556, Sep. 2002.

[55] V. Ganapathy, "Heat-recovery steam generators: Understand the basics", Chem. Eng. Prog. 92 (1996) 32–45.

[56] M.A. Neseli, O. Ozgener, L. Ozgener, "Energy and exergy analysis of electricity generation from natural gas pressure reducing stations", Energy Convers. Manag. 93 (2015) 109–120.

[57] S. Alharbi, M.L. Elsayed, L.C. Chow, "Exergoeconomic analysis and optimization of an integrated

system of supercritical CO2 Brayton cycle and multi-effect desalination", Energy. 197 (2020) 117-225.

[58] Z. Guo-Yan, W. En, T. Shan-Tung, "Techno-economic study on compact heat exchangers", Int. J. Energy Res. 32 (2008) 1119–1127.

[59] Y.M. El-Sayed, "Designing desalination systems for higher productivity", Desalination. 134 (2001) 129–158.

[60] J.A. Duffie (Deceased), W.A. Beckman, N. Blair, "Solar Engineering of Thermal Processes", Photovoltaics and Wind, 2020.

[61] C. Turchi, "Parabolic Trough Reference Plant for Cost Modeling with the Solar Advisor Model (SAM)", National Renewable Energy Laboratory (NREL), Golden CO, USA, NREL/TP-550-47605, July 2010.

[62] PORDATA, "Base de Dados Portugal Contemporâneo", (n.d.). https://www.pordata.pt (accessed July 3, 2020).

[63] Lazard, "Levelized Cost of Energy and Levelized Cost of Storage - 2020". "https://www.lazard.com/perspective/levelized-cost-of-energy-and-levelized-cost-of-storage-2020/" (accessed October 24, 2020).

Appendix A

A. Preliminary analysis complementary results

This appendix contains detailed results of the simulations conducted in chapter 3, complementing information presented in those sections. The outcomes of 5 simulations are presented, the first one under the previously defined standard conditions and the remaining 4 considering a seasonal representative day each.

A.1 Standard conditions

Table A. 1 Program inputs for the simulation, Standard conditions

G_0 $[W/m^2]$	T_{amb} $[K]$	p_r	r	T_5 $[K]$	A_{reg} $[m^2]$	T_{14} $[K]$	A_{col} $[m^2]$	η_{comp} [%]	η_{GT} [%]	η_{ST} [%]	η_{pump} [%]
1000	303	6.6	0.01	825	6	550	200	79.6	85.8	68	60

Table A. 2 Detailed results of the simulation, Standard conditions

State	Mass flow rate [kg/s]	Pressure [bar]	Temperature [K]	Specific enthalpy [kJ/kg]	Specific entropy [kJ/kg]	Specific flow exergy [kJ/kg]
1	0.471	1.000	308.000	514.280	2.767	0.035
2	0.471	6.600	489.081	682.335	2.839	147.185
3	0.471	6.468	490.730	684.054	2.846	146.662
4	0.471	6.145	781.412	1002.759	3.363	307.950
5	0.471	6.022	825.000	1053.868	3.431	338.543
6	0.471	1.041	646.366	850.398	3.485	118.504
7	0.466	1.041	646.366	850.398	3.485	118.504
8	0.466	1.020	320.170	524.803	2.797	1.560
9	0.005	1.041	646.366	850.398	3.485	118.504
10	0.005	1.020	489.081	684.195	3.195	40.325
11	0.471	1.020	322.003	526.402	2.802	1.649
12	0.187	1.000	308.000	-27.368	-0.087	0.076
13	0.187	20.000	309.523	-23.034	-0.081	2.708
14	0.187	19.600	550.000	785.514	1.791	244.124
15	0.187	1.020	486.364	671.569	1.904	95.842

A.2 Summer season

Table A. 3 Program inputs for the simulation, Summer season – Maximum efficiency scenario

G_0 $[W/m^2]$	T_{amb} $[K]$	p_r	r	T_5 $[K]$	A_{reg} $[m^2]$	T_{14} $[K]$	A_{col} $[m^2]$	η_{comp} [%]	η_{GT} [%]	η_{ST} [%]	η_{pump} [%]
672.15	300.7	6.6	0.01	825	6	550	200	79.6	85.8	68	60

Table A. 4 Detailed results of the simulation, Summer season – Maximum efficiency scenario

State	Mass flow rate [kg/s]	Pressure [bar]	Temperature [K]	Specific enthalpy [kJ/kg]	Specific entropy [kJ/kg]	Specific flow exergy [kJ/kg]
1	0.420	1.000	308.000	514.280	2.767	0.075
2	0.420	6.600	489.081	682.335	2.839	147.398
3	0.420	6.468	490.730	684.054	2.846	146.892
4	0.420	6.145	706.825	917.087	3.248	258.487
5	0.420	6.022	825.000	1053.868	3.431	340.140
6	0.420	1.041	646.366	850.398	3.485	120.226
7	0.416	1.041	646.366	850.398	3.485	120.226
8	0.416	1.020	320.170	524.803	2.797	1.670
9	0.004	1.041	646.366	850.398	3.485	120.226
10	0.004	1.020	489.081	684.195	3.195	41.367
11	0.420	1.020	322.003	526.402	2.802	1.771
12	0.167	1.000	308.000	-27.368	-0.087	0.164
13	0.167	20.000	309.523	-23.034	-0.081	2.809
14	0.167	19.600	550.000	785.514	1.791	248.623
15	0.167	1.020	486.364	671.569	1.904	100.608

Table A. 5 Program inputs for the simulation, Summer season – Maximum work output scenario

G_0 $[W/m^2]$	T_{amb} $[K]$	p_r	r	T_5 $[K]$	A_{reg} $[m^2]$	T_{14} $[K]$	A_{col} $[m^2]$	η_{comp} [%]	η_{GT} [%]	η_{ST} [%]	η_{pump} [%]
672.15	300.7	6.6	0.33	825	6	550	200	79.6	85.8	68	60

Table A. 6 Detailed results of the simulation, Summer season – Maximum work output scenario

State	Mass flow rate [kg/s]	Pressure [bar]	Temperature [K]	Specific enthalpy [kJ/kg]	Specific entropy [kJ/kg]	Specific flow exergy [kJ/kg]
1	0.539	1.000	308.000	514.280	2.767	0.075
2	0.539	6.600	489.081	682.335	2.839	147.398
3	0.539	6.468	540.637	735.568	2.946	168.190
4	0.539	6.145	706.825	917.087	3.248	258.487
5	0.539	6.022	825.000	1053.868	3.431	340.140
6	0.539	1.041	646.366	850.398	3.485	120.226
7	0.361	1.041	646.366	850.398	3.485	120.226
8	0.361	1.020	320.170	524.803	2.797	1.670
9	0.178	1.041	646.366	850.398	3.485	120.226
10	0.178	1.020	495.125	690.299	3.207	43.738
11	0.539	1.020	380.991	579.505	2.953	9.349
12	0.145	1.000	308.000	-27.368	-0.087	0.164
13	0.145	20.000	309.523	-23.034	-0.081	2.809
14	0.145	19.600	550.000	785.514	1.791	248.623
15	0.145	1.020	486.364	671.569	1.904	100.608

A.3 Fall season

Table A. 7 Program inputs for the simulation, Fall season – Maximum efficiency scenario

G_0 $[W/m^2]$	T_{amb} $[K]$	p_r	r	T_5 $[K]$	A_{reg} $[m^2]$	T_{14} $[K]$	A_{col} $[m^2]$	η_{comp} [%]	η_{GT} [%]	η_{ST} [%]	η_{pump} [%]
645.45	295.9	6.6	0.01	825	6	550	200	79.6	85.8	68	60

Table A. 8 Detailed results of the simulation, Fall season – Maximum efficiency scenario

State	Mass flow rate [kg/s]	Pressure [bar]	Temperature [K]	Specific enthalpy [kJ/kg]	Specific entropy [kJ/kg]	Specific flow exergy [kJ/kg]
1	0.426	1.000	308.000	514.280	2.767	0.203
2	0.426	6.600	489.081	682.335	2.839	147.871
3	0.426	6.468	490.730	684.054	2.846	147.399
4	0.426	6.145	695.745	904.566	3.230	253.661
5	0.426	6.022	825.000	1053.868	3.431	343.388
6	0.426	1.041	646.366	850.398	3.485	123.726
7	0.421	1.041	646.366	850.398	3.485	123.726
8	0.421	1.020	320.170	524.803	2.797	1.937
9	0.004	1.041	646.366	850.398	3.485	123.726
10	0.004	1.020	489.081	684.195	3.195	43.501
11	0.426	1.020	322.003	526.402	2.802	2.061
12	0.169	1.000	308.000	-27.368	-0.087	0.441
13	0.169	20.000	309.523	-23.034	-0.081	3.113
14	0.169	19.600	550.000	785.514	1.791	257.743
15	0.169	1.020	486.364	671.569	1.904	110.261

Table A. 9 Program inputs for the simulation, Fall season – Maximum work output scenario

G_0 $[W/m^2]$	T_{amb} $[K]$	p_r	r	T_5 $[K]$	A_{reg} $[m^2]$	T_{14} $[K]$	A_{col} $[m^2]$	η_{comp} [%]	η_{GT} [%]	η_{ST} [%]	η_{pump} [%]
645.45	295.9	6.6	0.34	825	6	550	200	79.6	85.8	68	60

Table A. 10 Detailed results of the simulation, Fall season – Maximum work output scenario

State	Mass flow rate [kg/s]	Pressure [bar]	Temperature [K]	Specific enthalpy [kJ/kg]	Specific entropy [kJ/kg]	Specific flow exergy [kJ/kg]
1	0.559	1.000	308.000	514.280	2.767	0.203
2	0.559	6.600	489.081	682.335	2.839	147.871
3	0.559	6.468	541.692	736.673	2.948	169.661
4	0.559	6.145	695.745	904.566	3.230	253.661
5	0.559	6.022	825.000	1053.868	3.431	343.388
6	0.559	1.041	646.366	850.398	3.485	123.726
7	0.369	1.041	646.366	850.398	3.485	123.726
8	0.369	1.020	320.170	524.803	2.797	1.937
9	0.190	1.041	646.366	850.398	3.485	123.726
10	0.190	1.020	496.584	691.777	3.210	46.525
11	0.559	1.020	383.320	581.664	2.959	10.834
12	0.148	1.000	308.000	-27.368	-0.087	0.441
13	0.148	20.000	309.523	-23.034	-0.081	3.113
14	0.148	19.600	550.000	785.514	1.791	257.743
15	0.148	1.020	486.364	671.569	1.904	110.261

A.4 Winter season

Table A. 11 Program inputs for the simulation, Winter season – Maximum efficiency scenario

G_0 $[W/m^2]$	T_{amb} $[K]$	p_r	r	T_5 $[K]$	A_{reg} $[m^2]$	T_{14} $[K]$	A_{col} $[m^2]$	η_{comp} [%]	η_{GT} [%]	η_{ST} [%]	η_{pump} [%]
618.44	282	6.6	0.01	825	6	550	200	79.6	85.8	68	60

Table A. 12 Detailed results of the simulation, Winter season – Maximum efficiency scenario

State	Mass flow rate [kg/s]	Pressure [bar]	Temperature [K]	Specific enthalpy [kJ/kg]	Specific entropy [kJ/kg]	Specific flow exergy [kJ/kg]
1	0.453	1.000	308.000	514.280	2.767	0.951
2	0.453	6.600	489.081	682.335	2.839	149.637
3	0.453	6.468	490.730	684.054	2.846	149.265
4	0.453	6.145	676.483	882.932	3.199	248.137
5	0.453	6.022	825.000	1053.868	3.431	353.343
6	0.453	1.041	646.366	850.398	3.485	134.424
7	0.449	1.041	646.366	850.398	3.485	134.424
8	0.449	1.020	320.170	524.803	2.797	3.095
9	0.005	1.041	646.366	850.398	3.485	134.424
10	0.005	1.020	489.081	684.195	3.195	50.169
11	0.453	1.020	322.003	526.402	2.802	3.288
12	0.180	1.000	308.000	-27.368	-0.087	2.048
13	0.180	20.000	309.523	-23.034	-0.081	4.798
14	0.180	19.600	550.000	785.514	1.791	285.445
15	0.180	1.020	486.364	671.569	1.904	139.538

Table A. 13 Program inputs for the simulation, Winter season – Maximum work output scenario

G_0 $[W/m^2]$	T_{amb} $[K]$	p_r	r	T_5 $[K]$	A_{reg} $[m^2]$	T_{14} $[K]$	A_{col} $[m^2]$	η_{comp} [%]	η_{GT} [%]	η_{ST} [%]	η_{pump} [%]
618.44	282	6.6	0.36	825	6	550	200	79.6	85.8	68	60

Table A. 14 Detailed results of the simulation, Winter season - Maximum work output scenario

State	Mass flow rate [kg/s]	Pressure [bar]	Temperature [K]	Specific enthalpy [kJ/kg]	Specific entropy [kJ/kg]	Specific flow exergy [kJ/kg]
1	0.622	1.000	308.000	514.280	2.767	0.951
2	0.622	6.600	489.081	682.335	2.839	149.637
3	0.622	6.468	543.139	738.190	2.951	173.658
4	0.622	6.145	676.483	882.932	3.199	248.137
5	0.622	6.022	825.000	1053.868	3.431	353.343
6	0.622	1.041	646.366	850.398	3.485	134.424
7	0.398	1.041	646.366	850.398	3.485	134.424
8	0.398	1.020	320.170	524.803	2.797	3.095
9	0.224	1.041	646.366	850.398	3.485	134.424
10	0.224	1.020	501.142	696.402	3.219	55.414
11	0.622	1.020	388.704	586.672	2.972	15.577
12	0.160	1.000	308.000	-27.368	-0.087	2.048
13	0.160	20.000	309.523	-23.034	-0.081	4.798
14	0.160	19.600	550.000	785.514	1.791	285.445
15	0.160	1.020	486.364	671.569	1.904	139.538

A.5 Spring season

Table A. 15 Program inputs for the simulation, Spring season – Maximum efficiency scenario

G_0 $[W/m^2]$	T_{amb} $[K]$	p_r	r	T_5 $[K]$	A_{reg} $[m^2]$	T_{14} $[K]$	A_{col} $[m^2]$	η_{comp} [%]	η_{GT} [%]	η_{ST} [%]	η_{pump} [%]
650.73	286.3	6.6	0.01	825	6	550	200	79.6	85.8	68	60

Table A. 16 Detailed results of the simulation, Spring season – Maximum efficiency scenario

State	Mass flow rate [kg/s]	Pressure [bar]	Temperature [K]	Specific enthalpy [kJ/kg]	Specific entropy [kJ/kg]	Specific flow exergy [kJ/kg]
1	0.446	1.000	308.000	514.280	2.767	0.663
2	0.446	6.600	489.081	682.335	2.839	149.038
3	0.446	6.468	490.730	684.054	2.846	148.635
4	0.446	6.145	689.036	897.011	3.219	254.166
5	0.446	6.022	825.000	1053.868	3.431	350.240
6	0.446	1.041	646.366	850.398	3.485	131.094
7	0.442	1.041	646.366	850.398	3.485	131.094
8	0.442	1.020	320.170	524.803	2.797	2.682
9	0.004	1.041	646.366	850.398	3.485	131.094
10	0.004	1.020	489.081	684.195	3.195	48.071
11	0.446	1.020	322.003	526.402	2.802	2.854
12	0.178	1.000	308.000	-27.368	-0.087	1.431
13	0.178	20.000	309.523	-23.034	-0.081	4.157
14	0.178	19.600	550.000	785.514	1.791	276.849
15	0.178	1.020	486.364	671.569	1.904	130.461

Table A. 17 Program inputs for the simulation, Spring season – Maximum work output scenario

G_0 $[W/m^2]$	T_{amb} $[K]$	p_r	r	T_5 $[K]$	A_{reg} $[m^2]$	T_{14} $[K]$	A_{col} $[m^2]$	η_{comp} [%]	η_{GT} [%]	η_{ST} [%]	η_{pump} [%]
650.73	286.3	6.6	0.34	825	6	550	200	79.6	85.8	68	60

Table A. 18 Detailed results of the simulation, Spring season – Maximum work output scenario

State	Mass flow rate [kg/s]	Pressure [bar]	Temperature [K]	Specific enthalpy [kJ/kg]	Specific entropy [kJ/kg]	Specific flow exergy [kJ/kg]
1	0.591	1.000	308.000	514.280	2.767	0.663
2	0.591	6.600	489.081	682.335	2.839	149.038
3	0.591	6.468	541.279	736.240	2.947	171.672
4	0.591	6.145	689.036	897.011	3.219	254.166
5	0.591	6.022	825.000	1053.868	3.431	350.240
6	0.591	1.041	646.366	850.398	3.485	131.094
7	0.390	1.041	646.366	850.398	3.485	131.094
8	0.390	1.020	320.170	524.803	2.797	2.682
9	0.201	1.041	646.366	850.398	3.485	131.094
10	0.201	1.020	497.834	693.044	3.213	51.780
11	0.591	1.020	383.785	582.095	2.960	13.243
12	0.157	1.000	308.000	-27.368	-0.087	1.431
13	0.157	20.000	309.523	-23.034	-0.081	4.157
14	0.157	19.600	550.000	785.514	1.791	276.849
15	0.157	1.020	486.364	671.569	1.904	130.461

Appendix B

B. MOO complementary results

This section presents complementary data resulting from the MOO conducted in chapter 4. It starts off by showcasing the set of Pareto-optimal solutions, followed by some important data used in the decision making process.

B.1 MOO results – Pareto-optimal solutions

Table B. 1 Pareto-optimal set of solutions, Model with regenerator

	Fitness value		Genes									Performance indicators								
#	C_{um} [€]	NPV [€]	p_r	τ	T_5 [K]	A_{reg} [m²]	T_{1A} [K]	A_{col} [m²]	η_{comp} [%]	η_{GT} [%]	η_{ST} [%]	η_{pump} [%]	η^{el} [%]	$\eta^{el,e}$ [%]	$\dot{P}_{el}$ [kW]	PBP [y]	IRR [%]	LEC [€/kWh]	f_{sol} [%]]	$\dot{m}_{CO_2\ emitted}$ [t/y]	$\dot{m}_{CO_2\ saved}$ [t/y]
1	113545.41	0.07	5.01	0.71	804.43	2.09	575.00	200.00	85.03	87.57	75.00	60.01	16.31	20.81	23.98	11	8.00	0.222	61.17	48.25	76.03
2	113545.43	0.09	5.01	0.71	804.43	2.09	575.00	200.00	85.03	87.57	75.00	60.01	16.31	20.81	23.98	11	8.00	0.222	61.17	48.25	76.03
3	113545.43	0.09	5.01	0.71	804.43	2.09	575.00	200.00	85.03	87.57	75.00	60.01	16.31	20.81	23.98	11	8.00	0.222	61.17	48.25	76.03
4	113545.45	0.12	5.01	0.71	804.43	2.09	575.00	200.00	85.03	87.57	75.00	60.01	16.31	20.81	23.98	11	8.00	0.222	61.17	48.25	76.03
5	113545.47	0.17	5.01	0.71	804.43	2.09	575.00	200.00	85.03	87.57	75.00	60.01	16.31	20.81	23.98	11	8.00	0.222	61.17	48.25	76.03
6	113545.49	0.18	5.01	0.71	804.43	2.09	575.00	200.00	85.03	87.57	75.00	60.01	16.31	20.81	23.98	11	8.00	0.222	61.17	48.25	76.03
7	113545.51	0.19	5.01	0.71	804.43	2.09	575.00	200.00	85.03	87.57	75.00	60.01	16.31	20.81	23.98	11	8.00	0.222	61.17	48.25	76.03
8	113545.52	0.21	5.01	0.71	804.43	2.09	575.00	200.00	85.03	87.57	75.00	60.01	16.31	20.81	23.98	11	8.00	0.222	61.17	48.25	76.03
9	113545.58	0.22	5.01	0.71	804.43	2.09	575.00	200.00	85.03	87.57	75.00	60.01	16.31	20.81	23.98	11	8.00	0.222	61.17	48.25	76.03
10	113545.59	0.25	5.01	0.71	804.43	2.09	575.00	200.00	85.03	87.57	75.00	60.01	16.31	20.81	23.98	11	8.00	0.222	61.17	48.25	76.03
11	113545.63	0.25	5.01	0.71	804.43	2.09	575.00	200.00	85.03	87.57	75.00	60.02	16.31	20.81	23.98	11	8.00	0.222	61.17	48.25	76.03
12	113545.69	0.47	5.01	0.71	804.43	2.09	575.00	200.00	85.03	87.57	75.00	60.01	16.31	20.81	23.98	11	8.00	0.222	61.17	48.25	76.03
13	113545.76	0.52	5.01	0.71	804.43	2.09	575.00	200.00	85.03	87.57	75.00	60.01	16.31	20.81	23.98	11	8.00	0.222	61.17	48.25	76.03
14	113545.81	0.59	5.01	0.71	804.43	2.09	575.00	200.00	85.03	87.57	75.00	60.01	16.31	20.81	23.98	11	8.00	0.222	61.17	48.25	76.03
15	113545.86	0.65	5.01	0.71	804.43	2.09	575.00	200.00	85.03	87.57	75.00	60.01	16.31	20.81	23.98	11	8.00	0.222	61.17	48.25	76.03
16	113545.95	0.78	5.01	0.71	804.43	2.09	575.00	200.00	85.03	87.57	75.00	60.01	16.31	20.81	23.98	11	8.00	0.222	61.17	48.25	76.03
17	113546.12	1.11	5.01	0.71	804.43	2.09	575.00	200.00	85.03	87.57	75.00	60.01	16.31	20.81	23.98	11	8.00	0.222	61.17	48.25	76.03
18	113546.46	1.44	5.01	0.71	804.43	2.09	575.00	200.00	85.03	87.57	75.00	60.01	16.31	20.81	23.98	11	8.00	0.222	61.17	48.25	76.03
19	113546.91	2.06	5.01	0.71	804.43	2.09	575.00	200.00	85.03	87.57	75.00	60.01	16.31	20.81	23.98	11	8.00	0.222	61.17	48.25	76.03
20	113547.96	3.40	5.01	0.71	804.43	2.09	575.00	200.00	85.03	87.57	75.00	60.01	16.31	20.81	23.98	11	8.00	0.222	61.17	48.26	76.03
21	113552.08	15.26	5.01	0.71	804.43	2.09	575.00	200.00	85.03	87.57	75.00	60.01	16.31	20.82	23.98	11	8.00	0.222	61.17	48.25	76.03
22	113556.78	29.04	5.01	0.71	804.43	2.09	575.00	200.00	85.04	87.57	75.00	60.03	16.31	20.82	23.98	11	8.00	0.222	61.18	48.25	76.03
23	116091.88	695.04	5.05	0.68	808.24	2.06	575.00	200.30	85.07	87.57	70.44	60.47	16.59	21.06	24.81	11	8.07	0.221	60.23	50.27	76.14
24	119429.90	17107.35	5.03	0.61	804.89	2.09	574.98	200.02	85.12	87.57	75.00	60.52	18.00	22.91	26.68	10	9.61	0.207	60.68	49.27	76.03
25	122672.14	26458.31	5.30	0.55	804.50	2.08	574.98	200.23	85.15	87.59	75.00	60.49	18.90	24.02	28.18	9	10.40	0.200	60.40	49.90	76.11
26	127324.13	43863.62	5.16	0.44	804.93	2.09	574.93	200.14	85.18	87.57	75.00	60.82	20.49	26.05	30.51	9	11.76	0.188	60.46	49.76	76.08
27	130542.25	49693.59	5.05	0.41	808.54	2.09	574.87	200.68	85.25	87.66	74.88	61.62	21.10	26.72	31.84	8	12.14	0.185	59.81	51.25	76.28
28	133213.67	52417.08	5.43	0.41	810.22	2.09	574.93	203.32	85.46	87.70	75.00	62.47	21.30	26.86	32.93	8	12.27	0.184	59.12	53.43	77.29
29	136561.98	75471.20	5.73	0.15	810.52	2.09	574.98	203.34	85.37	87.67	74.97	61.63	23.23	29.67	34.66	7	13.89	0.170	61.29	48.82	77.30
30	137965.84	77715.96	5.74	0.13	812.34	2.08	574.63	204.12	85.40	87.82	74.83	61.83	23.43	29.93	35.10	7	14.00	0.170	61.29	49.01	77.59
31	143372.19	82355.43	6.09	0.16	822.02	2.09	574.95	204.45	85.58	87.79	74.98	62.36	23.92	30.01	37.80	7	14.11	0.170	58.19	55.84	77.72
32	146318.19	86537.89	5.77	0.06	828.16	2.08	574.27	206.44	85.42	87.89	74.92	65.53	24.34	30.74	38.08	7	14.28	0.168	59.34	53.78	78.47
33	149799.67	91766.85	6.41	0.07	834.91	2.07	574.43	206.26	85.65	87.83	74.99	66.35	24.76	30.87	40.24	7	14.49	0.168	57.08	58.95	78.41
34	154711.87	96130.14	7.25	0.05	840.44	2.07	574.73	205.77	85.32	88.53	74.95	66.63	25.23	31.10	42.40	7	14.58	0.168	55.05	63.86	78.22
35	157341.54	101222.03	7.11	0.04	848.50	2.07	574.59	204.95	85.55	88.45	74.98	67.67	25.71	31.56	43.63	7	14.80	0.167	54.31	65.54	77.91
36	161031.65	102162.91	7.73	0.05	850.57	2.07	574.43	207.65	85.40	88.24	74.99	66.67	25.62	31.17	45.37	7	14.71	0.169	52.73	70.76	78.94
37	163484.25	105569.92	7.46	0.04	849.31	2.06	574.56	210.70	85.55	88.62	74.97	68.66	25.84	31.60	45.64	7	14.82	0.167	53.64	69.23	80.09
38	167341.62	108183.88	6.78	0.05	849.37	2.06	574.52	217.45	85.58	88.56	74.98	66.88	25.79	31.68	46.35	7	14.83	0.167	54.42	69.23	82.66
39	174321.89	113457.72	6.95	0.07	853.62	2.07	574.47	221.33	85.74	88.59	74.98	67.01	26.07	31.78	48.90	7	14.87	0.167	53.07	74.39	84.14
40	178548.46	118910.91	7.80	0.02	865.51	2.05	574.30	214.25	85.74	88.96	75.00	73.34	26.90	32.41	50.93	7	15.03	0.167	50.89	78.58	81.44
41	182491.36	122169.51	7.35	0.03	856.08	2.07	574.49	233.95	85.45	88.46	74.97	69.57	26.05	31.71	51.97	7	15.06	0.166	52.75	79.66	88.93
42	183465.43	123080.86	7.39	0.03	855.93	2.07	574.47	234.68	85.46	88.55	74.98	69.90	26.10	31.76	52.25	7	15.07	0.166	52.72	80.00	89.21
43	188097.00	125707.17	7.08	0.05	853.95	2.06	574.51	239.87	85.65	88.84	74.97	67.84	26.19	31.95	53.08	7	15.05	0.166	53.23	80.12	91.18
44	190379.00	128848.74	7.50	0.03	856.70	2.07	574.47	243.27	85.44	88.57	74.97	69.36	26.14	31.75	54.57	7	15.13	0.166	52.41	83.98	92.47
45	194027.00	131838.03	7.52	0.04	857.03	2.06	574.48	247.77	85.39	88.62	74.97	69.01	26.16	31.75	55.78	7	15.16	0.166	52.25	86.06	94.18
46	197955.36	135271.81	7.57	0.03	862.94	2.07	574.54	246.51	85.52	88.66	74.97	69.16	26.50	32.01	57.22	7	15.20	0.166	51.35	88.79	93.70
47	201046.18	137712.28	7.72	0.02	860.09	2.06	574.42	250.83	85.73	88.85	74.92	69.19	26.56	32.16	57.74	7	15.21	0.166	51.88	88.43	95.35
48	210878.46	146172.32	7.77	0.03	860.74	2.06	574.42	264.85	85.40	88.86	74.99	69.79	26.47	31.99	61.24	7	15.29	0.166	51.49	94.86	100.68
49	216552.37	148197.76	7.28	0.02	865.05	2.07	574.47	267.06	85.57	88.92	75.00	68.67	26.73	32.35	62.04	7	15.21	0.166	51.75	94.65	101.52
50	220154.33	153153.53	7.82	0.03	861.19	2.06	574.28	274.44	85.70	88.82	74.97	70.26	26.60	32.10	64.02	7	15.32	0.166	51.27	99.14	104.32
51	229614.01	161958.20	7.75	0.03	863.26	2.07	574.46	286.59	85.68	88.75	74.98	70.26	26.64	32.13	67.22	7	15.41	0.165	51.08	104.32	108.94
52	233674.82	165817.97	7.63	0.02	860.04	2.07	574.45	299.76	85.49	88.57	74.94	70.06	26.32	31.88	68.40	7	15.46	0.165	51.88	105.68	113.95
53	239432.21	169726.49	8.02	0.02	862.37	2.06	574.16	301.26	85.61	88.60	74.95	73.31	26.53	31.97	70.50	7	15.45	0.165	50.98	110.11	114.52
54	243517.42	172606.82	7.48	0.04	853.84	2.07	574.67	318.60	85.49	88.75	74.99	68.57	26.10	31.77	70.83	7	15.45	0.164	52.80	108.27	121.11
55	248532.34	175234.85	7.96	0.02	865.08	2.06	574.15	301.93	85.80	89.26	74.98	71.15	27.06	32.58	72.36	7	15.41	0.165	50.79	111.22	114.77
56	251550.63	178433.51	7.64	0.02	861.45	2.07	574.26	313.65	86.10	88.97	74.85	69.29	26.81	32.47	72.86	7	15.45	0.164	51.90	110.51	119.23
57	256372.47	185362.75	7.74	0.02	861.55	2.06	574.33	326.99	85.65	88.70	74.98	65.53	26.51	32.07	75.55	7	15.59	0.164	51.61	116.54	124.30
58	262352.22	190395.14	7.81	0.02	862.54	2.07	574.35	332.47	85.57	88.86	74.95	68.04	26.62	32.16	77.44	7	15.61	0.164	51.41	119.47	126.38
59	265361.79	192665.02	7.75	0.02	862.77	2.06	574.35	334.51	85.68	88.93	74.98	70.98	26.72	32.29	78.12	7	15.62	0.164	51.46	119.94	127.16
60	266690.86	193569.94	7.84	0.02	863.18	2.06	574.37	334.65	85.69	88.97	74.99	71.20	26.78	32.32	78.58	7	15.62	0.164	51.29	120.83	127.21
61	269756.02	195859.41	7.74	0.02	860.77	2.06	574.14	343.41	85.68	88.87	74.93	69.79	26.60	32.19	79.36	7	15.62	0.164	51.76	121.67	130.54
62	270738.18	197666.55	7.82	0.02	864.99	2.06	574.39	341.56	85.23	88.96	74.97	71.04	26.67	32.12	80.55	7	15.66	0.164	50.85	125.48	129.84
63	274409.42	200699.22	7.72	0.02	862.10	2.05	574.47	350.23	85.47	88.87	74.93	70.22	26.56	32.10	81.30	7	15.67	0.164	51.47	125.54	133.13
64	277770.67	202834.35	7.81	0.02	866.96	2.06	574.29	343.75	85.69	89.03	74.98	70.31	26.97	32.45	82.29	7	15.66	0.164	50.67	127.19	130.67
65	281668.86	204354.79	7.87	0.02	866.12	2.06	574.40	345.18	86.08	89.11	75.00	70.64	27.13	32.68	82.74	7	15.61	0.164	50.89	126.61	131.21
66	288584.28	212057.72	8.17	0.01	867.55	2.05	574.09	355.94	85.53	89.06	75.00	74.21	27.00	32.40	86.15	7	15.70	0.164	50.18	134.35	135.30
67	291152.16	213166.15	8.17	0.01	867.87	2.05	574.04	355.90	85.80	89.07	75.00	74.22	27.13	32.55	86.58	7	15.68	0.164	50.15	134.45	135.29
68	293369.25	213708.68	8.18	0.01	867.72	2.05	573.98	356.31	85.93	89.16	75.00	74.27	27.22	32.67	86.80	7	15.64	0.164	50.25	134.09	135.45
69	296328.00	214927.20	8.18	0.01	867.78	2.05	573.98	357.90	85.93	89.27	75.00	74.27	27.28	32.75	87.41	7	15.61	0.164	50.24	134.76	136.05
70	299354.93	215683.32	8.18	0.01	868.00	2.05	573.98	358.36	86.19	89.28	75.00	74.28	27.39	32.89	87.83	7	15.56	0.164	50.27	134.76	136.22

Table B. 2 Pareto-optimal set of solutions, System without regenerator

	Fitness value		Genes									Performance Indicators								
#	C_{inv} [€]	NPV [€]	p_r	r	T_h [K]	A_{reg} [m²]	T_{ts} [K]	A_{sol} [m²]	η_{comp} [%]	η_{HT} [%]	η_{ST} [%]	η_{pump} [%]	$\eta^{I,st}$ [%]	$\eta^{I,ex}$ [%]	$\dot{P}_{el}$ [kW]	PBP [y]	IRR [%]	LEC [€/kWh]	f_{cost} [%]]	$\dot{m}_{CO_2\,emitted}$ [t/y]	$\dot{m}_{CO_2\,saved}$ [t/y]
1																					
	118263.97	0.05	5.78	0.00	800.00	0.00	575.00	200.00	79.26	83.66	61.15	60.00	16.46	21.49	22.75	11	8.00	0.221	65.07	40.81	76.03
2	118263.97	0.05	5.78	0.00	800.00	0.00	575.00	200.00	79.26	83.66	61.15	60.00	16.46	21.49	22.75	11	8.00	0.221	65.07	40.81	76.03
3	118263.97	0.08	5.78	0.00	800.00	0.00	575.00	200.00	79.26	83.66	61.15	60.00	16.46	21.49	22.75	11	8.00	0.221	65.07	40.81	76.03
4	118263.97	0.12	5.78	0.00	800.00	0.00	575.00	200.00	79.26	83.66	61.15	60.00	16.46	21.49	22.75	11	8.00	0.221	65.07	40.81	76.03
5	118263.97	0.16	5.78	0.00	800.00	0.00	575.00	200.00	79.26	83.66	61.15	60.00	16.46	21.49	22.75	11	8.00	0.221	65.07	40.81	76.03
6	118263.97	0.16	5.78	0.00	800.00	0.00	575.00	200.00	79.26	83.66	61.15	60.00	16.46	21.49	22.75	11	8.00%	0.221	65.07	40.81	76.03
7	118263.97	0.20	5.78	0.00	800.00	0.00	575.00	200.00	79.26	83.66	61.15	60.00	16.46	21.49	22.75	11	8.00	0.221	65.07	40.81	76.03
8	118263.97	0.27	5.78	0.00	800.00	0.00	575.00	200.00	79.26	83.66	61.15	60.00	16.46	21.49	22.75	11	8.00	0.221	65.07	40.81	76.03
9	118263.97	0.30	5.78	0.00	800.00	0.00	575.00	200.00	79.26	83.66	61.15	60.00	16.46	21.49	22.75	11	8.00	0.221	65.07	40.81	76.03
10	118263.97	0.30	5.78	0.00	800.00	0.00	575.00	200.00	79.26	83.66	61.15	60.00	16.46	21.49	22.75	11	8.00	0.221	65.07	40.81	76.03
11	118263.97	0.38	5.78	0.00	800.00	0.00	575.00	200.00	79.26	83.66	61.15	60.00	16.46	21.49	22.75	11	8.00	0.221	65.07	40.81	76.03
12	118263.97	0.46	5.78	0.00	800.00	0.00	575.00	200.00	79.26	83.66	61.15	60.00	16.46	21.49	22.75	11	8.00	0.221	65.07	40.81	76.03
13	118263.97	0.53	5.78	0.00	800.00	0.00	575.00	200.00	79.26	83.66	61.15	60.00	16.46	21.49	22.75	11	8.00	0.221	65.07	40.81	76.03
14	118263.97	0.62	5.78	0.00	800.00	0.00	575.00	200.00	79.26	83.66	61.15	60.00	16.46	21.49	22.75	11	8.00	0.221	65.07	40.81	76.03
15	118263.97	0.76	5.78	0.00	800.00	0.00	575.00	200.00	79.26	83.66	61.15	60.00	16.46	21.49	22.75	11	8.00	0.221	65.07	40.81	76.03
16	118263.97	0.78	5.78	0.00	800.00	0.00	575.00	200.00	79.26	83.66	61.15	60.00	16.46	21.49	22.75	11	8.00	0.221	65.07	40.81	76.03
17	118263.97	1.03	5.78	0.00	800.00	0.00	575.00	200.00	79.26	83.66	61.15	60.00	16.46	21.49	22.75	11	8.00	0.221	65.07	40.81	76.03
18	118263.97	2.32	5.78	0.00	800.00	0.00	575.00	200.00	79.26	83.66	61.15	60.00	16.46	21.49	22.75	11	8.00	0.221	65.07	40.80	76.03
19	118263.98	2.90	5.78	0.00	800.00	0.00	575.00	200.00	79.27	83.66	61.15	60.00	16.46	21.49	22.75	11	8.00	0.221	65.07	40.81	76.03
20	118264.53	109.12	5.78	0.00	800.00	0.00	575.00	200.00	79.26	83.66	61.20	60.00	16.47	21.50	22.76	11	8.01	0.221	65.07	40.81	76.03
21	122018.05	45794.55	6.36	0.00	800.11	0.00	575.00	202.11	82.04	86.10	69.89	61.45	20.13	26.21	28.33	8	12.08	0.184	64.59	42.11	76.83
22	127602.24	72853.03	6.21	0.00	812.22	0.00	575.00	201.23	82.40	87.82	73.99	62.86	22.58	29.02	32.75	7	14.08	0.169	62.40	46.09	76.49
23	131102.48	75690.74	6.44	0.00	802.44	0.00	575.00	208.04	83.64	87.98	74.47	63.12	22.62	29.40	32.93	7	14.14	0.168	64.28	43.95	79.08
24	132950.85	79043.77	5.83	0.00	817.58	0.00	575.00	202.25	85.01	88.32	69.35	65.01	23.36	30.04	34.02	7	14.31	0.167	62.47	46.19	76.88
25	136216.39	88905.51	6.41	0.00	823.36	0.00	575.00	205.37	83.42	88.30	74.61	65.88	23.92	30.34	36.75	7	14.89	0.165	60.12	51.79	78.07
26	142484.97	98388.92	6.22	0.00	830.21	0.00	575.00	211.55	85.00	87.46	74.56	68.27	24.48	30.94	39.15	7	15.27	0.163	59.49	54.77	80.42
27	146596.00	104950.50	6.42	0.00	835.32	0.00	575.00	211.57	84.73	88.33	74.88	68.34	25.08	31.47	41.00	7	15.52	0.162	58.20	57.77	80.42
28	152858.10	111584.90	6.58	0.00	843.72	0.00	575.00	211.78	85.34	88.53	74.66	67.56	25.75	32.03	43.32	7	15.66	0.161	56.62	61.67	80.50
29	157399.29	115356.25	7.07	0.00	845.44	0.00	575.00	215.64	85.46	88.50	74.40	67.44	25.86	31.97	45.13	7	15.68	0.162	55.58	65.52	81.97
30	161802.14	120097.95	7.07	0.00	851.40	0.00	575.00	217.46	85.44	88.55	74.48	68.13	26.17	32.18	46.88	7	15.78	0.161	54.60	68.73	82.66
31	166721.46	124218.49	6.97	0.00	849.06	0.00	575.00	230.50	84.94	88.18	74.84	69.73	25.77	31.75	48.54	7	15.80	0.162	55.03	71.61	87.62
32	170593.72	127519.05	7.26	0.00	856.13	0.00	575.00	226.97	85.23	88.48	74.28	69.02	26.26	32.09	50.12	7	15.83	0.162	53.49	75.02	86.28
33	170671.85	127739.24	7.26	0.00	856.13	0.00	575.00	226.97	85.23	88.49	74.33	69.04	26.28	32.11	50.15	7	15.84	0.162	53.49	75.02	86.28
34	175155.63	131916.48	7.12	0.00	854.15	0.00	575.00	237.26	84.86	88.40	74.72	70.01	26.07	31.93	51.55	7	15.88	0.162	53.95	76.98	90.19
35	177802.15	134788.14	7.42	0.00	863.86	0.00	575.00	227.92	85.34	88.69	74.64	69.30	26.83	32.53	52.79	7	15.93	0.162	52.09	79.68	86.64
36	182221.00	140483.89	7.97	0.00	867.04	0.00	575.00	229.36	85.39	88.72	74.88	70.05	27.08	32.60	55.03	7	16.06	0.162	50.76	84.56	87.19
37	187533.32	143755.19	7.76	0.00	860.30	0.00	575.00	241.31	85.62	88.73	74.78	72.95	26.85	32.57	55.87	7	16.02	0.161	52.16	84.14	91.73
38	192573.02	148981.07	7.89	0.00	864.59	0.00	575.00	243.80	85.76	88.67	74.89	70.76	27.09	32.71	57.86	7	16.08	0.161	51.34%	87.85	92.68
39	200206.34	155340.35	7.67	0.00	868.10	0.00	575.00	252.65	85.48	88.72	74.73	71.99	27.13	32.72	60.34	7	16.11	0.161	51.09	91.94	96.04
40	206609.67	159679.64	6.99	0.00	855.69	0.00	575.00	277.05	85.46	88.65	74.66	68.07	26.44	32.41	60.94	7	16.08	0.160	54.05	89.51	105.31
41	210618.36	164979.03	7.39	0.00	858.33	0.00	575.00	279.07	85.53	88.57	74.79	69.90	26.62	32.44	63.00	7	16.18	0.160	53.02	93.99	106.08
42	213735.24	168562.58	7.83	0.00	866.09	0.00	575.00	270.89	85.60	88.85	74.96	70.16	27.19	32.80	64.73	7	16.23	0.161	51.17	98.25	102.97
43	216107.86	170005.84	7.40	0.00	860.94	0.00	575.00	281.67	85.68	88.71	74.90	72.07	26.88	32.69	64.70	7	16.21	0.160	52.63	96.37	107.07
44	219678.21	173157.53	7.29	0.00	855.81	0.00	575.00	296.19	85.59	88.35	74.91	70.86	26.43	32.31	65.70	7	16.23	0.160	53.59	97.51	112.59
45	223373.15	174916.03	7.71	0.00	866.83	0.00	575.00	283.45	85.75	88.77	74.37	69.73	27.13	32.75	67.44	7	16.18	0.161	51.28	102.37	107.75
46	228415.37	181616.40	7.76	0.00	861.75	0.00	575.00	297.37	85.63	88.64	74.92	70.09	26.89	32.57	69.25	7	16.29	0.160	51.93	104.64	113.04
47	231974.11	184280.87	7.47	0.00	862.21	0.00	575.00	304.38	85.56	88.57	74.72	70.08	26.80	32.53	70.12	7	16.29	0.160	52.31	105.47	115.70
48	238123.44	190663.91	7.53	0.00	862.81	0.00	575.00	311.94	85.60	88.55	74.89	70.63	26.86	32.58	72.28	7	16.35	0.160	52.13	108.88	118.58
49	244409.83	194321.69	7.28	0.00	862.90	0.00	575.00	321.62	85.56	88.53	74.70	69.74	26.78	32.54	73.77	7	16.29	0.160	52.50	110.60	122.26
50	249013.73	198384.17	7.35	0.00	855.92	0.00	575.00	333.71	85.41	88.87	74.66	71.86	26.60	32.49	74.71	7	16.31	0.159	53.43	110.57	126.85
51	253879.91	205493.81	7.70	0.00	864.18	0.00	575.00	329.85	85.58	88.73	74.92	69.84	27.02	32.68	77.61	7	16.43	0.160	51.65	117.40	125.39
52	256522.84	207175.64	7.78	0.00	864.36	0.00	575.00	331.12	85.85	88.66	74.93	70.85	27.10	32.77	78.28	7	16.42	0.160	51.56	118.26	125.87
53	260160.50	208624.28	7.27	0.00	861.80	0.00	575.00	344.42	85.73	88.49	74.67	69.75	26.77	32.57	78.63	7	16.36	0.159	52.73	117.38	130.93
54	266902.14	216933.14	7.89	0.00	864.27	0.00	575.00	345.11	85.66	88.78	74.94	69.72	27.09	32.72	81.88	6	16.47	0.159	51.36	124.25	131.19
55	271081.98	220484.77	7.36	0.00	861.52	0.00	575.00	357.00	85.71	88.75	74.97	73.57	26.95	32.77	82.24	6	16.47	0.159	52.62	122.20	135.71
56	274193.83	223083.73	7.80	0.00	860.16	0.00	575.00	363.65	85.46	88.66	74.87	70.98	26.76	32.44	84.05	6	16.47	0.159	52.07	127.27	138.23
57	276726.47	224528.14	7.36	0.00	859.85	0.00	575.00	367.74	85.87	88.61	74.71	70.65	26.81	32.65	83.83	6	16.45	0.159	52.90	124.47	139.79
58	279431.07	226239.29	7.22	0.00	849.07	0.00	575.00	392.93	85.54	88.25	74.90	71.69	26.05	32.05	84.06	7	16.44	0.158	54.76	123.42	149.36
59	280476.26	228849.38	7.56	0.00	865.45	0.00	575.00	372.73	85.17	88.29	74.73	73.29	26.68	32.26	86.70	6	16.50	0.160	51.59	132.96	141.69
60	28706.51	236772.22	7.77	0.00	867.87	0.00	575.00	370.50	85.63	88.63	74.99	74.31	27.19	32.77	88.81	6	16.58	0.159	51.01	135.27	140.84
61	289649.11	239214.90	7.82	0.00	868.09	0.00	575.00	373.74	85.46	88.77	74.88	71.04	27.18	32.73	89.84	6	16.59	0.159	50.85	137.30	142.07
62	292456.39	241776.89	7.85	0.00	868.91	0.00	575.00	375.12	85.59	88.77	74.92	71.09	27.27	32.82	90.72	6	16.60	0.159	50.72	138.57	142.59
63	296977.00	243561.96	7.45	0.00	867.40	0.00	575.00	382.67	85.81	88.78	74.97	72.76	27.26	32.97	90.89	6	16.54	0.159	51.61	136.37	145.47
64	299118.62	245550.49	7.73	0.00	866.97	0.00	575.00	383.41	86.08	88.68	74.91	73.26	27.32	32.98	91.80	6	16.55	0.159	51.31	138.31	145.74
65	303411.72	251948.58	7.71	0.00	867.64	0.00	575.00	392.70	85.55	88.80	74.94	71.63	27.21	32.81	93.99	6	16.64	0.159	51.12	142.72	149.28
66	309049.29	256699.28	7.87	0.00	869.15	0.00	575.00	394.98	85.81	88.77	74.95	71.13	27.37	32.94	95.87	6	16.64	0.159	50.71	145.92	150.14
67	314006.26	260259.61	7.82	0.00	870.93	0.00	575.00	397.08	85.81	88.90	74.91	73.93	27.51	33.08	97.24	6	16.62	0.159	50.53	147.78	150.94
68	317375.91	263755.52	7.89	0.00	871.92	0.00	575.00	398.95	85.75	89.00	75.00	73.54	27.60	33.13	98.51	6	16.64	0.159	50.27	150.03	151.65
69	326389.27	267077.45	8.08	0.00	872.30	0.00	575.00	400.00	86.15	89.21	74.98	74.51	27.89	33.44	100.33	6	16.52	0.159	50.01	152.00	152.05
70	328706.12	267373.31	8.09	0.00	872.37	0.00	575.00	400.00	86.22	89.30	75.00	74.72	27.97	33.53	100.63	6	16.47	0.159	50.00	152.05	152.05

B.2 Decision making complementary data

Scenario #1

Table B. 3 Stream cost rates of subject # 28, Summer and fall

	Summer				Fall			
	Base Case		Optimized Case		Base Case		Optimized Case	
State (n)	$c_n[€cents/kWh]$	$\dot{C}_n$ [€/h]	$c_n[€cents/kWh]$	$\dot{C}_n$ [€/h	$c_n[€cents/kWh]$	$\dot{C}_n$ [€/h]	$c_n[€cents/kWh]$	$\dot{C}_n$ [€/h
1	338.57	0.11	398.53	0.13	136.11	0.12	161.96	0.14
2	8.75	5.42	8.40	5.04	8.95	5.63	8.58	5.22
3	9.02	5.57	8.40	5.04	9.21	5.78	8.58	5.22
4	6.32	6.86	5.88	6.42	6.56	7.08	6.10	6.59
5	6.54	9.35	6.23	9.30	6.72	9.82	6.39	9.73
6	6.54	3.30	6.23	3.27	6.72	3.54	6.39	3.49
7	6.54	3.27	6.23	3.27	6.72	3.50	6.39	3.49
8	6.54	0.05	6.23	0.06	6.72	0.05	6.39	0.08
9	6.54	0.03	X	X	6.72	0.04	X	X
10	6.54	0.01	X	X	6.72	0.01	X	X
11	7.64	0.06	6.23	0.06	7.67	0.07	6.39	0.08
12	11731.91	3.20	12608.90	3.22	4971.20	3.71	5290.36	3.68
13	724.73	3.40	771.90	3.37	742.75	3.91	786.05	3.83
14	18.99	7.89	17.40	7.55	19.79	8.64	18.14	8.22
15	18.99	3.19	17.40	3.21	19.79	3.69	18.14	3.66

Table B. 4 Stream cost rates of subject # 28, Winter and Spring

	Winter				Spring			
	Base Case		Optimized Case		Base Case		Optimized Case	
State (n)	$c_n[€cents/kWh]$	$\dot{C}_n$ [€/h]	$c_n[€cents/kWh]$	$\dot{C}_n$ [€/h	$c_n[€cents/kWh]$	$\dot{C}_n$ [€/h]	$c_n[€cents/kWh]$	$\dot{C}_n$ [€/h
1	37.47	0.16	45.20	0.19	48.45	0.14	58.48	0.17
2	8.93	6.06	8.64	5.61	8.69	5.78	8.42	5.39
3	9.18	6.21	8.64	5.61	8.94	5.93	8.42	5.39
4	6.67	7.51	6.24	6.99	6.37	7.23	5.97	6.77
5	6.77	10.84	6.46	10.72	6.55	10.25	6.27	10.19
6	6.77	4.12	6.46	4.05	6.55	3.84	6.27	3.79
7	6.77	4.08	6.46	4.05	6.55	3.80	6.27	3.79
8	6.77	0.09	6.46	0.13	6.55	0.08	6.27	0.11
9	6.77	0.04	X	X	6.55	0.04	X	X
10	6.77	0.02	X	X	6.55	0.01	X	X
11	7.34	0.11	6.46	0.13	7.20	0.09	6.27	0.11
12	1448.61	5.35	1511.51	5.17	1856.99	4.72	1949.67	4.61
13	644.87	5.58	672.79	5.34	668.76	4.94	701.33	4.77
14	21.20	10.91	19.46	10.29	20.30	9.98	18.65	9.47
15	21.20	5.33	19.46	5.15	20.30	4.70	18.65	4.59

Scenario #2

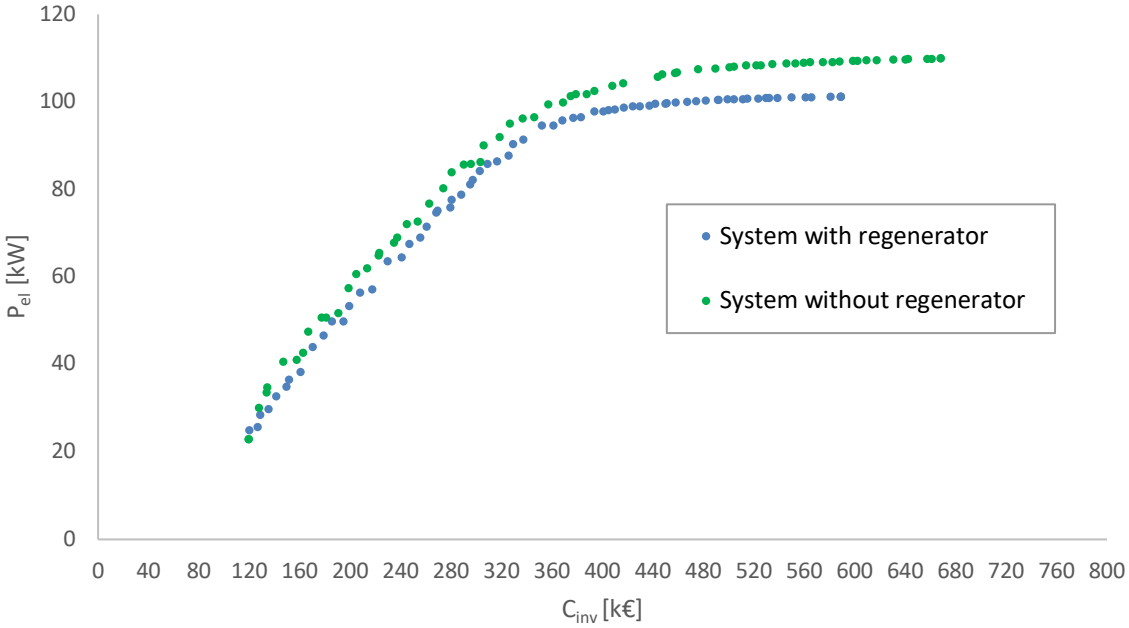

Figure B. 1 Pareto front of auxiliary MOO 1

Table B. 5 Stream cost rates of subject # 36, Summer and Fall

	Summer				Fall			
	Base Case		Optimized Case		Base Case		Optimized Case	
State (n)	c_n[€$cents/kWh$]	$\dot{C}_n$ [€/h]	c_n[€$cents/kWh$]	$\dot{C}_n$ [€/h	c_n[€$cents/kWh$]	$\dot{C}_n$ [€/h]	c_n[€$cents/kWh$]	$\dot{C}_n$ [€/h
1	338.57	0.11	391.17	0.15	136.11	0.12	159.40	0.16
2	8.75	5.42	8.88	7.08	8.95	5.63	9.03	7.33
3	9.02	5.57	8.88	7.08	9.21	5.78	9.03	7.33
4	6.32	6.86	6.41	8.57	6.56	7.08	6.62	8.82
5	6.54	9.35	6.60	12.54	6.72	9.82	6.74	13.12
6	6.54	3.30	6.60	4.09	6.72	3.54	6.74	4.36
7	6.54	3.27	6.60	4.09	6.72	3.50	6.74	4.36
8	6.54	0.05	6.60	0.08	6.72	0.05	6.74	0.10
9	6.54	0.03	X	X	6.72	0.04	X	X
10	6.54	0.01	X	X	6.72	0.01	X	X
11	7.64	0.06	6.60	0.08	7.67	0.07	6.74	0.10
12	11731.91	3.20	13071.15	3.94	4971.20	3.71	5469.86	4.51
13	724.73	3.40	800.27	4.12	742.75	3.91	813.31	4.69
14	18.99	7.89	18.07	9.25	19.79	8.64	18.78	10.09
15	18.99	3.19	18.07	3.92	19.79	3.69	18.78	4.49

Table B. 6 Stream cost rates of subject # 36, Winter and Spring

	Winter				Spring			
	Base Case		Optimized Case		Base Case		Optimized Case	
State (n)	$c_n[€cents/kWh]$	$\dot{C}_n$ [€/h]	$c_n[€cents/kWh]$	$\dot{C}_n$ [€/h	$c_n[€cents/kWh]$	$\dot{C}_n$ [€/h]	$c_n[€cents/kWh]$	$\dot{C}_n$ [€/h
1	37.47	0.16	44.97	0.23	48.45	0.14	58.13	0.20
2	8.93	6.06	9.05	7.92	8.69	5.78	8.86	7.59
3	9.18	6.21	9.05	7.92	8.94	5.93	8.86	7.59
4	6.67	7.51	6.76	9.41	6.37	7.23	6.49	9.08
5	6.77	10.84	6.79	14.49	6.55	10.25	6.62	13.77
6	6.77	4.12	6.79	5.09	6.55	3.84	6.62	4.76
7	6.77	4.08	6.79	5.09	6.55	3.80	6.62	4.76
8	6.77	0.09	6.79	0.16	6.55	0.08	6.62	0.13
9	6.77	0.04	X	X	6.55	0.04	X	X
10	6.77	0.02	X	X	6.55	0.01	X	X
11	7.34	0.11	6.79	0.16	7.20	0.09	6.62	0.13
12	1448.61	5.35	1559.10	6.38	1856.99	4.72	2017.34	5.67
13	644.87	5.58	695.05	6.59	668.76	4.94	726.71	5.87
14	21.20	10.91	20.10	12.72	20.30	9.98	19.32	11.67
15	21.20	5.33	20.10	6.36	20.30	4.70	19.32	5.65

Scenario #3

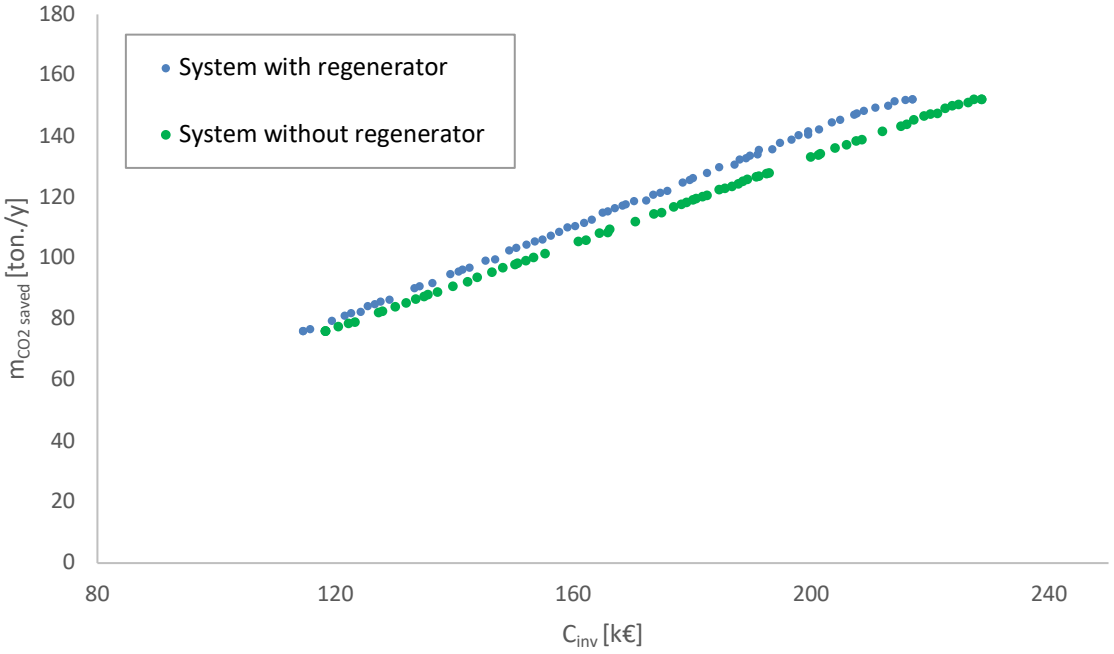

Figure B. 2 Pareto front of auxiliary MOO 2

Table B. 7 Stream cost rates of subject # 23, Summer and Fall

	Summer				Fall			
	Base Case		Optimized Case		Base Case		Optimized Case	
State (n)	$c_n[€cents/kWh]$	$\dot{C}_n$ [€/h]	$c_n[€cents/kWh]$	$\dot{C}_n$ [€/h	$c_n[€cents/kWh]$	$\dot{C}_n$ [€/h]	$c_n[€cents/kWh]$	$\dot{C}_n$ [€/h
1	338.57	0.11	679.35	0.21	136.11	0.12	278.91	0.24
2	8.75	5.42	8.53	5.02	8.95	5.63	8.81	5.25
3	9.02	5.57	8.53	5.02	9.21	5.78	8.81	5.25
4	6.32	6.86	5.95	6.37	6.56	7.08	6.22	6.60
5	6.54	9.35	6.24	8.36	6.72	9.82	6.46	8.83
6	6.54	3.30	6.24	2.77	6.72	3.54	6.46	2.98
7	6.54	3.27	6.24	2.77	6.72	3.50	6.46	2.98
8	6.54	0.05	6.24	0.13	6.72	0.05	6.46	0.16
9	6.54	0.03	X	X	6.72	0.04	X	X
10	6.54	0.01	X	X	6.72	0.01	X	X
11	7.64	0.06	6.24	0.13	7.67	0.07	6.46	0.16
12	11731.91	3.20	12310.20	2.57	4971.20	3.71	5210.06	2.96
13	724.73	3.40	753.12	2.69	742.75	3.91	772.64	3.09
14	18.99	7.89	16.97	6.01	19.79	8.64	17.84	6.61
15	18.99	3.19	16.97	2.56	19.79	3.69	17.84	2.95

Table B. 8 Stream cost rates of subject # 23, Winter and Spring

	Winter				Spring			
	Base Case		Optimized Case		Base Case		Optimized Case	
State (n)	$c_n[€cents/kWh]$	$\dot{C}_n$ [€/h]	$c_n[€cents/kWh]$	$\dot{C}_n$ [€/h	$c_n[€cents/kWh]$	$\dot{C}_n$ [€/h]	$c_n[€cents/kWh]$	$\dot{C}_n$ [€/h
1	37.47	0.16	77.06	0.33	48.45	0.14	99.66	0.29
2	8.93	6.06	8.99	5.74	8.69	5.78	8.67	5.45
3	9.18	6.21	8.99	5.74	8.94	5.93	8.67	5.45
4	6.67	7.51	6.44	7.09	6.37	7.23	6.11	6.80
5	6.77	10.84	6.61	9.85	6.55	10.25	6.35	9.28
6	6.77	4.12	6.61	3.53	6.55	3.84	6.35	3.27
7	6.77	4.08	6.61	3.53	6.55	3.80	6.35	3.27
8	6.77	0.09	6.61	0.24	6.55	0.08	6.35	0.21
9	6.77	0.04	X	X	6.55	0.04	X	X
10	6.77	0.02	X	X	6.55	0.01	X	X
11	7.34	0.11	6.61	0.24	7.20	0.09	6.35	0.21
12	1448.61	5.35	1505.83	4.21	1856.99	4.72	1924.96	3.72
13	644.87	5.58	667.91	4.36	668.76	4.94	690.18	3.86
14	21.20	10.91	19.37	8.37	20.30	9.98	18.39	7.64
15	21.20	5.33	19.37	4.20	20.30	4.70	18.39	3.71